

THE DECOMPOSITION OF 2-PROPANOL OVER VANADIUM PENTOXIDE
AND MODIFIED VANADIUM PENTOXIDE CATALYSTS

BY

DAVID V. FIKIS

A THESIS SUBMITTED TO THE DEPARTMENT OF CHEMISTRY
IN PARTIAL FULFILLMENT OF THE REQUIREMENTS FOR
THE DEGREE OF MASTER OF SCIENCE

LAKEHEAD UNIVERSITY

THUNDER BAY, ONTARIO, CANADA.

AUGUST, 1977.

ProQuest Number: 10611599

All rights reserved

INFORMATION TO ALL USERS

The quality of this reproduction is dependent upon the quality of the copy submitted.

In the unlikely event that the author did not send a complete manuscript and there are missing pages, these will be noted. Also, if material had to be removed, a note will indicate the deletion.



ProQuest 10611599

Published by ProQuest LLC (2017). Copyright of the Dissertation is held by the Author.

All rights reserved.

This work is protected against unauthorized copying under Title 17, United States Code
Microform Edition © ProQuest LLC.

ProQuest LLC.
789 East Eisenhower Parkway
P.O. Box 1346
Ann Arbor, MI 48106 - 1346

© DAVID V. FIKIS 1978

Canadian Thesis on Microfiche
No. 34731

252873

ACKNOWLEDGEMENTS

The work in preparation for this thesis was carried out at Lakehead University from August, 1974, to August 1977. The author wishes to thank his supervisor Dr. R.A. Ross, B.Sc., A.R.C.S.T., F.R.I.C., and Dr. W.J. Murphy for their continual encouragement and direction.

In addition, the author would like to acknowledge the expert assistance provided by the technical staff of the Faculty of Science.

The financial assistance of the National Research Council of Canada and Lakehead University is also gratefully acknowledged.

TABLE OF CONTENTS

CHAPTER	PAGE
ACKNOWLEDGEMENTS	ii
TABLE OF CONTENTS	iii
ABSTRACT	v
1. INTRODUCTION	1
1.1 General	1
1.2 Dehydration	4
1.3 Dehydrogenation	11
1.4 Modified Metal Oxide Catalysts	15
1.5 Objective of the Present Investigation	16
2. EXPERIMENTAL	18
2.1 General	18
2.2 Flow System	20
2.3 Analysis	24
2.4 Surface Area Measurements	28
2.5 X-ray Analysis	32
2.6 Catalyst Preparation	32
2.7 Reagents	34
3. RESULTS	35
3.1 Tests for Diffusion	35
3.1.1 Flow Rate Effects	36
3.1.2 The Effect of Particle Size	39
3.2 The Catalytic Decomposition of 2-propanol	40
3.2.1 The Effect of Exposure Time on the Reaction Components	40
3.2.2 The Effect of Temperature on the Reaction	40
3.2.3 The Effect of 2-propanol Partial Pressure on the Reaction Rates	50
3.2.4 The Effect of Acetone	50
3.2.5 The Effect of Water Vapour	55
3.2.6 The Effects of Hydrogen, Propylene and Propane	55

CHAPTER	PAGE
3.3 Activation Energies	55
3.4 Surface Area Determinations	76
3.5 X-ray Diffraction	76
4. DISCUSSION	80
4.1 Diffusion Effects	80
4.2 Catalytic Decomposition of 2-propanol	82
4.2.1 Conditioning Effects	82
4.2.2 Selectivities for Acetone Formation	82
4.2.3 Activation Energies	83
4.2.4 Reaction Rates and Kinetics	86
4.2.5 Reaction Mechanisms	88
4.3 Surface Areas	93
4.4 X-ray Analysis	95
5. CONCLUSION	98
6. SUGGESTIONS FOR FURTHER WORK	98
REFERENCES	99
APPENDIX I	105
APPENDIX II	111

ABSTRACT

The catalytic decomposition of 2-propanol has been investigated in a flow system from 200-300°C on vanadium pentoxide and modified vanadium pentoxide catalysts.

Dehydration, dehydrogenation and propane formation were observed over the temperature range studied. The propane reaction was predominant at higher temperatures.

Kinetic experiments showed the dehydration and dehydrogenation reactions to be zero order with respect to all components while the propane-forming reaction was found to have a rate order of 0.3 with respect to 2-propanol. The kinetics for the reactions were interpreted in terms of the Langmuir-Hinshelwood model and elimination type mechanisms have been proposed to account for the 2-propanol decomposition.

Trends in activity and activation energies for the dehydration reaction have been correlated with the mobility of surface oxygen previously reported in the literature. Some correlations were obtained with activation energies for dehydration reactions in similar systems.

The reduction of the catalysts used, as indicated by changes in surface area and X-ray powder diffraction patterns, has been related to oxygen mobility and to the surface 'Tammann' temperature of the additive.

1. INTRODUCTION

1.1 General

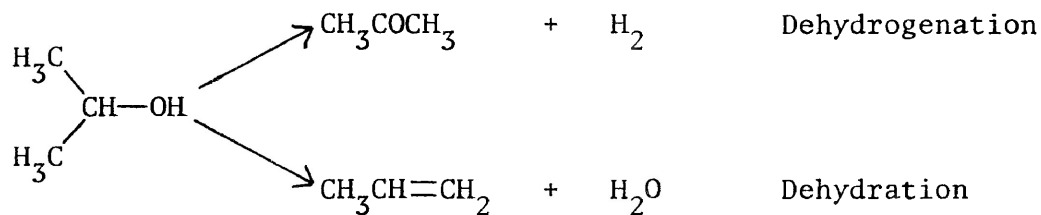
Dehydration and dehydrogenation reactions are the two main reaction paths followed in alcohol decompositions over metal oxide catalysts.

Dehydrogenation of primary alcohols results in aldehyde formation while with secondary alcohols ketones are produced. Dehydration of alcohols generally gives olefins and water (1). At high temperatures (300-600°C) carbon-carbon cleavage may occur yielding paraffins, CO, CO₂ and other cleavage products, whereas at near ambient temperatures the major product is ether (1). More recently it has been shown that these reactions are of a more complex nature and may also involve condensation processes (2).

Numerous studies of the various reactions involved in alcohol decompositions have shown that each type proceeds at specific surface sites which may be subject to activity and selectivity variations through changes in reaction conditions as well as catalyst preparation procedures.

Dehydrogenation is the preferred reaction on metals (3, 4) while on metal oxides both dehydration and dehydrogenation take place (1). Since this study has been focused on the decomposition of 2-propanol on selected metal oxides, selectivity in 2-propanol decomposition is of interest.

The decomposition of 2-propanol serves as a good example for the two contributing processes:



This reaction has often been used as a model for studying the principles of catalyst selection (1).

The various parameters which must be considered when selecting a catalyst have been outlined by Krylov (1).

The rate limiting step for dehydrogenation is believed to be the migration of vacancies whereas for dehydration it is thought to be the migration of free electrons. Thus, in terms of the electronic theory of catalysis, dehydrogenation should take place on "p-type" semiconducting oxides while dehydration should be favoured on "n-type" semiconducting oxides. However, several authors (5,6) have reported conflicting evidence and possible explanations for these discrepancies will be discussed later.

Balandin's "multiplet theory of catalysis" suggested that alcohol decompositions involved a two point adsorption mechanism. Thus the interatomic spacing between surface atoms of the catalyst should affect the decomposition.

Krylov (1) reports that interatomic spacing is more critical for adsorption processes giving rise to dehydration reactions than for adsorption processes involving dehydrogenation reactions. Increasing

crystal lattice parameters would augment dehydration activity while decreasing the crystal lattice parameters aids dehydrogenation.

The majority of catalytic reactions can be classified into two general types, oxidation-reduction (electronic) and acid-base (ionic) (1).

Dehydrogenation reactions fall into the electronic category and should therefore be catalyzed by solids possessing 'free' or easily excited electrons, e.g. metals and semiconductors. The mechanism of catalytic dehydrogenation is usually interpreted as involving the transfer of an electron from the catalyst to the reactant or vice versa (1).

Dehydration reactions belong to the ionic category and should therefore be affected by the nature and preponderance of surface acid or base sites. The mechanism has been reported as proceeding via the transfer of protons or the production of a heteropolar donor-acceptor pair (1).

If catalysis is considered to involve the formation of an adsorbed cyclic intermediate then two-point adsorption of alcohol to electropositive and electronegative surface atoms should occur. Thus, an increase in the metal-oxygen distance would be expected to facilitate dehydrogenation, while a decrease in this distance should facilitate dehydration.

Krylov (1) has also discussed the role of the width of the forbidden zone and specific conductivity of semiconductor catalysts. Thus, the rate of alcohol dehydrogenation would be expected to increase with a decrease in the width of the forbidden zone, while dehydration should not be so affected, since it follows the mechanism of an acid

catalysed reaction rather than an electronic one related to band theory concepts.

Other criteria for explaining the selectivity of oxide catalysts towards dehydrogenation or dehydration have also been considered.

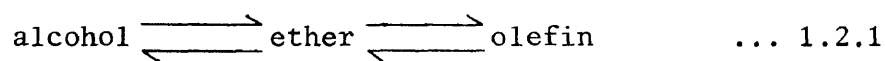
Schwab et.al. (7) proposed that, on alumina, selectivity was not an inherent chemical property but that dehydrogenation occurred mainly on the flat surface of the catalyst whereas dehydration was restricted to sub-microscopical holes, cracks, pores, or channels between particles.

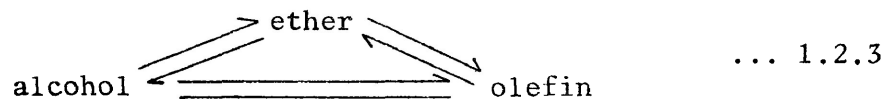
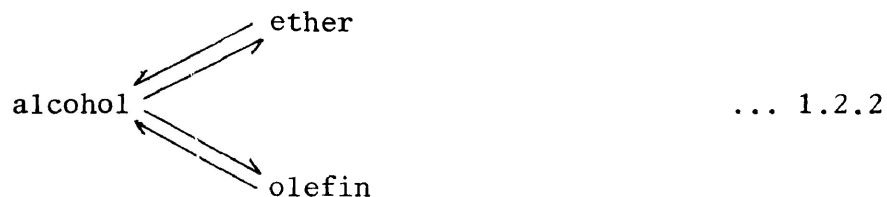
Eucken (8, 9) concluded that dehydrogenation predominated with large oxide cations of low valency and the converse was true for dehydration. It was suggested that when small cations were involved the surface of the oxide consisted mainly of oxygen atoms whereas with larger cations, these were also present on the surface. Thus, dehydrogenation involved adsorption on the metal atoms and dehydration involved adsorption on oxygen atoms.

The mechanisms proposed for the catalytic dehydrogenation and dehydration of alcohols may support or contradict these various hypotheses regarding selectivity.

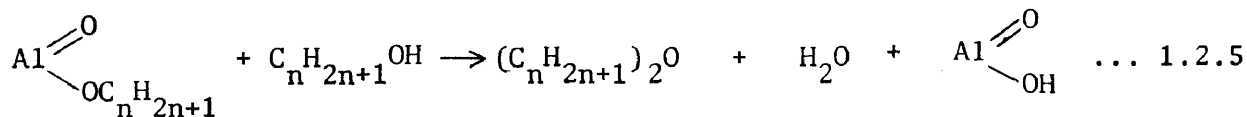
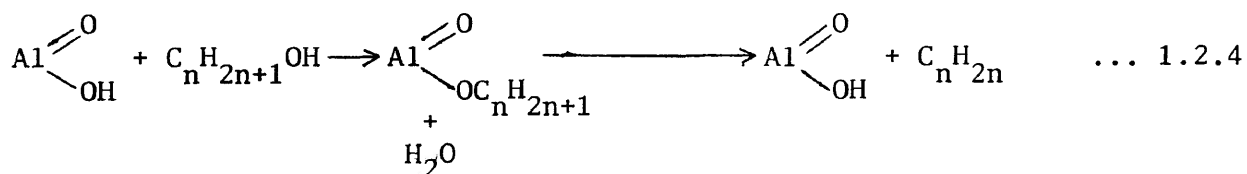
1.2 Dehydration

The dehydration of alcohols to olefins and ethers can result through three possible reaction mechanisms commonly identified (10) as (1) "consecutive", (2) "parallel", or (3) "simultaneous". Thus:





Ipatieff (11) favoured the so called "consecutive" mechanism. From studies of alcohol decomposition on alumina he concluded that the alumina formed a "hydrate-type intermediate". This intermediate could undergo subsequent reaction with another alcohol species to form the corresponding ether, or, if another alcohol species was not available, decompose to the olefin:



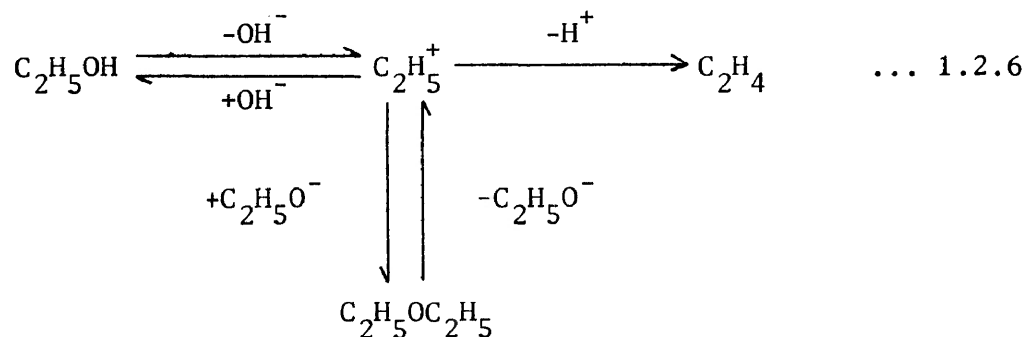
A similar intermediate of the type (Al-O-Et) was proposed by Sabatier (12).

Pease and Yung (13) showed that the dehydration of ethanol to ether was reversible and that water vapour and ethylene vapour

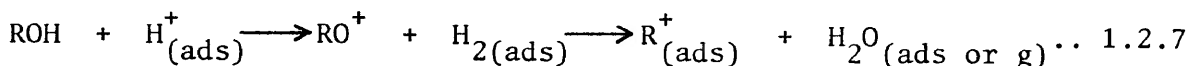
reduced the alcohol dehydrating efficiency of the catalyst. Although the data of Pease and Yung could be accommodated by the "consecutive" mechanism proposed earlier, there were indications that olefin production proceeded directly from the alcohol, rather than through an ether intermediate.

Adkins et.al. (14,15) illustrated the inadequacy of the "consecutive" mechanism from their studies of butyl alcohol dehydration. The butene obtained could not have resulted from an ether intermediate, thus ether need not necessarily be an intermediate for olefin formation.

A "simultaneous" mechanism, involving a carbonium ion intermediate was proposed by Whitmore (16). The carbonium ion may be formed from either the alcohol or the ether and can then react to form either olefin or ether (17). The decomposition of ethanol via this "simultaneous" mechanism is illustrated below.



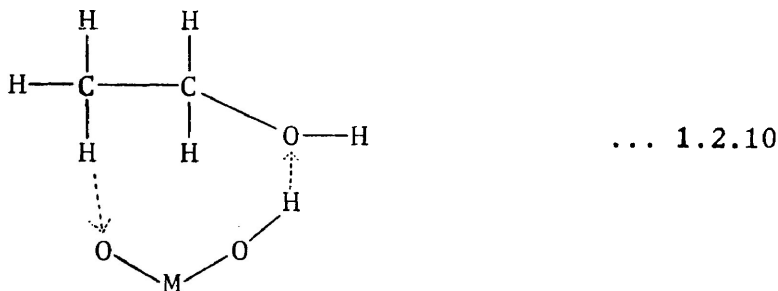
According to Bremner (18) the adsorbed carbonium ion could be formed via an oxonium ion, the conjugate acid, resulting from proton donation from the catalyst to an alcohol molecule.



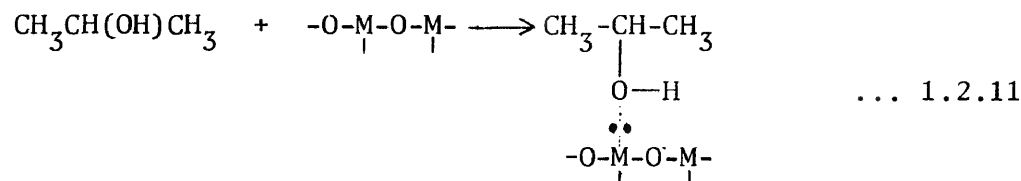
pyridine adsorption may involve proton addition to the nitrogen atom, giving an analog of an oxonium ion, these results were believed to provide indirect evidence in support of the oxonium ion mechanism (20).

From a statistical analysis of published experimental data Krylov (1) suggested that catalytic activity towards dehydration was inversely proportional to the increasing electronegativity difference between anion and cation in the metal oxides which supports the carbonium ion mechanism since acid oxides have small electronegativity differences.

Eucken (8,9) and Wicke (21) reported mechanisms involving a cyclic transition complex:

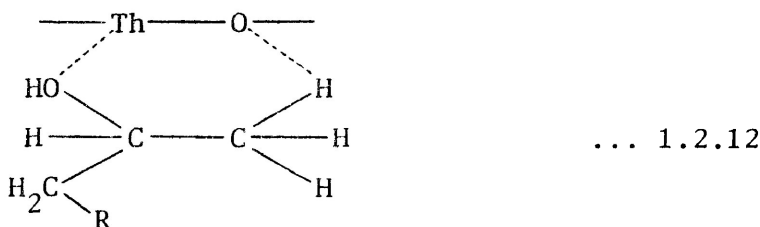


but Krylov (1) has not found any correlation between interatomic distances and catalyst activity towards dehydration reactions. He further suggested (22) that dehydration involved one point adsorption which resulted in the formation of coordinate bonds between Lewis acid sites on the metal atom and the oxygen atom of the alcohol:



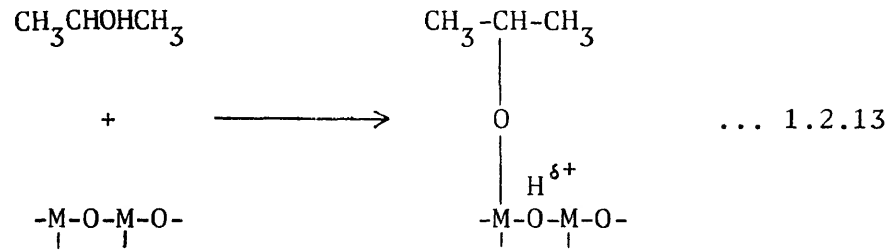
Generally, there is uncertainty as to which atom of the alcohol loses hydrogen in the subsequent dehydration process. In most cases, as predicted by 'Ingold's rule', the elimination occurs trans to the hydroxyl group.

The dehydration of secondary alcohols over ThO_2 , however, gives only α -olefins, while over the oxides of W, Mg, Al, Ti, and Zr, a mixture of α - and β -olefins are obtained (23). There is no clear explanation for the difference between ThO_2 and the other oxides. Perhaps the reactions involving ThO_2 involve the formation of a cyclic complex and thus become an exception to Krylov's single point adsorption concept (1), e.g. :

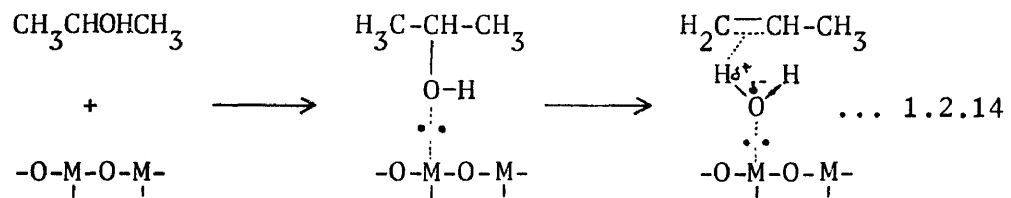


Again, according to Krylov (1), if there is an excess of charge on a surface metal atom (e.g. a "positive free valency"), formation of a strong

bond can occur which impedes catalysis, e.g.:



If this charge was cancelled, however, by the capture of an electron, the number of active centres should increase, e.g.:



Thus alcohol dehydration via a carbonium-oxonium ion mechanism on Lewis acid centres would be enhanced as well.

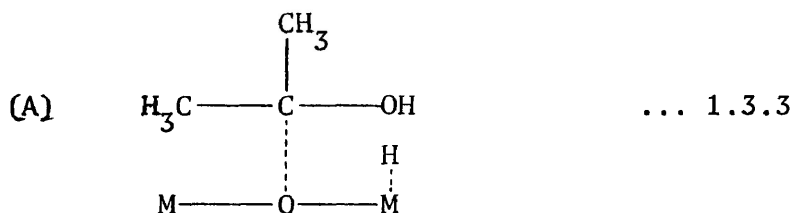
Doping experiments, in which the electronic conductivity of the catalyst was increased, showed that the rate of dehydration increased also (24) and thus it would be expected that "n-type" semiconductors would be more active than "p-type" semiconductors for dehydration.

Krylov (1) concluded that although Brønsted acid sites do participate in dehydration of alcohols, in general, positive centres such as surface "positive free valencies" on metal ions contribute most to the catalytic activity.

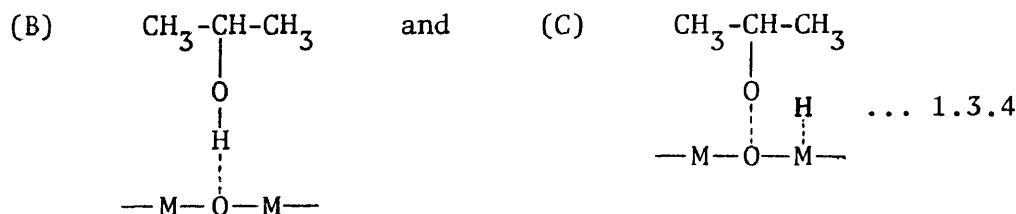
discussed in terms of Balandin's "Multiplet Theory of Catalysis".

Balandin (28) concluded that dehydrogenation on metal oxides resulted from interactions with metal atoms, but participation of the oxygen atoms was not entirely ruled out. Krylov (22), however, reported that the electronegative surface atom was responsible for interactions leading to dehydrogenation. This conclusion was based on the high catalytic activity of bases (29), the increased value of ΔH_{ads} for 2-propanol and acetone when oxygen was preadsorbed (30) and also from spectroscopic studies (31).

The most probable type of adsorption leading to dehydrogenation, may involve the alcohol attachment through a carbon atom to a surface anion, e.g. (22)



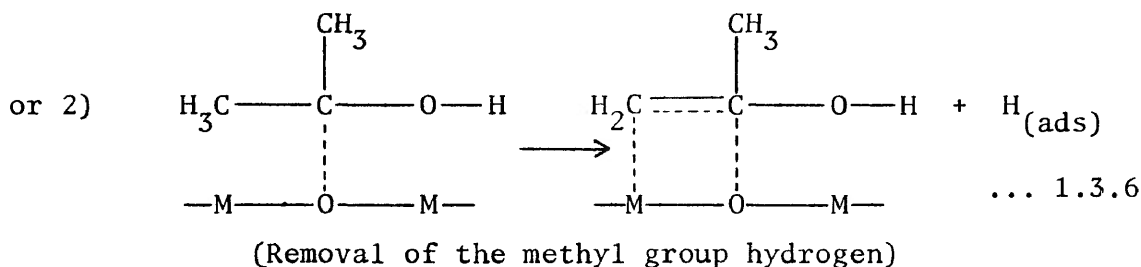
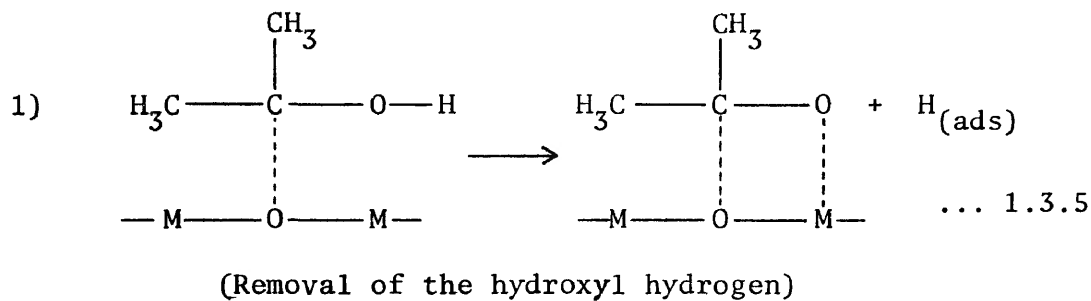
Two other suggested forms:



are not favoured since they would not lead to dehydrogenation, or, as

in the case of (C) there is no experimental evidence indicating that they are formed (22). Type (B) adsorption has been observed on NiO and ZnO but does not lead to dehydrogenation (22). A transition from (B) type to (A) type adsorption may account for the strengthening of the alcohol-oxide bond (22) as observed by Keier (32) in thermodesorption studies of adsorbed ethanol on ZnO.

Once type (A) adsorption has occurred the reaction can then proceed via the formation of a cyclic complex which results in the loss of the second hydrogen. There are two possible mechanisms for this process (22):



The preferred pathway has yet to be determined. Although complexes of the type produced in 1) have been observed on alumina, they were very stable and did not lead to dehydrogenation (31). Schwab and Wandinger (33) have reported evidence in favour of a reaction via path 2). Their study of the dehydrogenation of $\text{CH}_3\text{CD}_2\text{OH}$ and $\text{CH}_3\text{CH}_2\text{OD}$ showed

that hydrogen was removed from methyl, methylene and hydroxyl groups.

Dehydrogenation is not inhibited by the addition of hydrogen, but there is considerable controversy as to the effect of the addition of acetone on the reaction rate. In a 'static' flow system the addition of acetone strongly inhibited the initial reaction rate which indicated that the rate-determining step was the dehydrogenation of the alcohol in the adsorbed phase (34). However, it has also been reported that acetone did not inhibit the dehydrogenation of 2-propanol over an "aged" zinc oxide catalyst (35). From a study of 2-propanol dehydrogenation over NiO the desorption of acetone was shown to be the rate-determining step (36).

In recent work in these laboratories it was concluded that the rate-controlling step in both dehydration and dehydrogenation reactions over a series of oxides was either the adsorption of 2-propanol or the reaction of the adsorbed alcohol (37, 38). It was shown further that the decomposition of 2-propanol over manganese (II) oxide was more complex than had been previously reported in that condensation reactions were also possible (37).

Some of the conflicting results can be interpreted in terms of the effects of surface oxygen (30, 38, 39). Gale et.al. (30) suggested that preadsorbed oxygen may activate acetone to form a chemisorbed species. The oxygen would, in effect, decrease the activation energy for acetone adsorption and hence the desorption of acetone, which agrees with the view that acetone desorption is the rate-determining step in 2-propanol dehydrogenation over nickel oxide (36).

McCaffrey et.al. (38, 39) also reported relationships between

oxygen content and mobility of surface oxygen with the catalytic activity of various metal oxides. In general, the selectivity for dehydrogenation increased with increasing oxygen content (39).

1.4 Modified Metal Oxide Catalysts

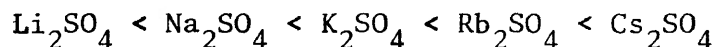
Several studies have been made on the effects of added impurities, on the activity of metal oxide catalysts towards alcohol decomposition (36, 40, 41) and it has been reported that additives which increased "p-type" semiconductivity also increased dehydrogenation activity, while those which increased "n-type" semiconductivity, have the reverse activity effect. However, with zinc oxide ("n-type") increasing the "n-type" character (i.e. increasing the "free" electron concentration) also increased the rate of dehydrogenation (42, 43). Other studies have also indicated that maxima and minima exist in relationships between the rate of dehydrogenation and the concentration of additives in zinc oxide (44, 45, 46).

Deren et.al. (47) studied the effects of lithium oxide doping of zinc oxide on the semiconductivity and rates of dehydrogenation of 2-propanol (at approximately 1 atom % lithium, semiconductivity reversed from "n" to "p-type") and found that the maximum activity corresponded to a maximum value in the electrical conductivity. It was shown that initially a lowering of the Fermi level caused an increase in the rate of dehydrogenation (a donor reaction) to a maximum. The rate then decreased with a further shift in the Fermi level towards the valence band (an acceptor reaction). Consequently dehydrogenation can be regarded as either an 'acceptor' or 'donor' reaction depending on the position of the Fermi level .

The introduction of additives has been discussed so far in terms of effects on conductivity and the electronic nature of the catalyst, however, other factors may contribute to the changes produced.

Boreskov (48) reported that the presence of alkali metal sulphates in vanadium pentoxide catalysts, used in sulphuric acid production, had a pronounced effect on catalytic activity. Similarly, Bibin and Kasatkina (49) found that the addition of alkali metal sulphates to vanadium pentoxide promoted exchange between molecular oxygen and the oxygen of vanadium pentoxide. The effects on catalyst activity were attributed to changes in mobility of the oxygen in the pentoxide (49, 50, 51, 52).

The promoting action for oxygen exchange (49,50) was found to be:



and studies of the catalytic oxidation of sulphur dioxide showed similar trends (53).

1.5 Objective of the Present Investigation

From the above survey, it is apparent that the mechanism of the heterogeneous decomposition of 2-propanol is still not well understood. Much of the previous work has been concerned with the effects of electronic and lattice factors and quite often the data obtained have been confusing and contradictory.

The effect of oxygen mobility on the decomposition of 2-propanol has only recently received limited study. Thus, McCaffrey

et.al. (38, 39) have proposed relationships between the catalytic activity of alkaline earth oxides in 2-propanol decomposition and both the mobility of surface oxygen and non-stoichiometric oxygen content. Since the addition of alkali metal sulphates to vanadium pentoxide has been shown to affect surface oxygen mobility, the decomposition of 2-propanol over modified vanadium pentoxide was investigated primarily in an attempt to gain further information on these effects.

2. EXPERIMENTAL

2.1 General

The investigation of kinetic parameters, such as reaction rate and factors influencing the reaction rate, is of prime importance to catalytic research. Generally, kinetic data are used to develop rate equations which are consistent with observations of the reaction mechanism.

Kinetic studies are mainly concerned with the slower reaction steps, since these are rate-determining, and thus it is not always possible to obtain a complete description of a catalytic reaction from kinetic measurements alone. Frequently, different kinetic methods are used to study a catalytic reaction. The major methods, the 'static' method, the 'plug-type flow' method, and the 'pulse' method employ different types of reactors and to some extent differ in the type of information obtained (54).

The 'static' reactor system was one of the earliest used to study catalytic reactions (55, 56). The reactants were introduced into a constant volume reactor at the start of an experiment and then the system was closed. The rate was followed by changes in concentration or pressure. 'Static' reactors are seldom used today because of the many experimental uncertainties involved with the technique.

The two other principal methods are variations of flow techniques. They differ in that the 'plug-type flow' method operates under steady-state conditions whereas the 'pulse' method operates under

non-steady state conditions.

In the 'plug-type flow' system a mixture of reactants, often diluted by a carrier gas, is passed continuously, at a known rate of flow, through a reaction vessel containing the catalyst to be studied (57). The reaction products and unreacted starting materials are continuously removed from the system for analysis.

These systems are generally in conditions where the catalyst has attained 'steady-state activity'. Reaction rates and activities are then determined after this condition has been established. The steady state situation is achieved by passing the reactant gas(es) over the catalyst for a period of time, which depends on the particular catalyst. Reaching steady-state activity, however, creates one of the inherent problems of this method—the chemical and physical nature of the catalyst after conditioning. For example, Balandin and co-workers (58, 59) have shown that during alcohol decompositions on transition metal oxides the conditioning period caused reduction and in some cases carbonization of many catalysts.

The 'pulse' method utilizes a fixed bed reactor with a continuously flowing carrier gas stream. In contrast to the "plug-type flow" method the catalyst is not continuously exposed to the reactants but to a micro quantity of reactant(s) (a pulse) injected into the carrier gas stream (60). The carrier gas removes products and unreacted starting material from the system for analysis. This method makes it possible to study the process of 'conditioning' by pretreating with reactants under non-steady state conditions. However, the non-steady state condition usually does not allow rate data to be obtained, which

is a major disadvantage.

2.2 Flow System

High purity helium (>99.99%) was passed through a molecular sieve (Davison, Grade 564) drying column, which also acted as a pressure stabilizer, into a common junction, see Figure 2.2.1. Flow rates were maintained using 'Matheson Rotameters' fitted with 'Matheson Millimite' fine-control needle valves. In addition, lines (a), (b), and (c) contained differential-pressure capillary flow meters, filled with di-n-butyl phthalate as the manometric liquid, in series with the rotameters. This ensured accurate flow measurements as the rotameters tended to stick occasionally due to static charge build up created by the dry helium passing through the glass rotameter tubes. The rotameters and differential flow meters were calibrated, for the gas used, with a soap bubble burette.

From the differential flow meter in line (a) the helium passed through an alcohol saturator. The alcohol-saturated helium was channeled into a common manifold where it was allowed to mix with helium carrier gas and other reactants, depending on the experimental requirements. The reaction mixture next entered a preheater which raised the temperature of the gas stream close to that of the reaction. The stream was then directed through the reactor where it contacted the catalyst.

The reaction products were conducted from the reactor through heated lines and sampled periodically, by means of a gas sampling valve, and fed into a gas chromatograph for analysis. The remainder of the reaction products were vented to a fume hood.

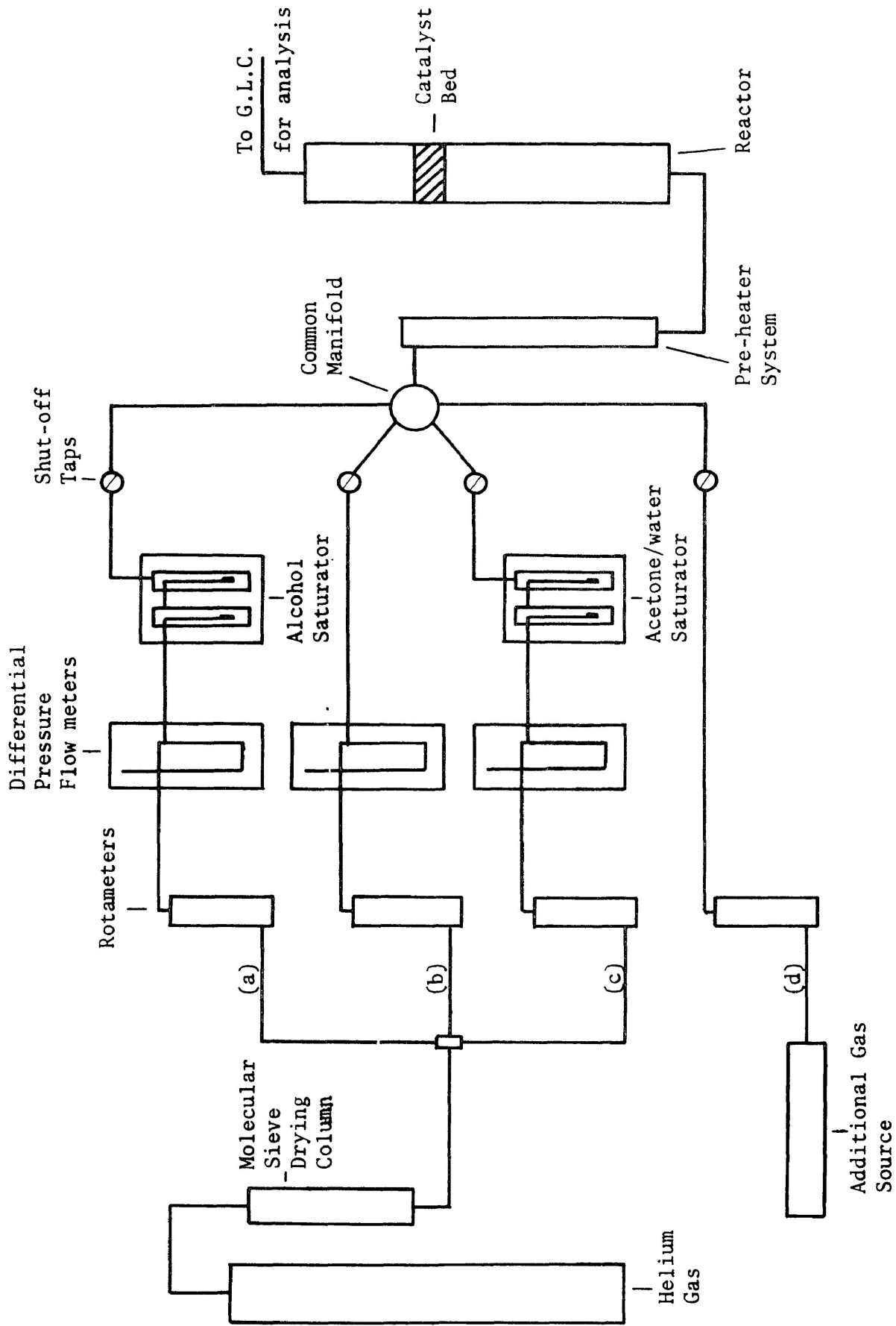


Figure 2.2.1 Flow System

Flow line (b), Figure 2.2.1, was used for the addition of pure helium carrier gas to maintain a constant total flow of 300 ml. min⁻¹ (NTP) in the system. Lines (c) and (d) were used in studies of the effects of the addition of acetone, water, propylene, propane and hydrogen on catalysis. All gas streams could be mixed in desired proportions in the common manifold prior to entry into the preheater.

The alcohol saturator was maintained at a constant temperature by means of a water bath equipped with a 'Braun Thermomix II' circulatory heater which maintained the temperature at 17.4[±] 0.05°C. The partial pressure of alcohol fed into the gas stream was controlled by varying the flow of helium through the saturator. The saturator efficiency, with respect to saturation by alcohol vapour, was checked by weighing the amount of alcohol removed and delivered to a cold trap in separate experiments. The amount collected at a flow rate of 100 ml. min⁻¹ (NTP) through the saturator, when compared to the amount theoretically present, assuming complete saturation, corresponded to a saturator efficiency of 98.7%. Unless otherwise stated, the flow through the alcohol saturator was maintained at 100 ml. min⁻¹ (NTP).

Since it was necessary in some experiments to vary the flow through the alcohol saturator the effect of flow rate on saturator efficiency was also examined. The efficiency was found to deviate by less than 1% when the flow was varied between 40 ml. min⁻¹ and 120 ml. min⁻¹ (NTP). The efficiency of the acetone/water saturator was determined in a similar manner and values of 99.5% for acetone and 96.8% for water were observed.

Prior to use, saturator liquids were degased for 30 minutes

by purging with dry helium. The shut-off taps, Figure 2.2.1, were then opened and the gas stream was allowed to enter the common manifold.

The catalytic reactor was constructed from 20 mm. I.D. quartz tubing and had an overall length of 58 cm. with B24/40 ground joints at each end. The catalyst samples were sandwiched between quartz wool plugs supported on three dimples in the reactor wall 32 cm. from the entry port of the reactor.

The reactor was resistance heated by 5.14 m. of Chromel A resistance wire ($5.45 \text{ ohms. m}^{-1}$) uniformly and non-inductively wound in grooves in the quartz tube. The tube was then covered with asbestos tape to a thickness of 1.5 cm. giving an outside diameter of 7 cm. The reactor was finally wrapped tightly with several layers of aluminum foil.

Reactor temperatures were monitored by a chromel/alumel thermocouple, positioned in a thermometer well 5 mm. above the catalyst bed, and controlled to within $\pm 0.2^{\circ}\text{C}$ with a 'Thermo Electric 400' indicating controller. A variable resistance was connected in series with the resistance element of the reactor and adjusted with temperature in order to eliminate slow cycling. All of the inter-connecting lines from the outlets of the saturators to the inlet of the gas chromatograph were tightly wound with thermal tape and maintained at a temperature of not less than 120°C in order to avoid condensation of vapour from the gas stream.

Blank run experiments, in which 2-propanol was passed through the reactor containing quartz wool plugs, indicated no catalysis on the reactor walls or plugs in the range from 150° to 350°C .

2.3 Analysis

The gas stream containing reaction products was analyzed using a dual column 'Hewlett Packard Research Chromatograph Model 5750' with flame ionization and thermal conductivity detectors. Samples were injected via a temperature controlled dual-loop gas sampling valve which was maintained at 195°C. The analytical columns were constructed from 1.5 m. of 0.32 cm. O.D. stainless steel tubing packed with 'Porapak Q' (150-200 mesh).

Prior to each injection the column oven was maintained at 100°C. The temperature was held for a post-injection interval of 4 minutes which allowed water, propylene and propane to be eluted. The column oven was then heated by linear-temperature programming at 20°C. min⁻¹ to a maximum of 140°C. The columns were maintained at this upper limit for 7 minutes. During this period, acetone and 2-propanol were eluted. The column oven was then recycled to 100°C. With the chromatograph programmed in this manner the gas stream could be sampled every 15 minutes.

A helium flow of 30 ml. min⁻¹ (NTP) was passed through the columns. Compressed air and pure hydrogen (99.9%), with flow rates of 300 ml. min⁻¹ and 30 ml. min⁻¹ (NTP) respectively, were used as a source for the jet flame of the ionization detector. In addition a 'make-up' gas stream of 40 ml. min⁻¹ (NTP) helium was passed through the flame detector.

The flame detector oven was maintained at 175°C. The oven containing the thermal conductivity detector was maintained at 200°C with a current of 245 mA passing through the detector filaments.

The detector amplifiers were adjusted where necessary to enable the peaks of the individual components to remain on the recorder scale. The chromatograms were recorded on a dual pen Linear Instruments 10" Strip Chart recorder.

Table 2.3.1 gives the retention times for the reaction components using the 'Porapak Q' (150-200 mesh) column. Figures 2.3.1 and 2.3.2 show the chromatograms for the flame ionization and conductivity detectors, respectively. Peak areas of the individual components were used in quantitative estimations and these areas were determined from the print-outs by a planimeter.

Table 2.3.1

Retention times for reaction components using a "Porapak Q" (150-200 mesh) column.

Reaction Component	Retention Time (min)
Water	2.00
Propylene	3.47
Propane	3.85
Acetone	11.55
2-propanol	12.30

Detectors were calibrated for concentrations of gaseous components by the exponential dilution method (61). This method involves the injection of a gas sample into a mixing vessel of known volume with a constant flow of helium passing through it. If at time, $t=0$, the initial concentration of the injected sample was C_0 then at any

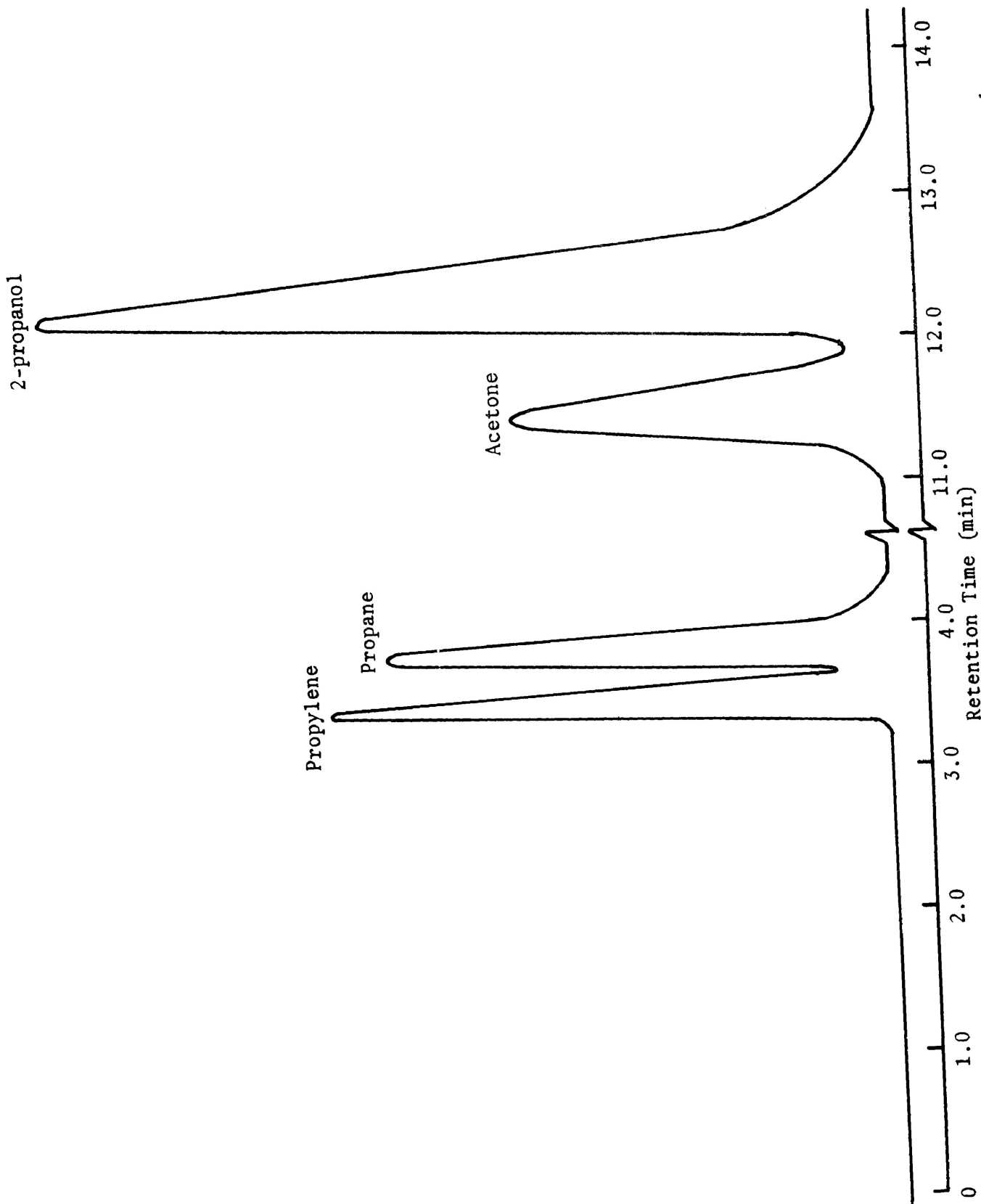


Figure 2.3.1 Typical Flame Ionization chromatogram for decomposition of 2-propanol

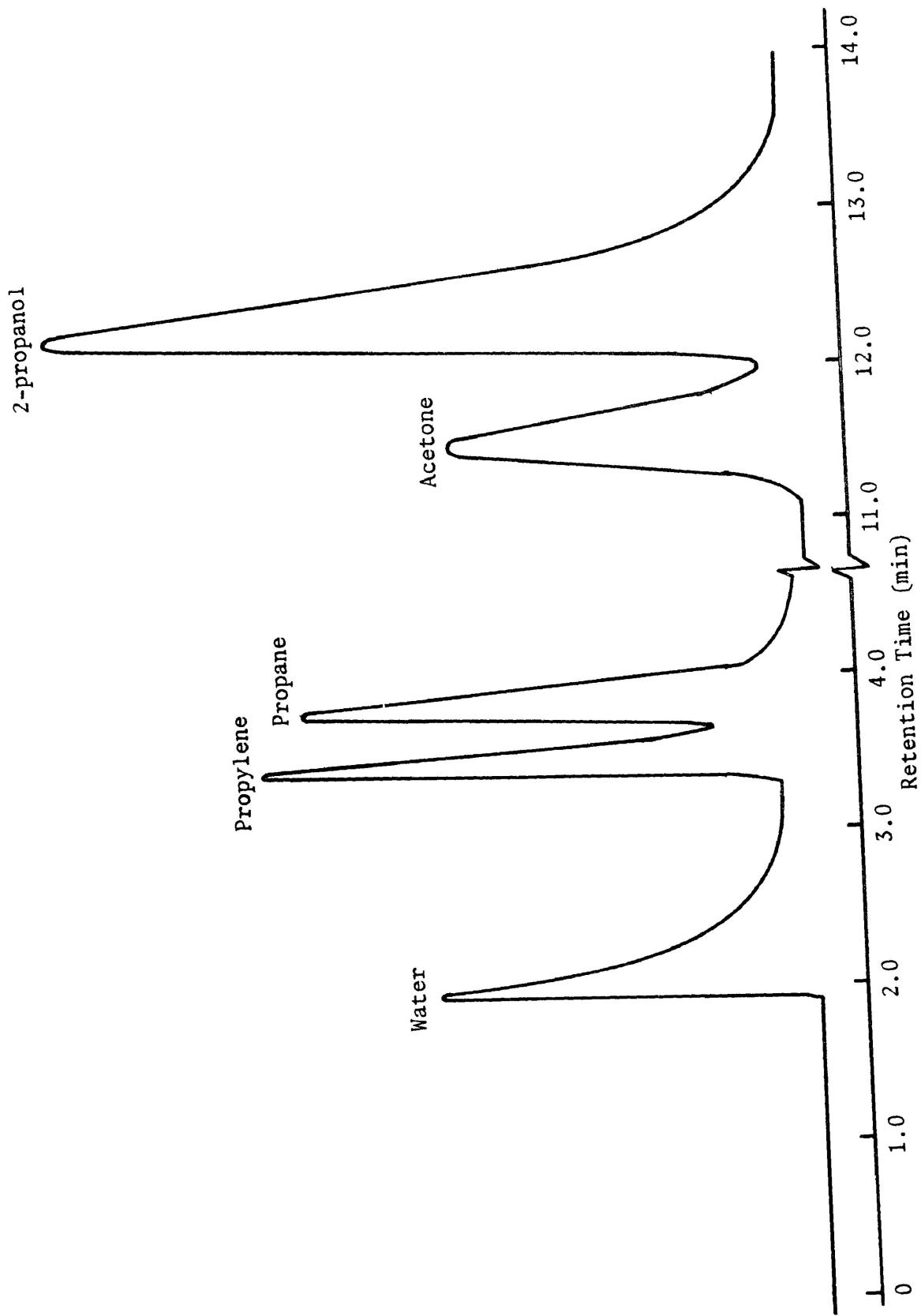


Figure 2.3.2 Typical Thermal Conductivity Chromatogram for decomposition of 2-propanol

time, t , the concentration, C_t , of the gas can be calculated using the equation:

$$C_t = C_o \cdot \exp^{-(F/V) \cdot t} \quad \dots 2.3.1$$

where F is the flow of helium through the vessel and V is the volume of the mixing vessel. At various times the helium stream from the vessel was sampled via the gas sampling loop of the chromatograph and calibration curves of peak area against partial pressure were constructed as illustrated in Figure 2.3.3.

Calibration for the vapours, such as alcohol, acetone, and water, was carried out by varying flow rates through the appropriate saturator, see Figure 2.2.1, at a fixed temperature and calculating the concentration of vapour which should be present in the gas stream. A sample of the gas stream was analyzed via the gas sampling loop of the chromatograph. Calibration curves of peak area against partial pressure were constructed, see Figure 2.3.4. The accuracy of this method was confirmed by injecting known amounts of the liquids into the chromatograph by 'Hamilton micro-syringes' fitted with Chaney adapters.

2.4 Surface Area Measurements

Surface area determinations involved the measurement of the amount of gas necessary to form a monomolecular layer on the solid surfaces. From the number of molecules adsorbed and the area occupied by each molecule the surface area of the material can be determined.

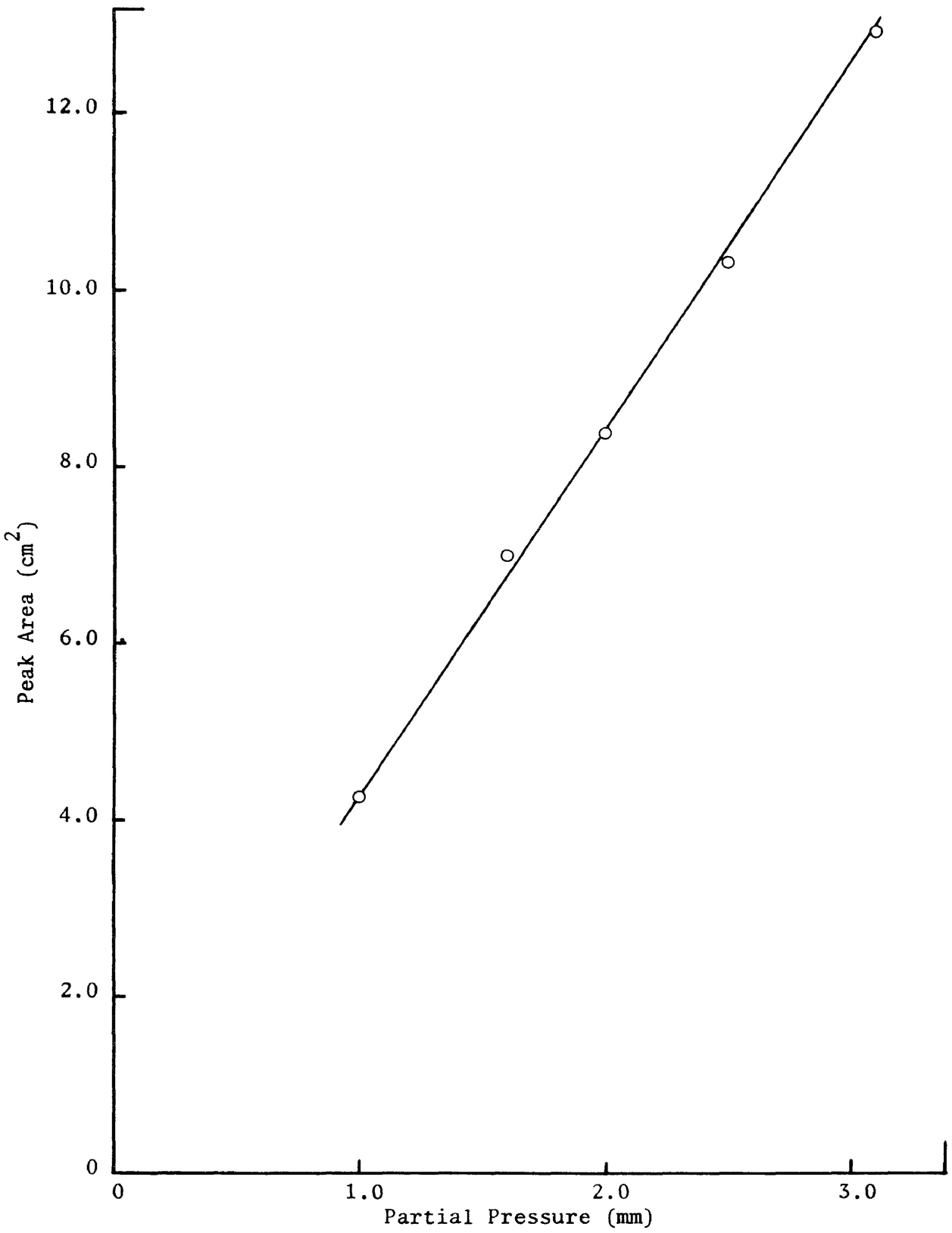


Figure 2.3.3 Peak Area vs. Partial Pressure of propylene for Flame Ionization Detector sensitivity of 3200

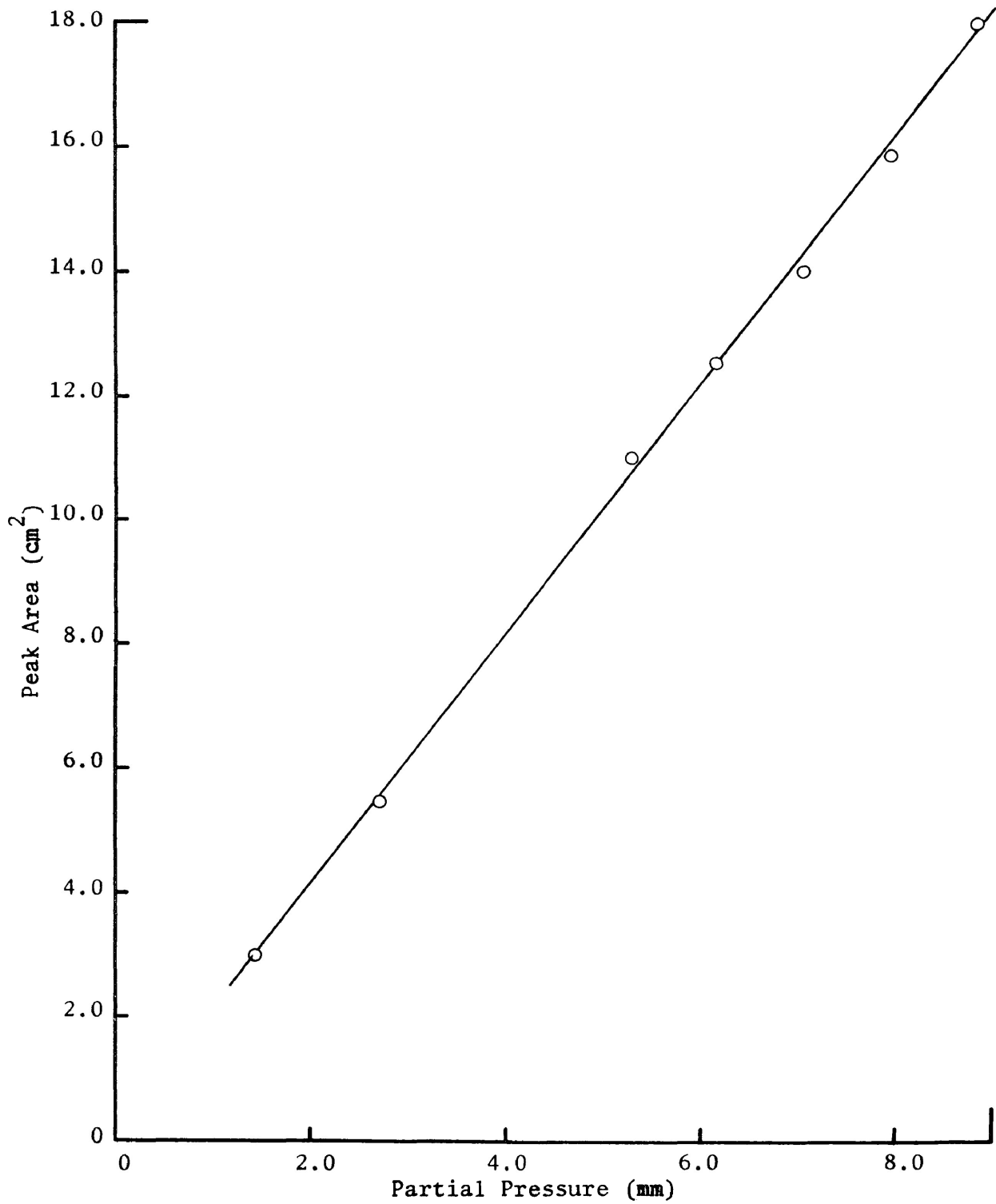


Figure 2.3.4 Peak Area vs. Partial Pressure of 2-propanol for Flame Ionization Detector sensitivity of 3200

This technique has been widely used and gives very dependable results for relative surface area values (62).

Brunauer, Emmett and Teller (63) derived the following general equation relating the monolayer volume (V_m) at saturation pressure of the adsorbate gas (P_o) to the total volume of gas adsorbed (V) at a measured pressure (P), thus:

$$\frac{P}{V(P_o - P)} = \frac{1}{V_m C} + \frac{(C-1)P}{V_m \cdot C \cdot P_o} \quad \dots 2.4.1$$

where C is a constant related to the heats of adsorption and liquefaction of the gas.

A plot of $P/\Sigma V(P_o - P)$ against P/P_o gives a straight line of slope $(C-1)/V_m C$ and intercept $1/V_m C$ valid for relative pressures, P/P_o , between 0.05 and 0.35 (64).

The relatively small surface areas of the oxides, 0.36 to 12.7 $m^2 \cdot g^{-1}$, used in this work permitted the use of krypton as the adsorbate (65). The apparatus is shown in Figure 2.4.1.

Approximately 10 mg. of sample was weighed into the sample tube which was then positioned on the apparatus and evacuated at 10^{-4} Torr for 12 hours at $100^\circ C$. Krypton was then admitted to volume V_a , see Figure 2.4.1, and the pressure measured on the McLeod gauge. The gas was then expanded into the sample tube which was immersed in liquid nitrogen. After equilibrium was achieved, approximately 30 minutes,

The pressure was again measured and the volume of krypton adsorbed was calculated in the usual way (66) utilizing the computer programme 'KRBET' (see Appendix I).

2.5 X-ray Analysis

The catalysts in this work were analyzed by x-ray powder diffraction techniques before and after use in the reactor.

The finely ground powders were sealed in capillary tubes and diffraction patterns obtained using a Philipps X-ray Generator, operating at 40 kV and 20 mA, using a nickel-filtered, copper-K α radiation source, equipped with a 114.83 mm. Debye-Scherrer camera. The diffracted x-rays were recorded on strips of photographic film to give the familiar powder photographs of lines of varying intensities. By measurement of the lines, since the radius of the camera and the wavelength (λ) of the x-rays are known, the interplanar spacings were calculated and the sample identified by comparison with standards in the usual fashion (67).

2.6 Catalyst Preparation

The catalysts used were vanadium pentoxide and a series of vanadium pentoxide melts containing, individually, 9.09 mole percent of the sulphates of lithium, sodium, potassium, rubidium and cesium. In addition a series of catalysts containing 1.01, 2.00 and 4.98 mole percent potassium sulphate were prepared.

Vanadium pentoxide (>99.9% pure) and the alkali metal sulphates (>99.9% pure) were obtained from Ventron and were used without any further purification. The melts containing the alkali metal sulphates were prepared (49) by mixing vanadium pentoxide powder and the correspond-

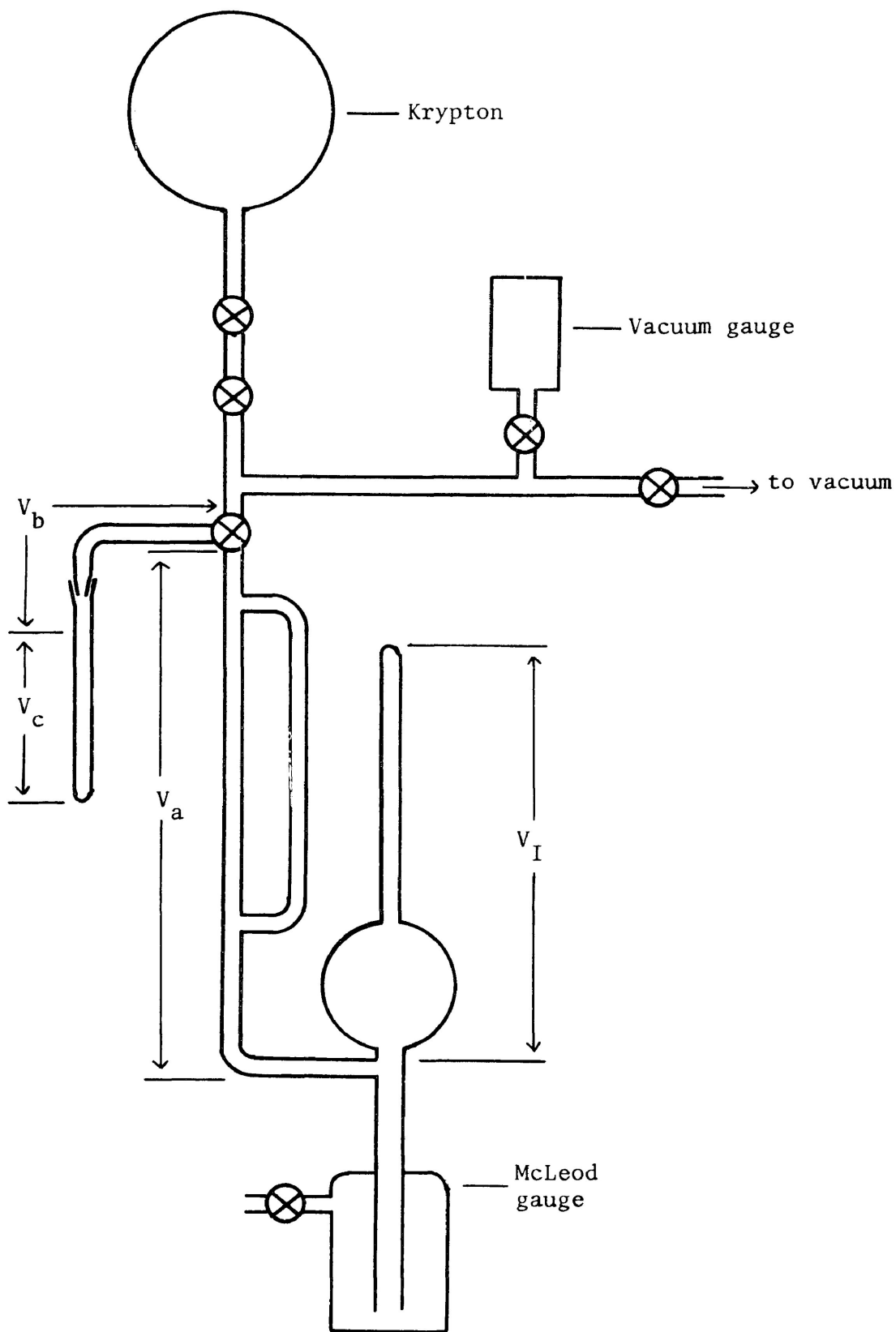


Figure 2.4.1 Krypton BET apparatus; $V_a = 13.6$ ml, $V_b = 1.855$ ml, $V_c = 0.865$ ml, $V_I = 47.37$ ml.

ing weight of the appropriate sulphate additive in a 'ball mill' for 2 hours. This mixture was placed in a quartz dish and heated at 720°C for 4 hours. The liquid melts were cooled rapidly, ground, and pelletized in a 1.27 cm. die at a ram pressure of 3 tons for 2 minutes. These pellets and pellets of pure vanadium pentoxide, prepared in the same manner, were calcined at 520°C for 10 hours with the exception of the cesium and rubidium sulphate melts which were calcined at 430°C. The pellets were crushed, and sieved material with a particle diameter between 0.063 and 0.074 mm. used for the catalytic studies.

2.7 Reagents

"Spectranalyzed" grade 2-propanol and acetone were supplied by Fisher Scientific.

Certified grade helium (>99.99 %), hydrogen (99.9%) and compressed air were supplied by Canadian Liquid Air Limited.

Instrument Grade propane (99.5%) and C.P. Grade propylene (99.0%) were obtained from Canadian Liquid Air Limited.

3. RESULTS

3.1 Tests for Diffusion

In heterogeneous processes the transport of species "through the gas phase to or from the catalyst surface" is dependent on conditions of temperature, pressure and gas flow (68). More specifically, when transport phenomena such as flow, diffusion or convection are such that they control the rate of the reaction then the contributions of 'intrinsic chemical properties' of the surface reaction may be obscured (69,70).

Catalytic reactions which are chemically controlled (i.e. independent of transport phenomena) can be interpreted using the Arrhenius equation:

$$k = A \exp (-E_a/RT) \qquad \dots 3.1.1$$

where k is the rate constant, A, the 'pre-exponential factor' and, E_a, the activation energy. For chemically controlled reactions the activation energy is usually greater than 10 kcal.mole⁻¹ (71). In the case of diffusion controlled reactions the estimation of activation energies becomes more complex and values in the range of 2-4 kcal.mole⁻¹ are frequently observed for diffusion processes (71). The evaluation of transport effects, therefore, is important in any catalytic investigation.

Tests for gas phase diffusion normally involve examination

of the effects of varying flow rate (72) and particle size (72, 73).

Preliminary investigations of the catalysts used in this work indicated that the melt containing 9.09 mole percent potassium sulphate was the most active catalyst and it was used as a standard for diffusion tests and also in detailed kinetic studies.

3.1.1 Flow Rate Effects

The effect of varying flow rates, or space velocities, on 2-propanol decomposition was examined in order to establish a range of flow rates within which 'intrinsic chemical activity' would be observed. In these experiments the catalyst temperature and partial pressure of 2-propanol from the saturator were kept constant. The helium flow rate was the only variable from 150 to 400 ml.min⁻¹ (NTP). The flow effects were studied at 230^o and 300^oC. In each experiment 1 g. of catalyst (V₂O₅:9.09%K₂SO₄, particle size 0.063 to 0.074 mm.) was placed in the reactor. The alcohol saturator was kept at 17.4±0.05^oC and a partial pressure of 8.84 mm. 2-propanol maintained.

Prior to each experiment the catalyst was conditioned for 24 hours in order to bring the system to a steady state, see section 3.2.1. For each flow rate 4 successive samples were analyzed over a 1 hour period.

The effects of varying flows on the rates, r_1 = rate of acetone formation; r_2 = rate of propylene formation; r_3 = rate of propane formation and r_4 = overall rate of 2-propanol decomposition, and product formation are shown in Figures 3.1.1 and 3.1.2 for reactor temperatures of 230^o and 300^oC respectively. Figure 3.1.1 shows that at 230^oC the overall and component reaction rates were unaffected by changes in flow

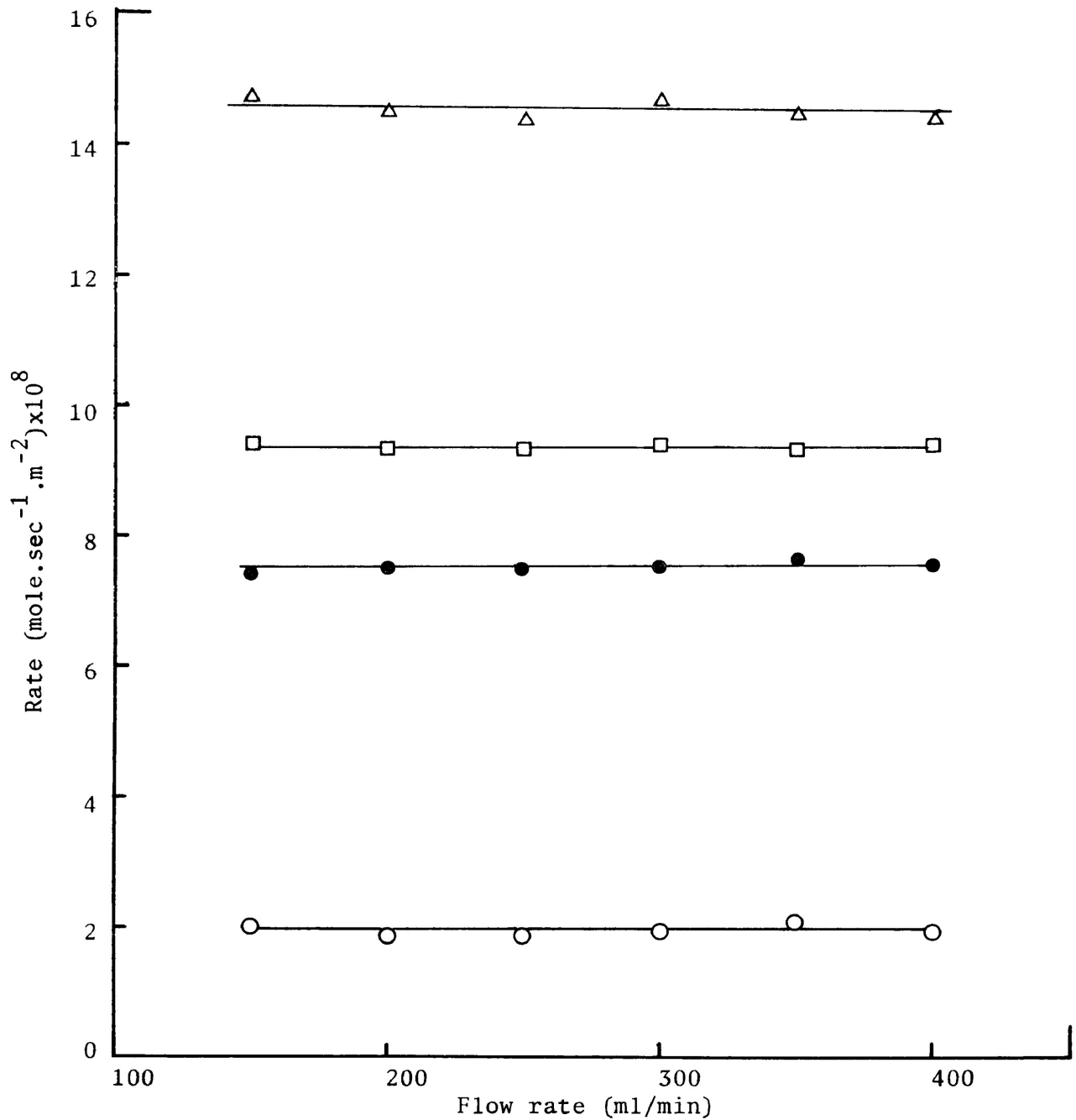


Figure 3.1.1 The effect of flow rate on the rates of: acetone formation \square, r_1 ; propylene formation \circ, r_2 ; propane formation \triangle, r_3 and 2-propanol consumption \bullet, r_4 , over $V_2O_5:9.09\%K_2SO_4$ using 8.84 mm alcohol partial pressure at $230^\circ C$.

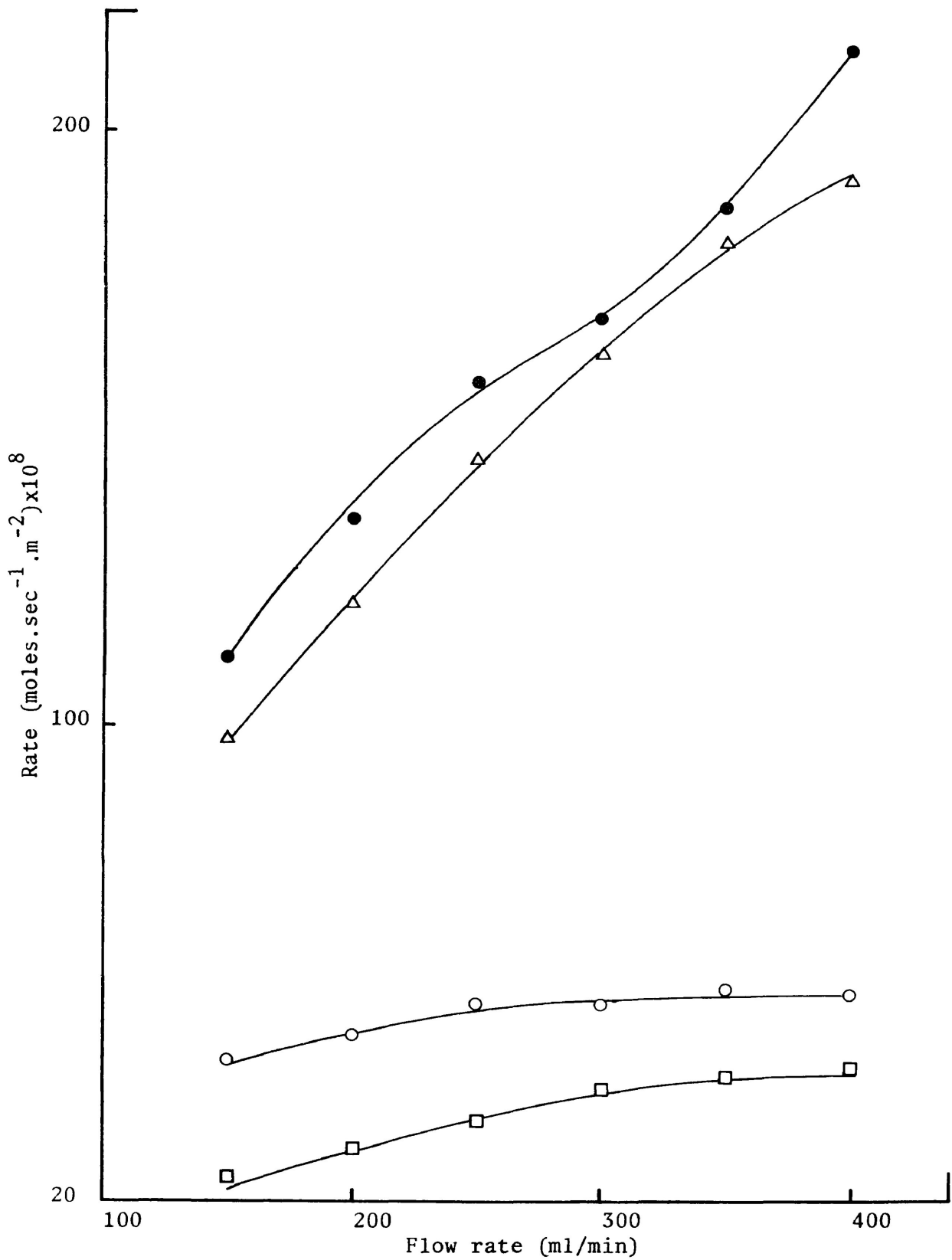


Figure 3.1.2 The effect of flow rate on the rates of: acetone formation \square , r_1 ; propylene formation \circ , r_2 ; propane formation \triangle , r_3 and 2-propanol consumption \bullet , r_4 , over $V_2O_5:9.09\%K_2SO_4$ using 8.84 mm alcohol partial pressure at $300^\circ C$.

rate, while Figure 3.1.2 indicates that at 300°C reaction rates increase with increase in flow rate. The reaction rates for formation of propylene and acetone show a fair tendency to level at $\sim 300 \text{ ml. min}^{-1}$ (NTP) at the higher temperature. However, the overall rate of reaction is still climbing at this flow rate as a consequence of the increase in the rate of formation of propane. Thus it appears that the latter rate may be subject to transport influences in these conditions and hence all subsequent experiments concerned with the evaluation of chemical kinetic features were carried out at lower temperatures with a flow rate of 300 ml. min^{-1} (NTP).

3.1.2 The Effect of Particle Size

The effect of varying particle size on the reaction rates was examined at 230°C and 300°C using 1 g. of catalyst (V_2O_5 :9.09% K_2SO_4) and a partial pressure of 8.84 mm. 2-propanol. The rates were found to be independent of particle size at both temperatures, see Table 3.1.1.

Table 3.1.1 Effect of particle size on the reaction rates: r_1 , acetone formation; r_2 , propylene formation and r_3 , propane formation.

Particle size range (mm)	Rates at 230°C (moles.sec ⁻¹ .m ⁻²)x10 ⁸			Rates at 300°C (moles.sec ⁻¹ .m ⁻²)x10 ⁸		
	r_1	r_2	r_3	r_1	r_2	r_3
0.088 - 0.105	9.38	1.93	14.45	35.91	63.24	145.33
0.074 - 0.088	9.42	1.94	14.30	35.87	63.01	147.19
0.063 - 0.074	9.40	1.94	14.56	35.90	63.08	147.20
< 0.063	9.42	1.96	14.80	35.85	63.15	148.60

In all further experiments a particle size range from 0.063 to 0.074 mm. was used.

3.2 The Catalytic Decomposition of 2-propanol

3.2.1 The Effect of Exposure Time on the Reaction Components

The effect of time on the decomposition of 2-propanol over the catalyst containing 9.09 mole percent potassium sulphate, at 300°C with 8.84 mm. alcohol partial pressure, is shown in Figure 3.2.1.

Initially the alcohol concentration dropped very quickly but reached a steady level after approximately 12 hours. The acetone production increased slowly while the propane increased at a faster rate. Propylene formation increased very rapidly but fell off quickly with time. The rate of decrease in propylene was in close step with the rate of increase of propane, see Figure 3.2.1.

In all experiments thereafter the catalysts were exposed to 8.84 mm. 2-propanol for 24 hours at 300°C before commencing a run. The lengthy conditioning period ensured that catalyst samples had reached a steady state activity. Results on all catalyst samples were reproducible for at least 12 hours after the conditioning period.

3.2.2 The Effect of Temperature on the Reaction

Experiments were carried out, on vanadium pentoxide and the series of catalysts containing alkali metal sulphate additives, with 8.84 mm. partial pressure 2-propanol, at various temperatures, from 200° to 300°C, in which the rates of conversion of alcohol to acetone, r_1 , propylene, r_2 , and propane, r_3 , were measured along with the overall rate of consumption of 2-propanol, r_4 , Figures 3.2.2 to 3.2.9.

The selectivity ratio for acetone formation, $r_1/(r_1+r_2+r_3)$,

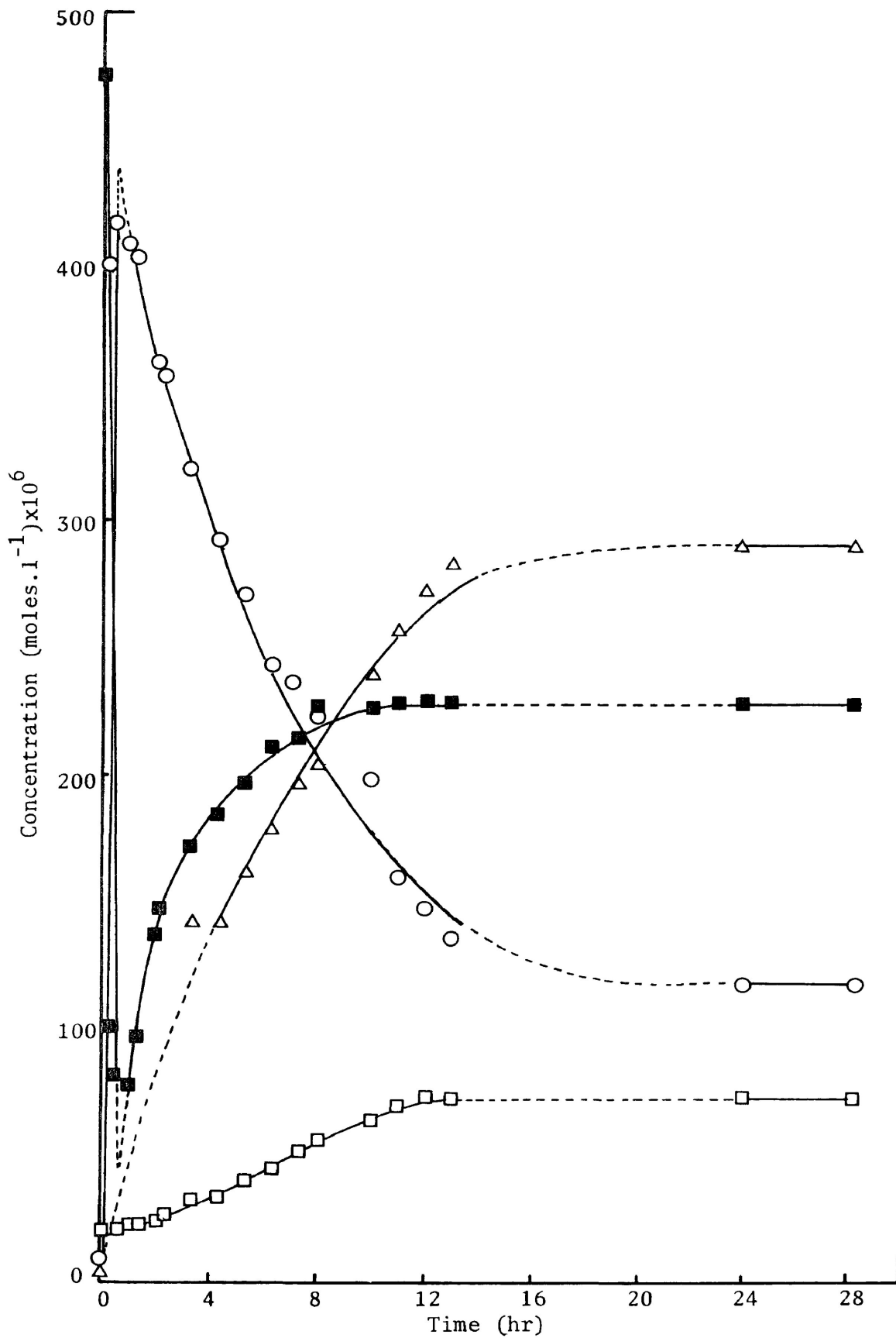


Figure 3.2.1 The effect of exposure time on the reaction components from the decomposition of 2-propanol over $\text{V}_2\text{O}_5:9.09\%\text{K}_2\text{SO}_4$ at 300°C : Δ propane; \square acetone; \circ propylene; \blacksquare 2-propanol.

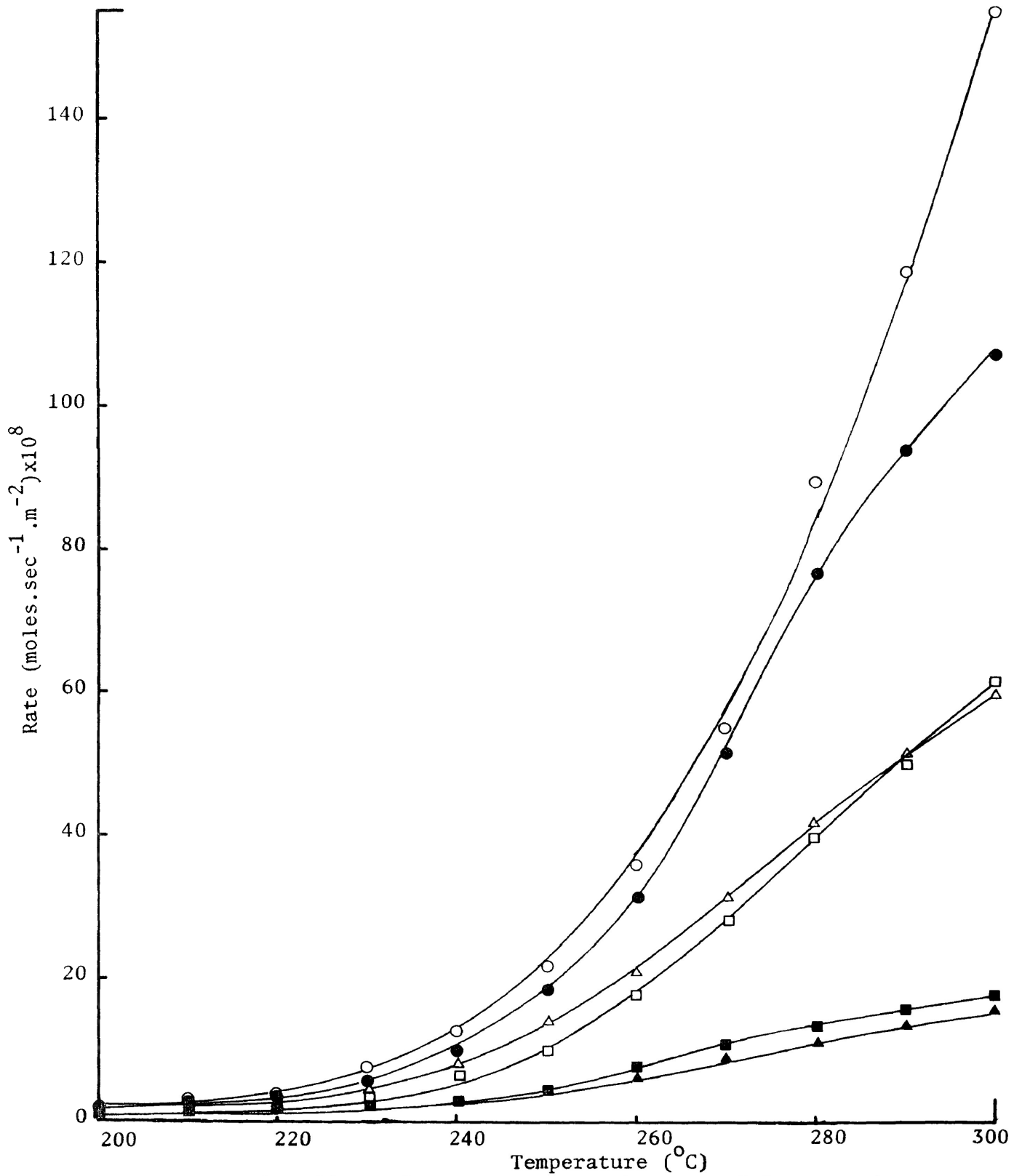


Figure 3.2.2 The effect of temperature on the rate of 2-propanol consumption for, ■ V₂O₅, and V₂O₅ melts containing 9.09 mole percent of: ▲ Li₂SO₄; ● Na₂SO₄; ○ K₂SO₄; △ Rb₂SO₄ and □ Cs₂SO₄.

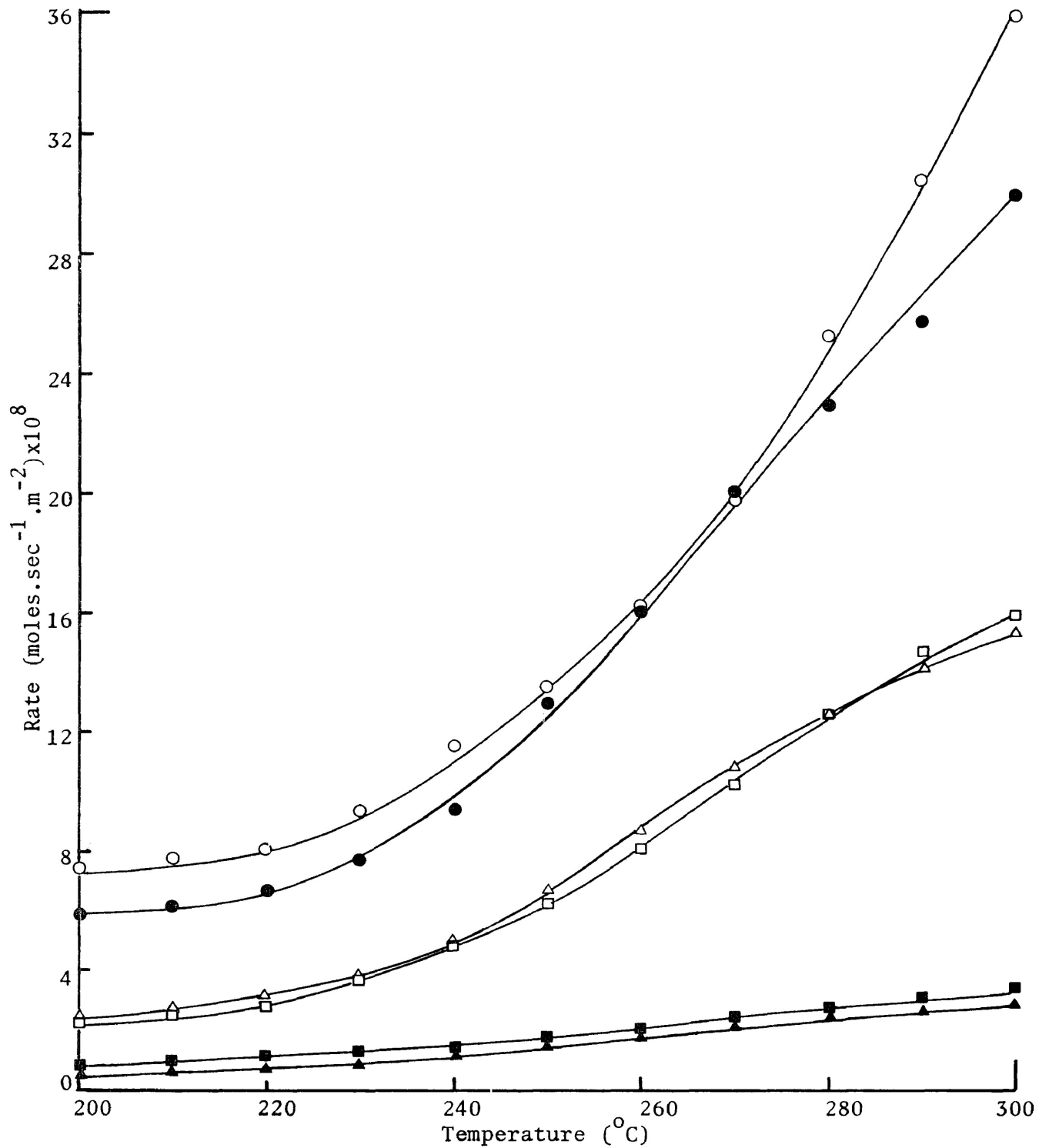


Figure 3.2.3 The effect of temperature on the rate of acetone production for, ■ V₂O₅, and V₂O₅ melts containing 9.09 mole percent of: ▲ Li₂SO₄; ● Na₂SO₄; ○ K₂SO₄; △ Rb₂SO₄ and □ Cs₂SO₄.

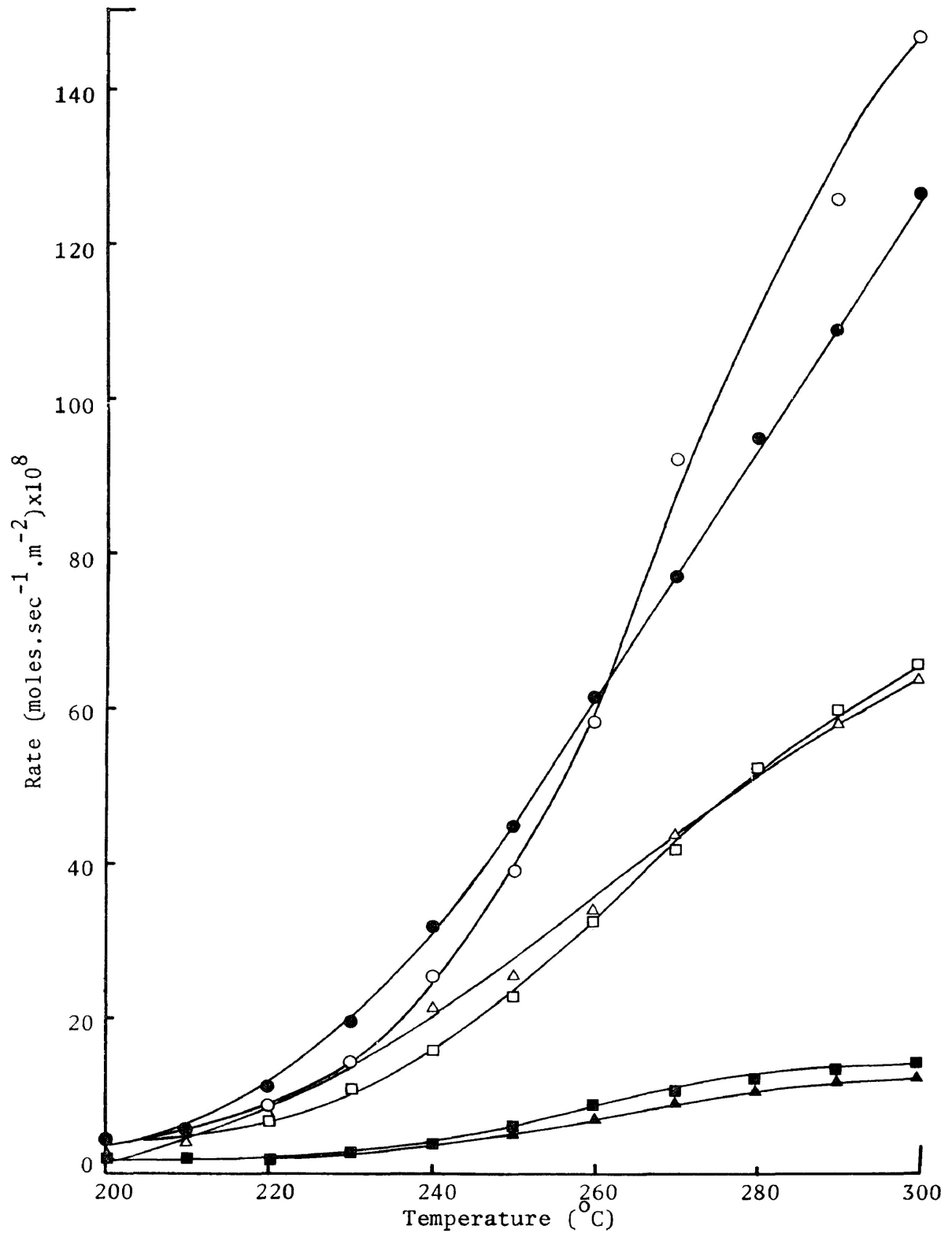


Figure 3.2.4 The effect of temperature on the rate of propane production for, \blacksquare V_2O_5 , and V_2O_5 melts containing 9.09 mole percent of: \blacktriangle Li_2SO_4 ; \bullet Na_2SO_4 ; \circ K_2SO_4 ; \triangle Rb_2SO_4 and \square Cs_2SO_4 .

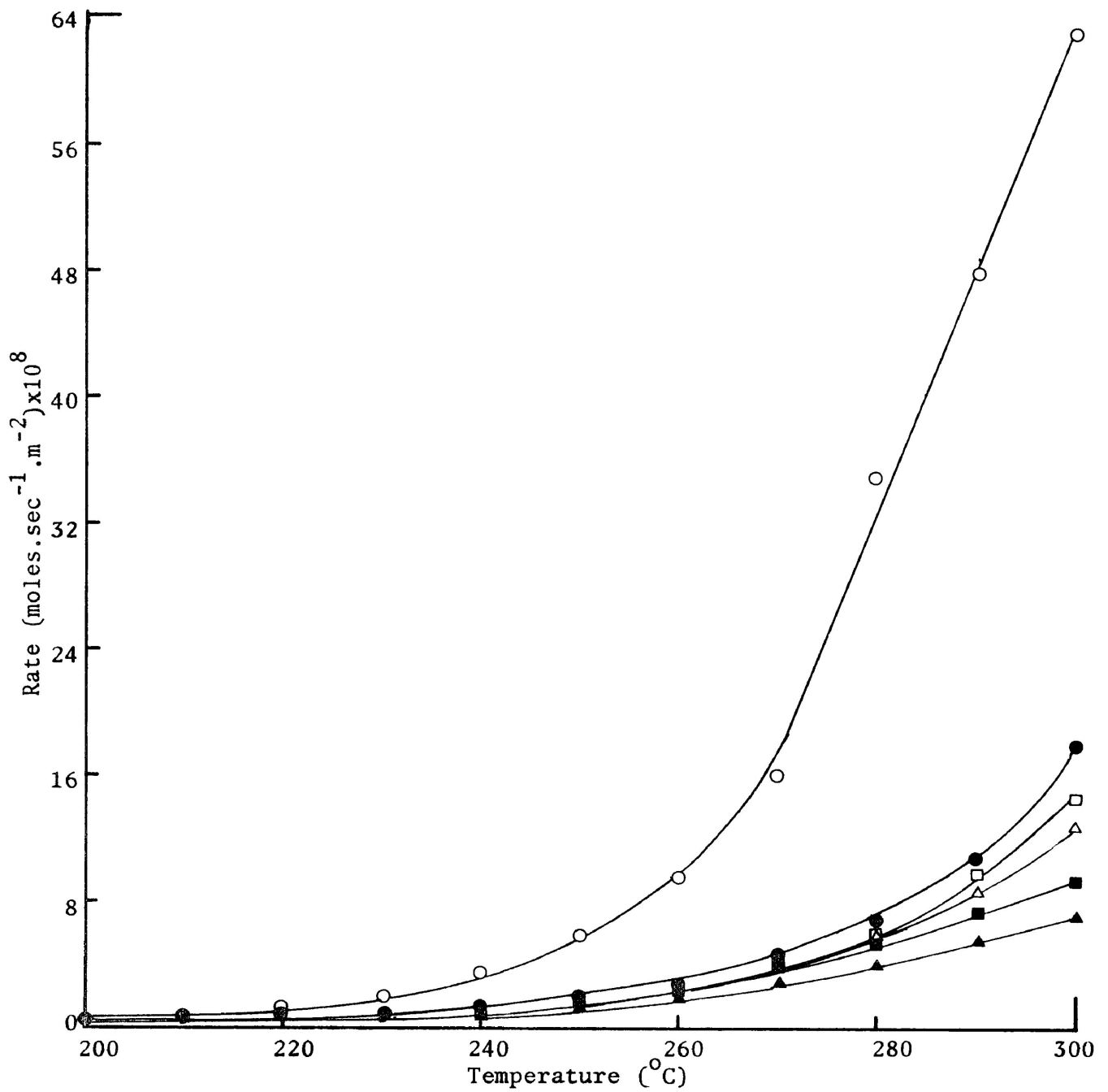


Figure 3.2.5 The effect of temperature on the rate of propylene production for, \blacksquare V_2O_5 , and V_2O_5 melts containing 9.09 mole percent of: \blacktriangle Li_2SO_4 ; \bullet Na_2SO_4 ; \circ K_2SO_4 ; \triangle Rb_2SO_4 and \square Cs_2SO_4 .

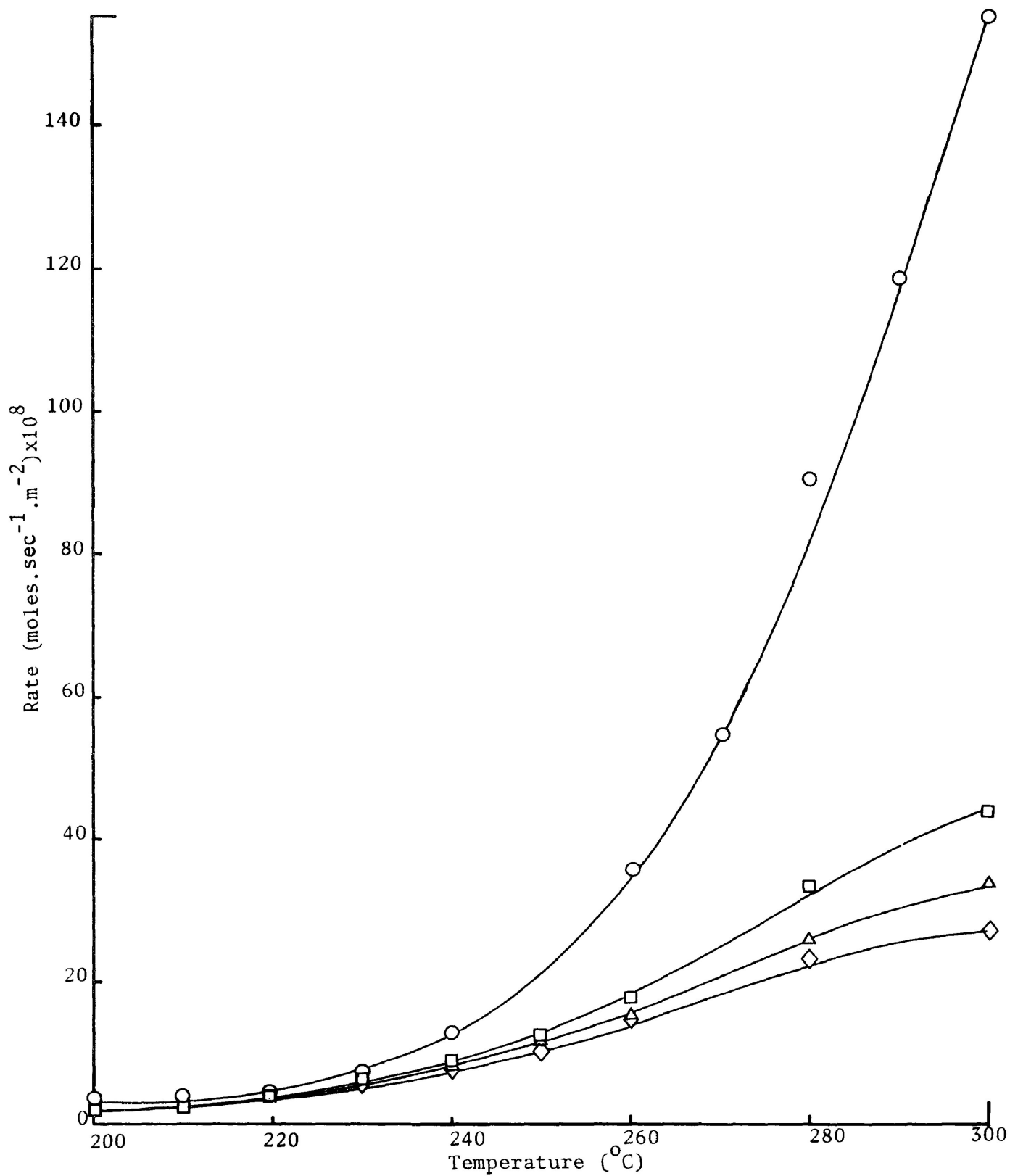


Figure 3.2.6 The effect of temperature on the rate of 2-propanol consumption for V_2O_5 melts containing the following mole percent of K_2SO_4 : \circ 9.09%; \square 4.98%; \triangle 2.00% and \diamond 1.01%.

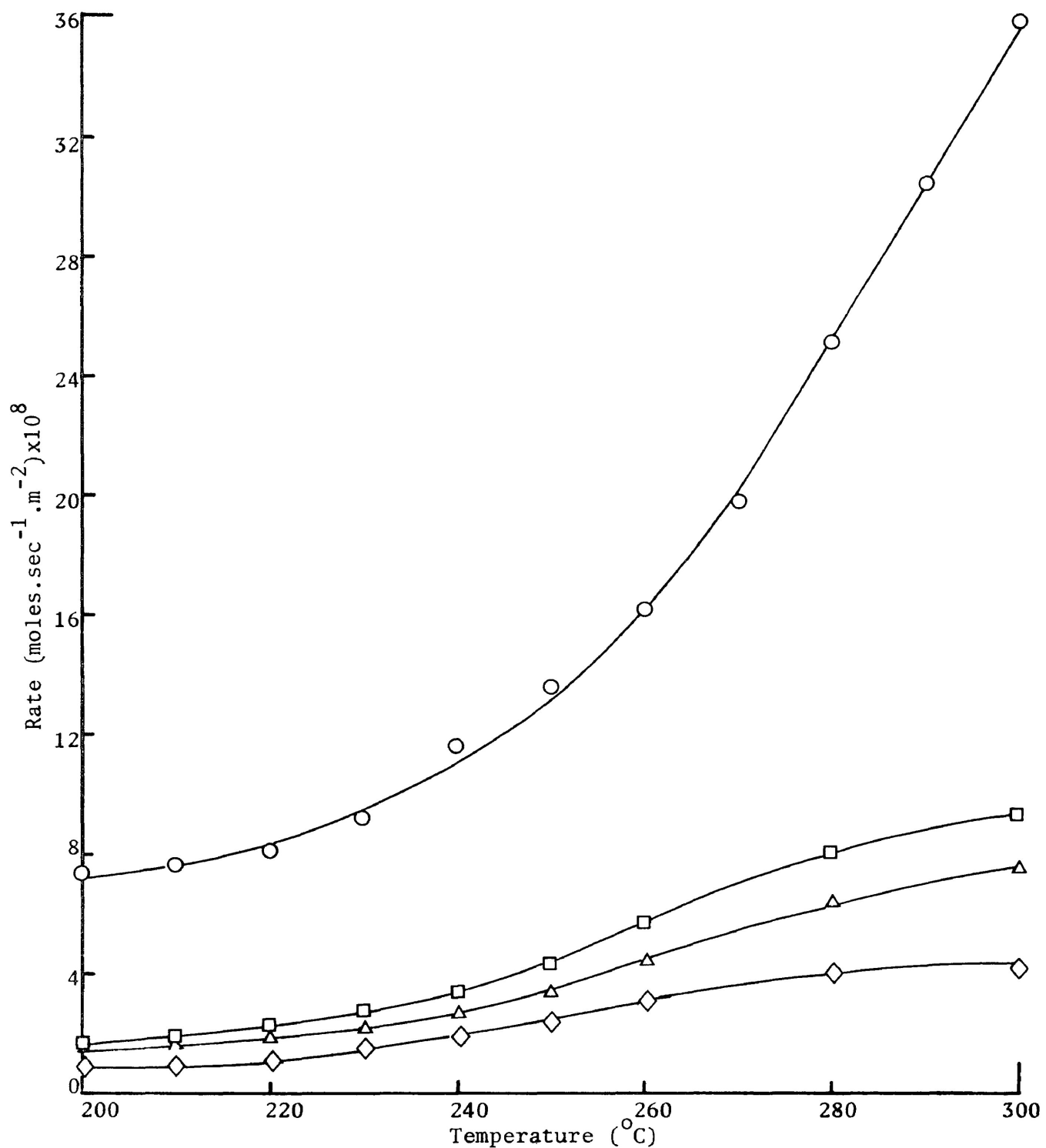


Figure 3.2.7 The effect of temperature on the rate of acetone production for V₂O₅ melts containing the following mole percent of K₂SO₄: ○ 9.09%; □ 4.98%; △ 2.00% and ◇ 1.01%.

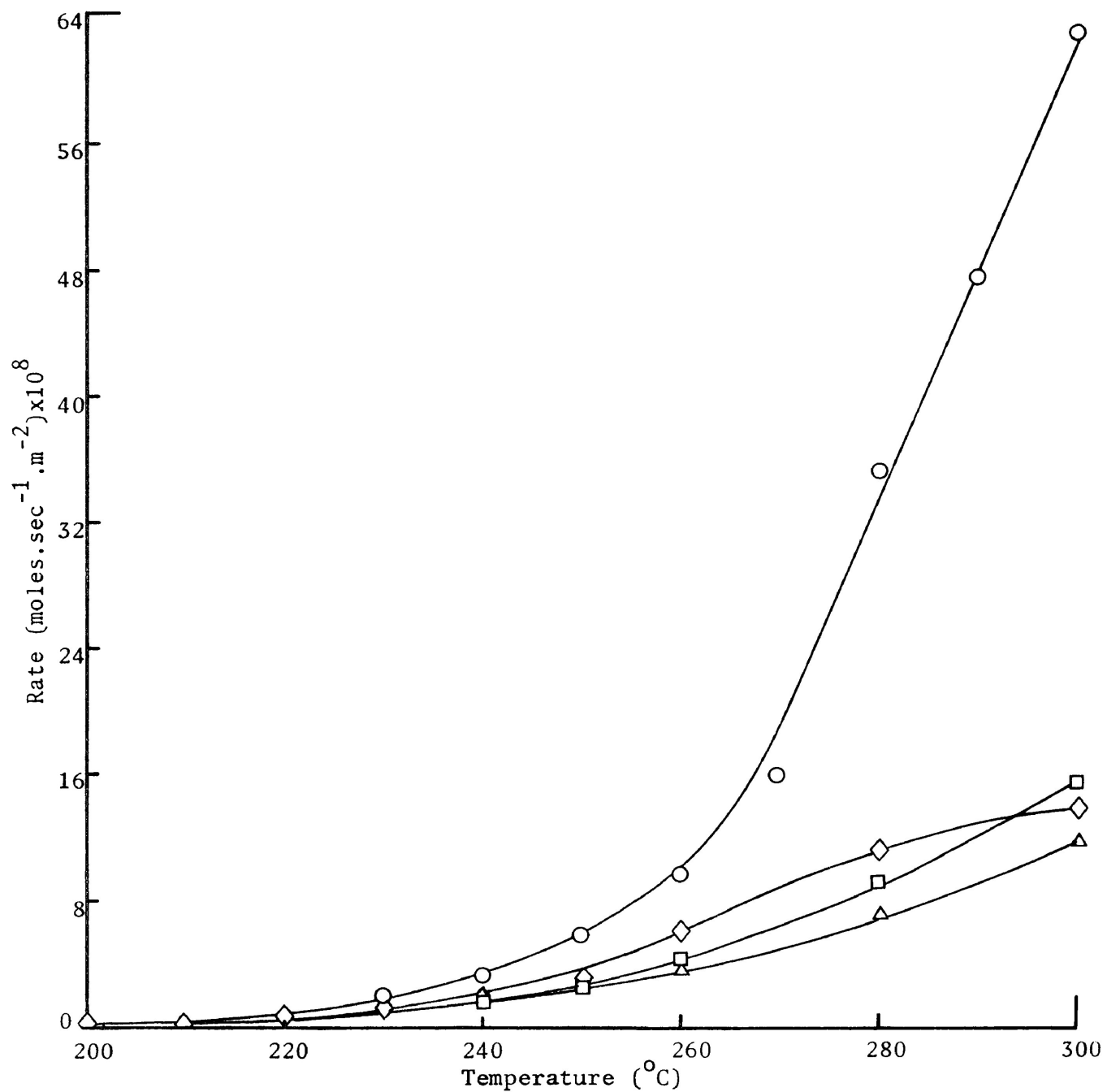


Figure 3.2.8 The effect of temperature on the rate of propylene production for V₂O₅ melts containing the following mole percent of K₂SO₄: ○ 9.09%; □ 4.98%; △ 2.00% and ◇ 1.01%.

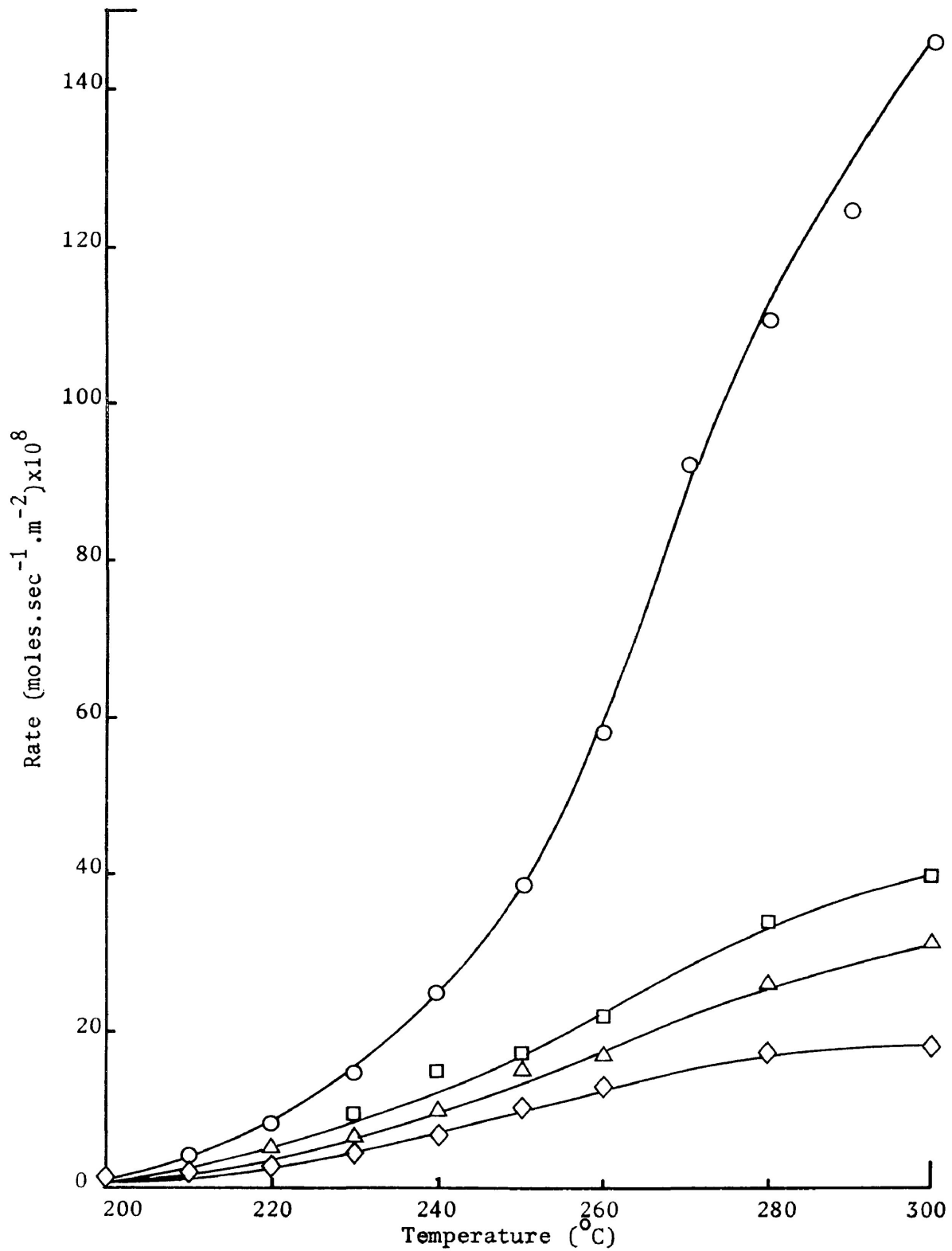


Figure 3.2.9 The effect of temperature on the rate of propane production for V₂O₅ melts containing the following mole percent of K₂SO₄: ○ 9.09%; □ 4.98%; △ 2.00% and ◇ 1.01%.

was calculated for each catalyst as shown in Table 3.2.1.

The propane forming reaction was dominant although dehydration to propylene and dehydrogenation to acetone also took place to a significant extent. The contribution of these latter reactions, to the overall reaction, decreased at higher temperatures. No other organic compounds could be detected in the temperature range studied while water was difficult to determine quantitatively with the chromatograph columns used.

3.2.3 The Effect of 2-propanol Partial Pressure on the Reaction Rates

The partial pressure of 2-propanol was varied between 3.57 and 8.84 mm. over $V_2O_5:9.09\%K_2SO_4$ at $230^{\circ}C$ and 300 ml. min^{-1} (NTP) total flow, see Figure 3.2.10. The amount of propane produced increased directly with increase in the partial pressure of 2-propanol while propylene was unaffected and acetone varied very slightly. A logarithmic plot of rate against partial pressure of alcohol indicated a reaction order for propane of 0.3 with respect to 2-propanol partial pressure, Figure 3.2.11. The other products showed zero order reaction rate dependencies with respect to 2-propanol partial pressure.

3.2.4 The Effect of Acetone

At $230^{\circ}C$ and 8.84 mm. partial pressure 2-propanol, over $V_2O_5:9.09\%K_2SO_4$, the reaction was initially unsettled by the introduction of 0.58 mm. acetone but returned to steady values shortly afterwards, see Figure 3.2.12. Once the system had returned to steady conditions, no further effects of acetone on the reaction were detected as the partial pressure of this component was increased step wise from 0.5 to 3.0 mm Hg.

Table 3.2.1 The effect of temperature on catalyst selectivity for acetone formation.

Reactor Temperature (°C)	Catalyst selectivity = $\frac{r_1}{r_1 + r_2 + r_3}$									
	V ₂ O ₅	V ₂ O ₅ :9.09% Li ₂ SO ₄	V ₂ O ₅ :9.09% Na ₂ SO ₄	V ₂ O ₅ :9.09% K ₂ SO ₄	V ₂ O ₅ :9.09% Rb ₂ SO ₄	V ₂ O ₅ :9.09% Cs ₂ SO ₄	V ₂ O ₅ :1.01% K ₂ SO ₄	V ₂ O ₅ :2.00% K ₂ SO ₄	V ₂ O ₅ :4.98% K ₂ SO ₄	
300	0.125	0.129	0.172	0.146	0.168	0.166	0.115	0.147	0.144	
290	0.130	0.140	0.178	0.150	0.176	0.174	-----	-----	-----	
280	0.138	0.145	0.184	0.147	0.179	0.177	0.125	0.160	0.159	
270	0.144	0.154	0.197	0.154	0.186	0.185	-----	-----	-----	
260	0.140	0.171	0.208	0.185	0.195	0.191	0.136	0.180	0.178	
250	0.185	0.190	0.220	0.233	0.205	0.208	0.141	0.157	0.187	
240	0.217	0.213	0.223	0.290	0.183	0.233	0.184	0.188	0.165	
230	0.250	0.220	0.281	0.363	0.201	0.263	0.180	0.212	0.202	
220	0.287	0.238	0.369	0.461	0.264	0.290	0.227	0.278	0.270	
210	0.311	0.267	0.481	0.546	0.350	0.388	0.302	0.355	0.393	
200	0.341	0.298	0.572	0.575	0.491	0.491	0.377	0.457	0.442	

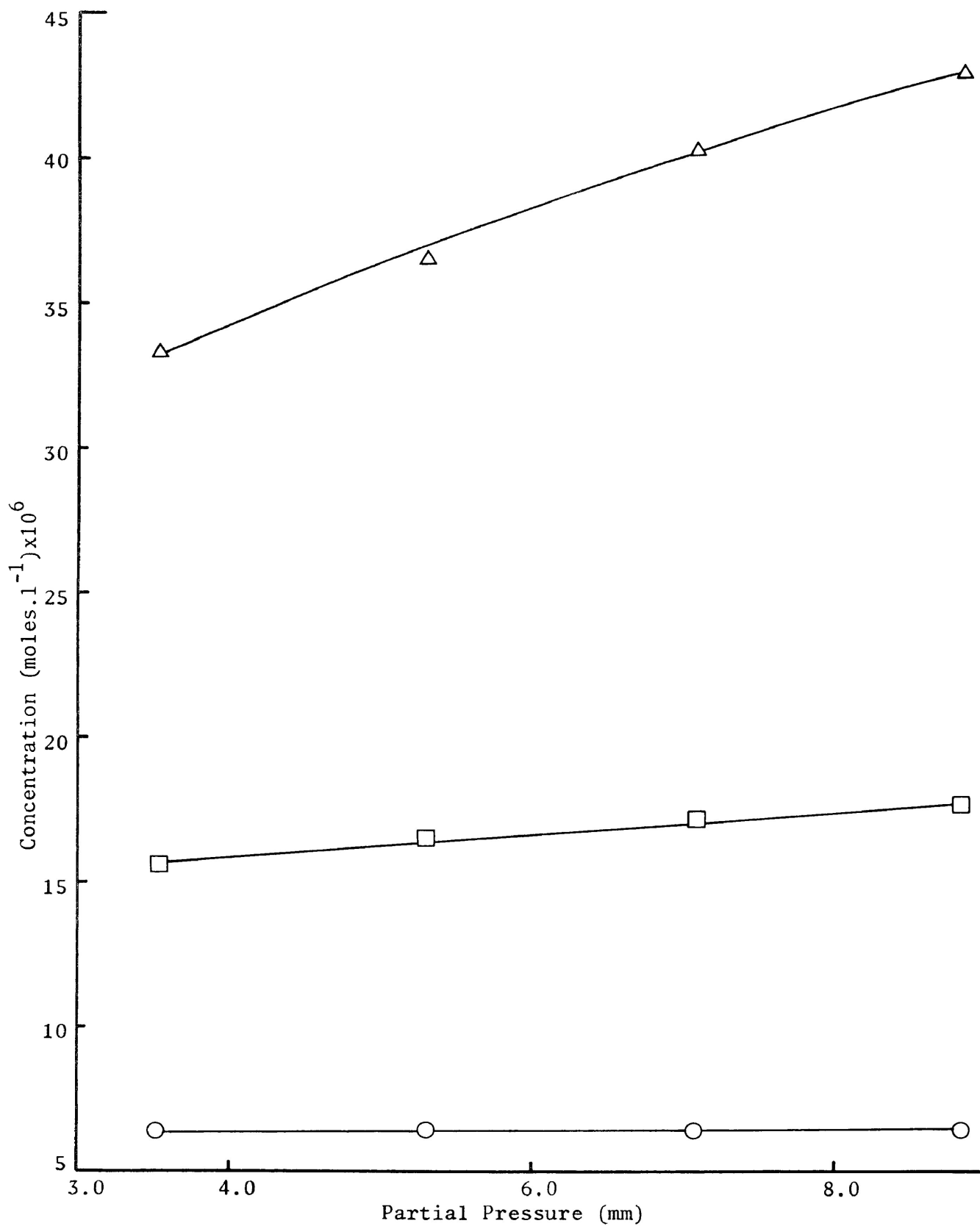


Figure 3.2.10 The effect of 2-propanol partial pressure on the products of the decomposition of 2-propanol over $V_2O_5:9.09\%K_2SO_4$ at $230^\circ C$: Δ propane; \square acetone; \circ propylene.

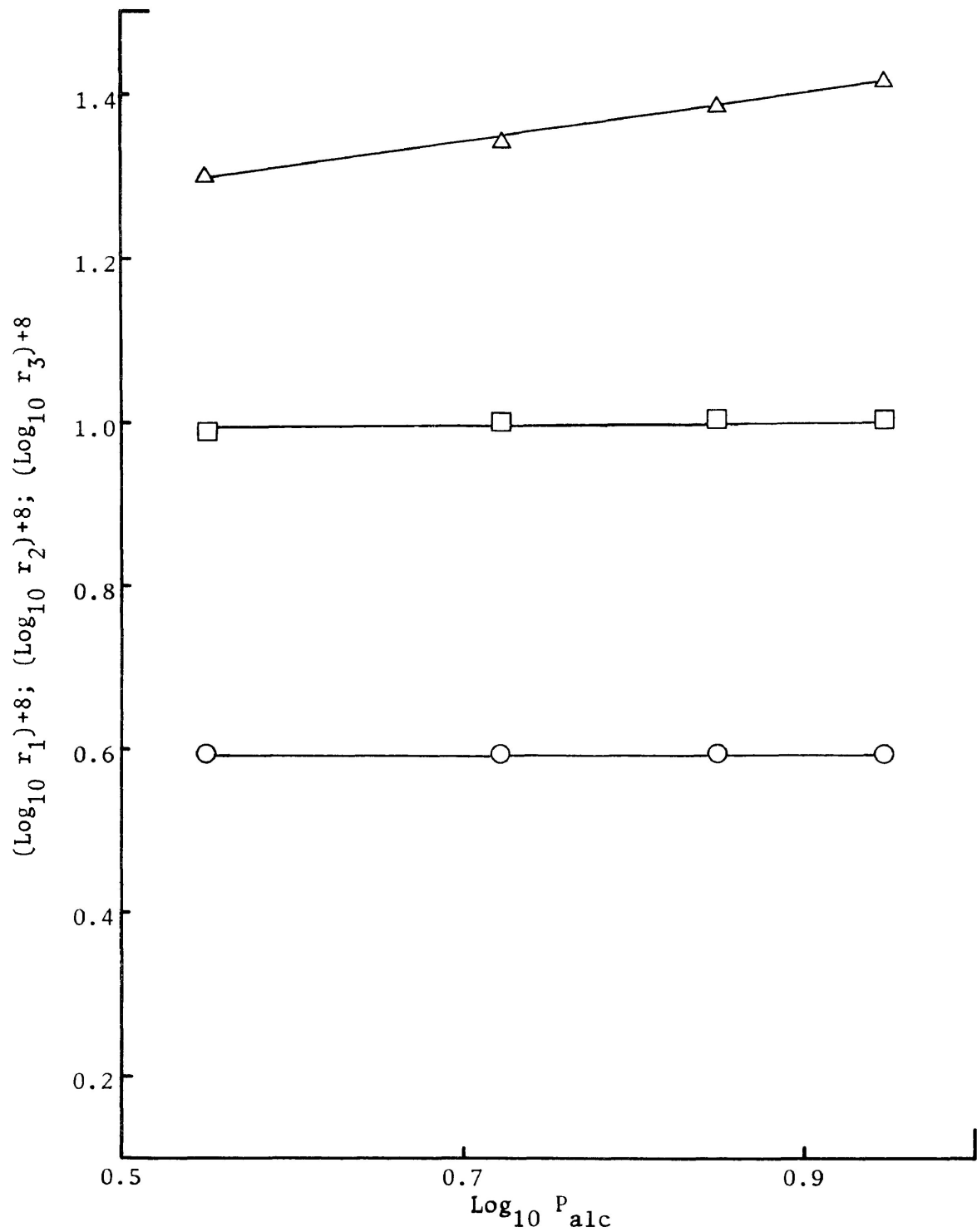


Figure 3.2.11 Logarithmic plot of the rate of: \square acetone formation, r_1 ; \circ propylene formation, r_2 , and Δ propane formation, r_3 , over $V_2O_5:9.09\%K_2SO_4$ at 230°C , against 2-propanol partial pressure.

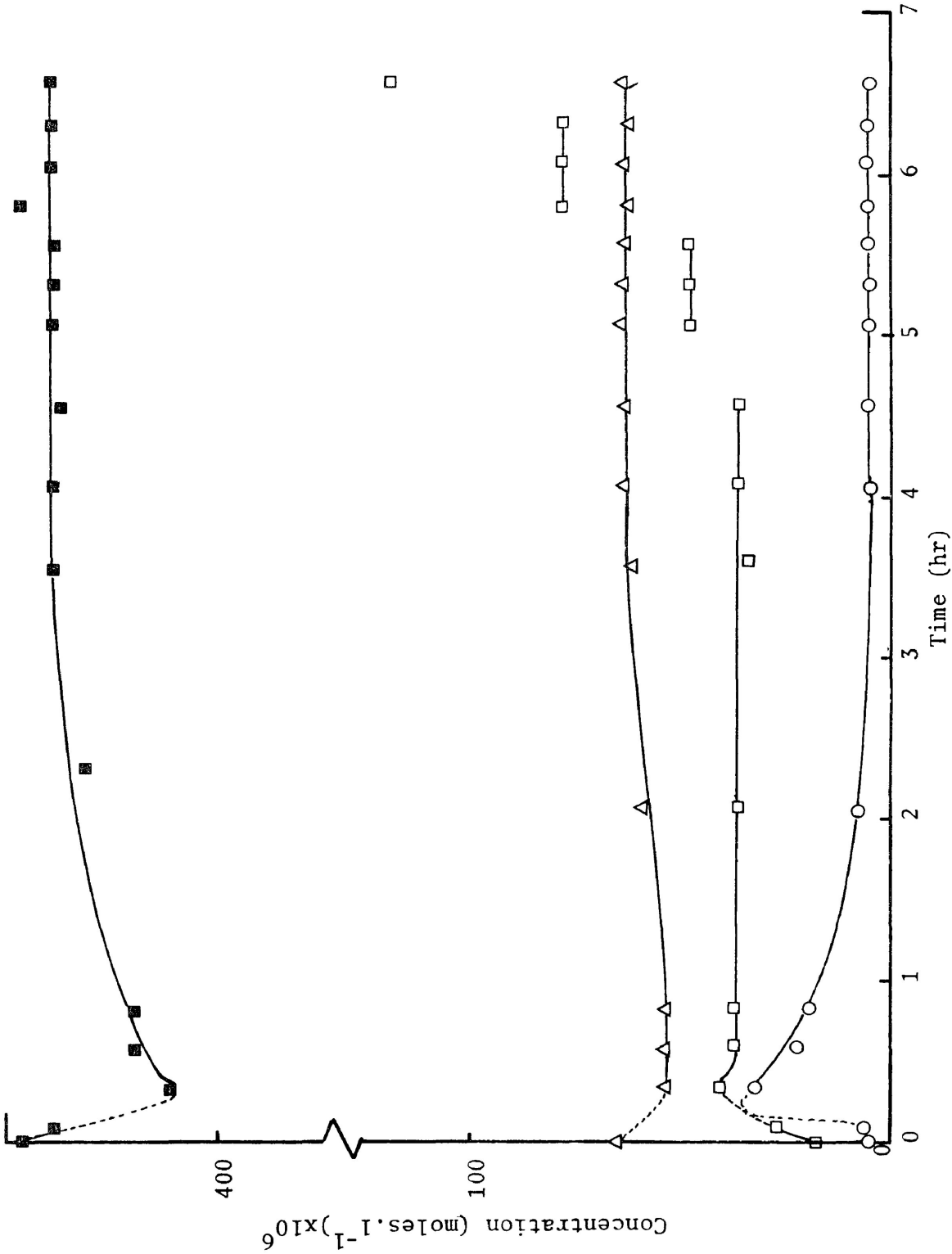


Figure 3.2.12 The effect of acetone partial pressure on the components for the decomposition of 2-propanol over V₂O₅:9.09%K₂SO₄ at 230°C: □ acetone; ○ propylene; Δ propane and ■ 2-propanol.

3.2.5 The Effect of Water Vapour

At 230°C and 8.84 mm. partial pressure 2-propanol and a total flow of 300 ml.min⁻¹ (NTP), over V₂O₅:9.09%K₂SO₄, the initial steady-state condition was disturbed as water vapour was introduced. The system returned to steady conditions shortly afterwards and then remained unaffected as the partial pressure of water was varied from 0.75 to 3.0 mm., Figure 3.2.13.

3.2.6 The Effects of Hydrogen, Propylene and Propane

Under similar reaction conditions, 230°C, 8.84 mm. partial pressure 2-propanol and a total flow of 300 ml.min⁻¹ (NTP), over V₂O₅:9.09%K₂SO₄, the main course of the reaction was not affected, aside from the recurring initial settling, as the partial pressures of propylene and hydrogen were varied between 4.2 and 10.0 mm., Figures 3.2.14 and 3.2.15. A similar result was observed for propane but, unfortunately, insufficient data are available to plot a meaningful graph.

3.3 Activation Energies

The apparent activation energies for the reactions involved were calculated from rate equations formulated from the experimental results. The order of the reaction for propane with respect to 2-propanol concentration was taken as 0.3 while the net effects of the other components were considered to be zero order.

Since the dehydrogenation reaction, acetone formation, was found to be zero order with respect to all components the reaction may be treated as overall zero order, i.e.

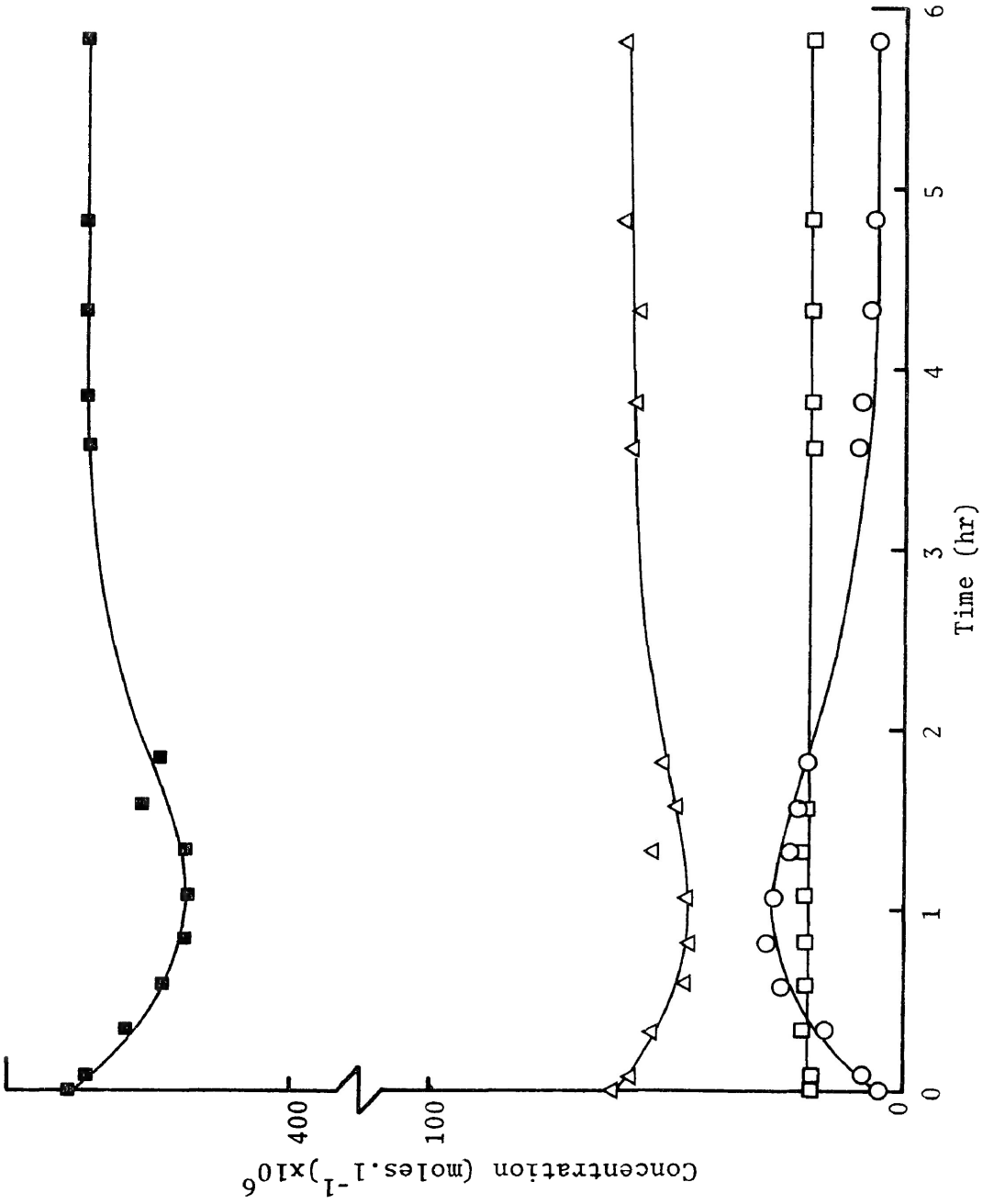


Figure 3.2.13 The effect of water partial pressure on the components for the decomposition of 2-propanol over $V_2O_5:9.09\%K_2SO_4$ at $230^\circ C$: \square acetone; \circ propylene; Δ propane and \blacksquare 2-propanol.

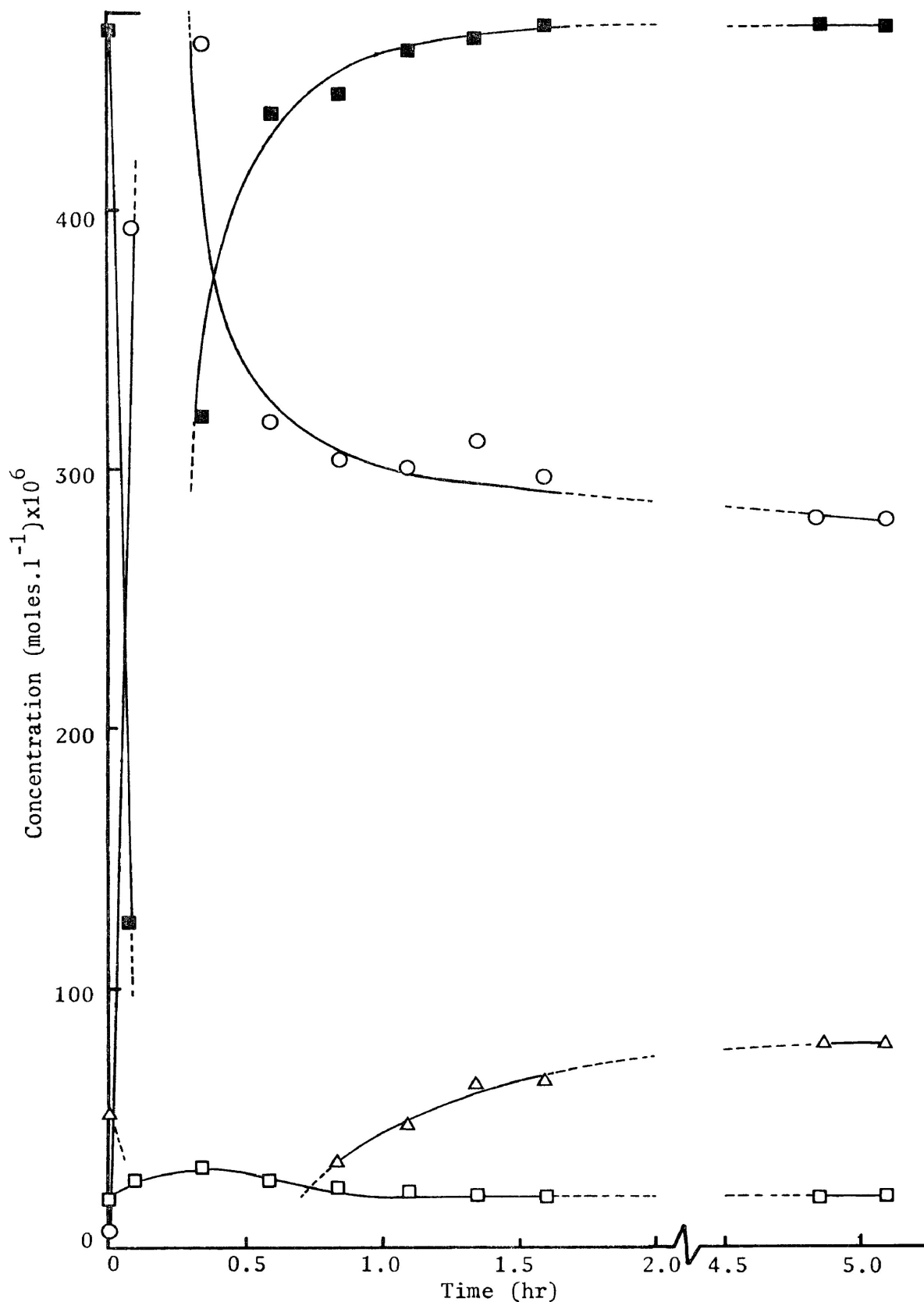


Figure 3.2.14 The effect of propylene partial pressure on the components for the decomposition of 2-propanol over $V_2O_5:9.09\%K_2SO_4$ at $230^\circ C$: \square acetone; \circ propylene; Δ propane and \blacksquare 2-propanol.

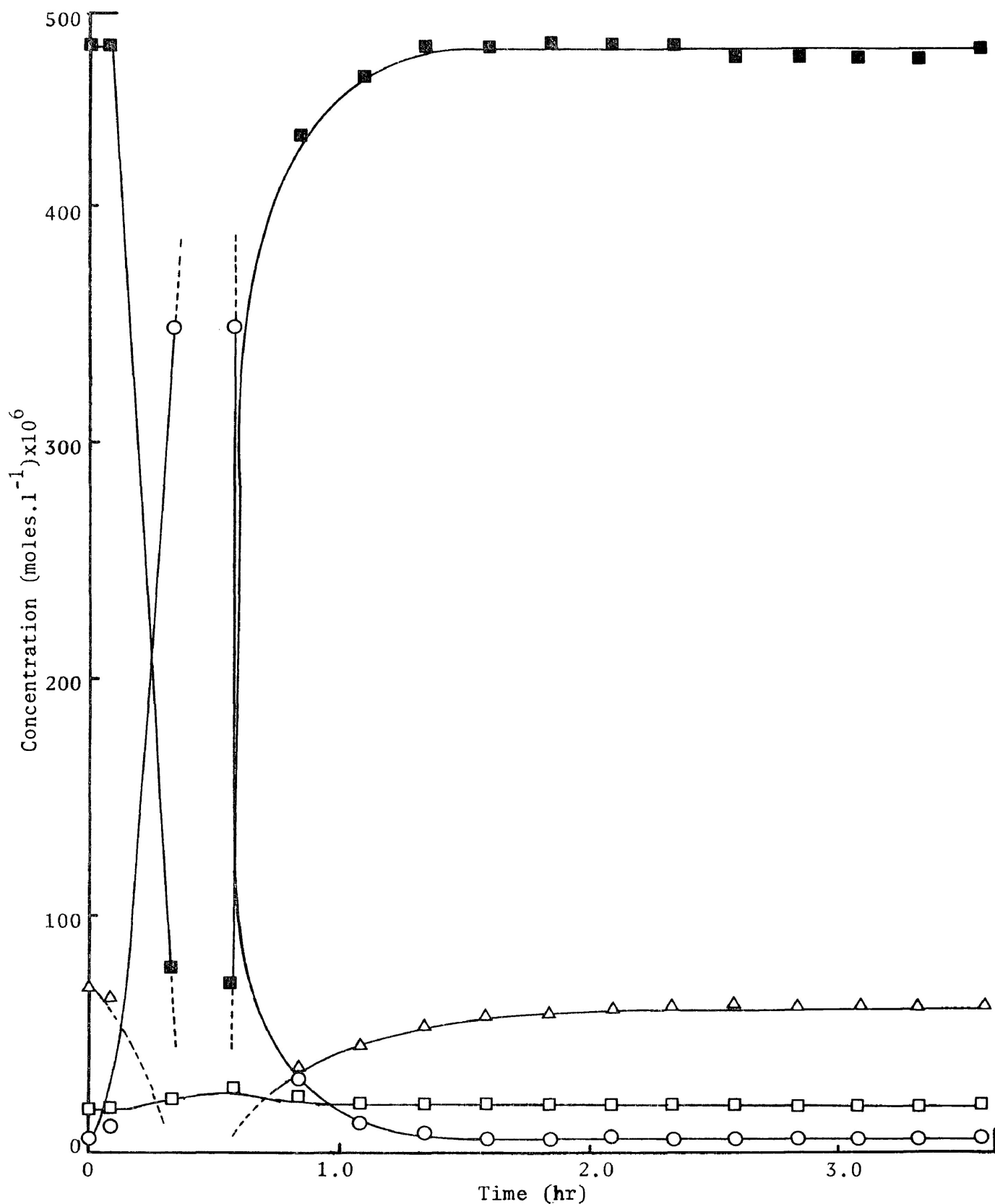


Figure 3.2.15 The effect of hydrogen partial pressure on the components for the decomposition of 2-propanol over $V_2O_5:9.09\%K_2SO_4$ at $230^\circ C$: □ acetone; ○ propylene; △ propane and ■ 2-propanol.

$$\frac{dC_{ac}}{dt} = k_1' \cdot C_{ac}^o \cdot C_{alc}^o \cdot C_{pro}^o \cdot C_{py}^o \cdot C_w^o \quad \dots 3.3.1$$

or

$$\frac{dC_{ac}}{dt} = k_1' \quad \dots 3.3.2$$

where C refers to concentration and the subscripts ac, alc, pro, py and w refer to acetone, 2-propanol, propane, propylene and water, respectively. Separating variables and integrating gives:

$$\left[C_{ac} \right]_{C_{ac}(i)}^{C_{ac}(f)} = k_1' \cdot t \quad \dots 3.3.3$$

where the subscripts i and f refer to initial and final concentrations.

Since

$$C_{ac}(i) = 0$$

then

$$C_{ac}(f) = k_1' \cdot t \quad \dots 3.3.4$$

or

$$k_1' = \frac{C_{ac}(f)}{t} \quad \dots 3.3.5$$

It is normal to assume that time, t, is inversely proportional to the flow, i.e.

$$t \propto \frac{1}{V} \propto \frac{1}{S.V.}$$

Where $V =$ flow rate

S.V. = space velocity in cc. gas.cc.⁻¹ catalyst.sec⁻¹
corrected for catalyst temperature (Reference 2)

Therefore $k_1'' = C_{ac}(f) \cdot S.V. \quad \dots 3.3.6$

But $C_{ac} = \frac{P_{ac} \times 298}{24.47 \times 760 \times T} \text{ (moles.l}^{-1}\text{)} \quad \dots 3.3.7$

where $P_{ac} =$ partial pressure acetone in mm.

and $T =$ catalyst temperature in °K

and $S.V. = \frac{300 \times T}{298 \times 1.1 \times 60} \text{ sec}^{-1} \quad \dots 3.3.8$

since the catalyst volume was 1.1 cc.

Therefore $k_1'' = \frac{P_{ac} \times 300}{24.47 \times 760 \times 1.1 \times 60} \text{ (moles.sec}^{-1}\text{.l}^{-1}\text{)} \quad \dots 3.3.9$

The specific rate constant k_1 is given by:

$$k_1 = k_1'' \cdot (S.A.)^{-1}$$

where S.A. = the surface area of the catalyst present in the reactor.

Therefore $k_1 = \frac{P_{ac} \times 300}{24.47 \times 760 \times 1.1 \times 60 \times S.A.} \text{ (moles.l}^{-1}\text{.sec}^{-1}\text{.m}^{-2}\text{)} \quad \dots 3.3.10$

For propane formation the following rate equation was formulated

$$\frac{dC_{pro}}{dt} = k_3' \cdot C_{alc}^{0.3} \quad \dots 3.3.11$$

Separating variables and integrating gives:

$$\left[\frac{C_{\text{pro}}}{C_{\text{alc}}^{0.3}} \right]_{C_{\text{pro}(i)}}^{C_{\text{pro}(f)}} = k_3' t \quad \dots 3.3.12$$

Since $C_{\text{pro}(i)} = 0$

then $k_3' = \frac{C_{\text{pro}}}{C_{\text{alc}}^{0.3} \cdot t} \quad \dots 3.3.13$

or $k_3'' = \frac{C_{\text{pro}}}{C_{\text{alc}}^{0.3}} \cdot \text{S.V.} \quad \dots 3.3.14$

where S.V. = space velocity, see equation 3.3.8

and $C_{\text{pro}} = \text{concentration of propane}$
 $= \frac{P_{\text{pro}} \times 298}{24.47 \times 760 \times T} \text{ (moles.l}^{-1}\text{)} \quad \dots 3.3.15$

where $P_{\text{pro}} = \text{partial pressure of propane in torr}$

and $C_{\text{alc}} = \text{concentration of 2-propanol}$
 $= \frac{P_{\text{alc}} \times 298}{24.47 \times 760 \times T} \text{ (moles.l}^{-1}\text{)} \quad \dots 3.3.16$

where $P_{\text{alc}} = \text{partial pressure of 2-propanol in torr}$

Therefore $k_3'' = \left(\frac{P_{\text{pro}} \times 300}{24.47 \times 760 \times 1.1 \times 60} \right) \cdot \left(\frac{P_{\text{alc}} \times 298}{24.47 \times 760 \times T} \right)^{-0.3}$
 $\text{(moles}^{0.7}\text{.l}^{-0.7}\text{.sec}^{-1}\text{)} \quad \dots 3.3.17$

and the specific rate constant for propane formation is given by:

$$k_3 = \left(\frac{P_{\text{pro}} \times 300}{24.47 \times 760 \times 1.1 \times 60 \times \text{S.A.}} \right)^{-0.3} \left(\frac{P_{\text{alc}} \times 298}{24.47 \times 760 \times T} \right) \quad \dots 3.3.18$$

(moles^{0.7} .l^{-0.7} .sec⁻¹ .m⁻²)

The apparent activation energy for each reaction was obtained by plotting the specific rate constant, k , in the Arrhenius fashion.

$$\text{Log}_{10} k = \text{Log}_{10} A - \frac{E_a}{2.303 \times R \times T} \quad \dots 3.3.19$$

A plot of $\text{Log}_{10} k$ against $1/T$ yields a line of slope $E_a/2.303 \times R$ where E_a is the apparent activation energy, R the gas constant, T the temperature in $^{\circ}\text{K}$ and A the 'pre-exponential factor'.

The specific rate constants for acetone formation, k_1 , propylene formation, k_2 , propane formation, k_3 , and 2-propanol consumption, k_4 , were calculated. The surface areas used in these calculations were those obtained after conditioning, see Table 3.4.1. The surface areas measured after the conditioning period and those after subsequent reaction were found to be the same in all cases. The rates of propylene formation and alcohol consumption were zero order with respect to all components thus the rate constants were determined in a manner similar to that used for acetone. Plots of $\text{Log}_{10} k$ against $1/T$ were constructed, Figure 3.3.1.

Since all other catalysts were found to behave in a similar kinetic manner to the melt containing 9.09 mole percent potassium sulphate the same rate equations were used to evaluate specific reaction rate constants and plots of $\text{Log}_{10} k$ against $1/T$ were constructed, Figures 3.3.2 to 3.3.9.

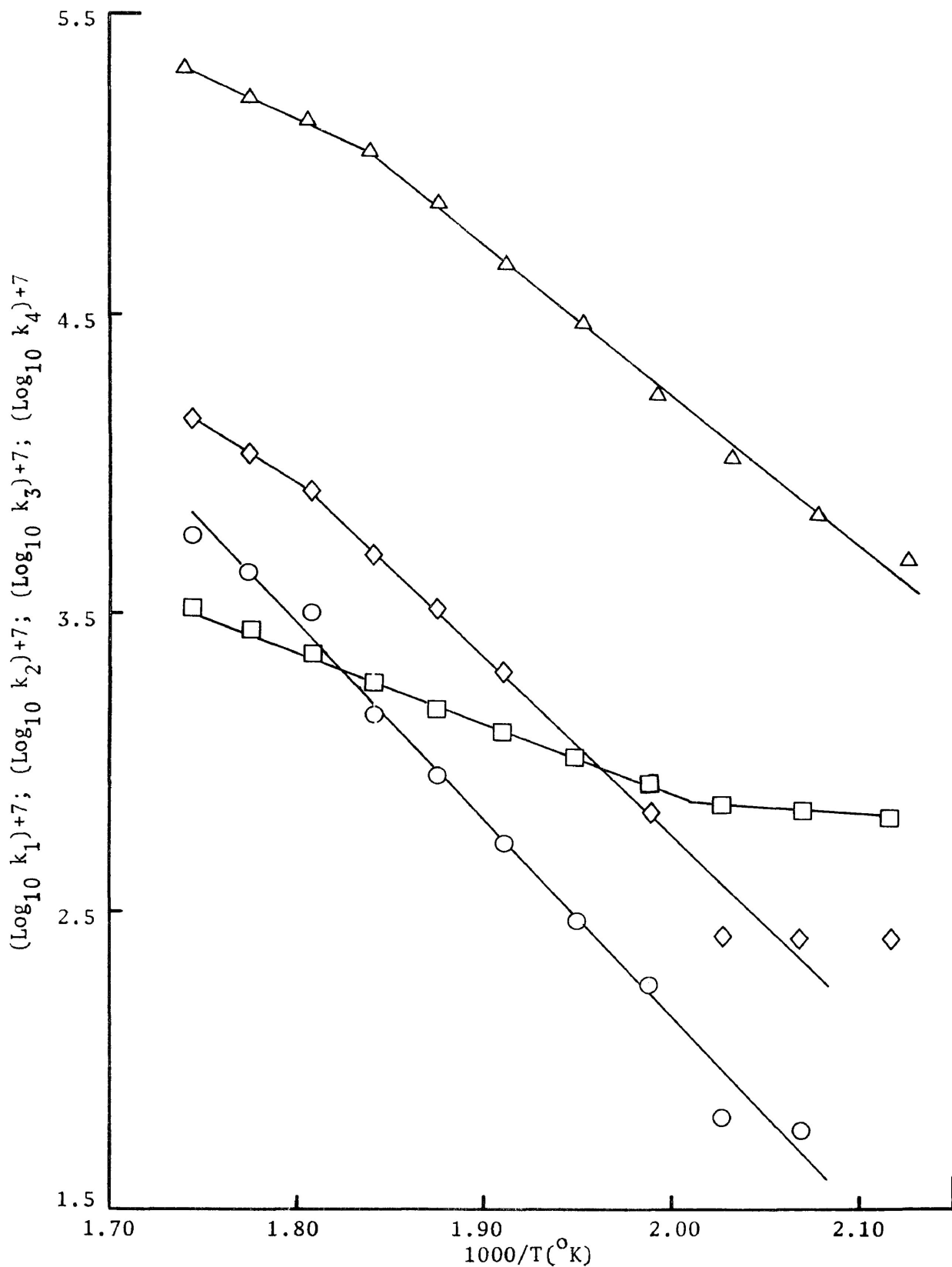


Figure 3.3.1 Arrhenius plots for the decomposition of 2-propanol over $\text{V}_2\text{O}_5:9.09\%\text{K}_2\text{SO}_4$: \square k_1 , acetone formation; \circ k_2 , propylene formation; Δ k_3 , propane formation and \diamond k_4 , 2-propanol consumption.

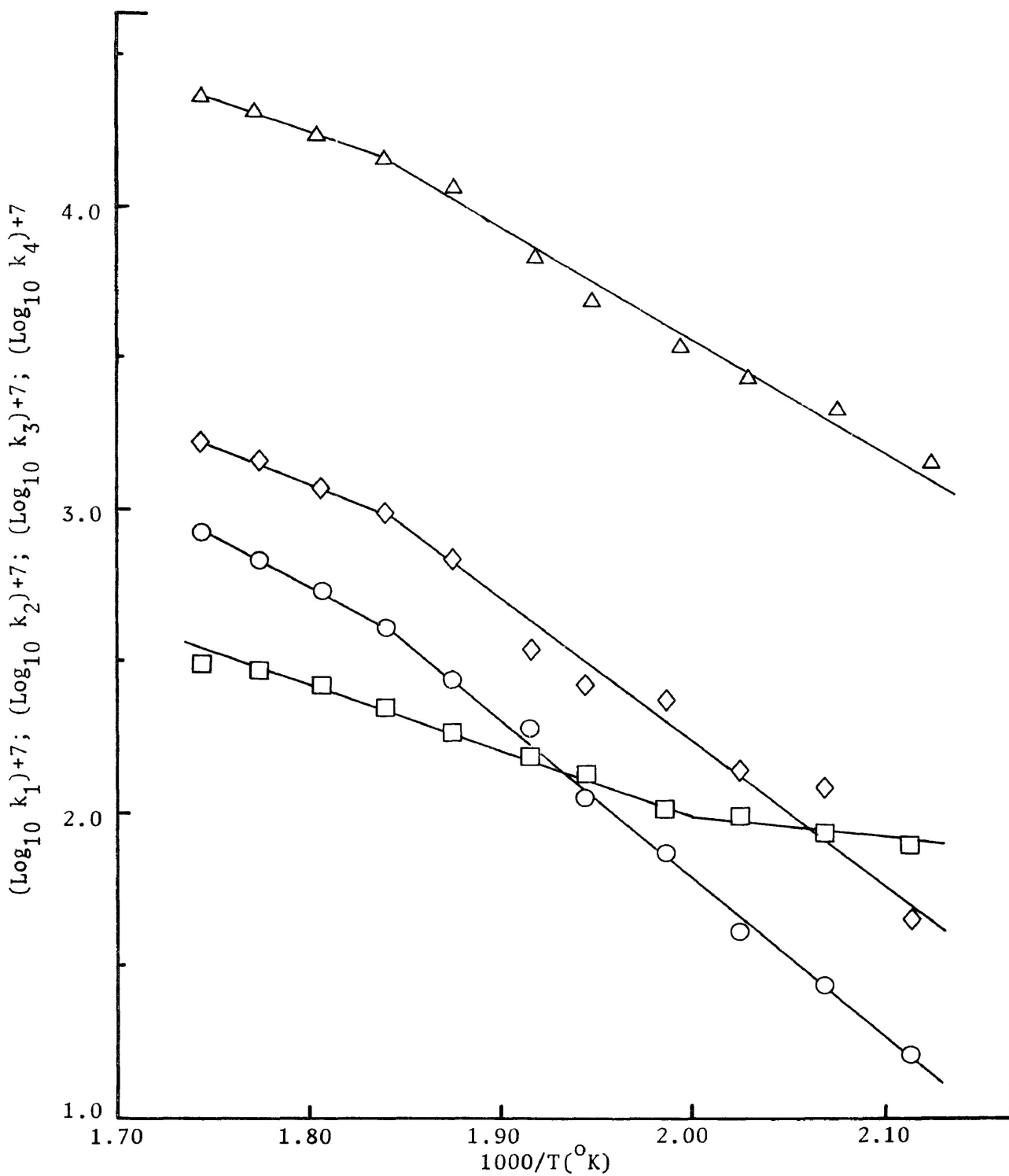


Figure 3.3.2 Arrhenius plots for the decomposition of 2-propanol over V_2O_5 : \square k_1 , acetone; \circ k_2 , propylene; Δ k_3 , propane and \diamond k_4 , 2-propanol consumption.

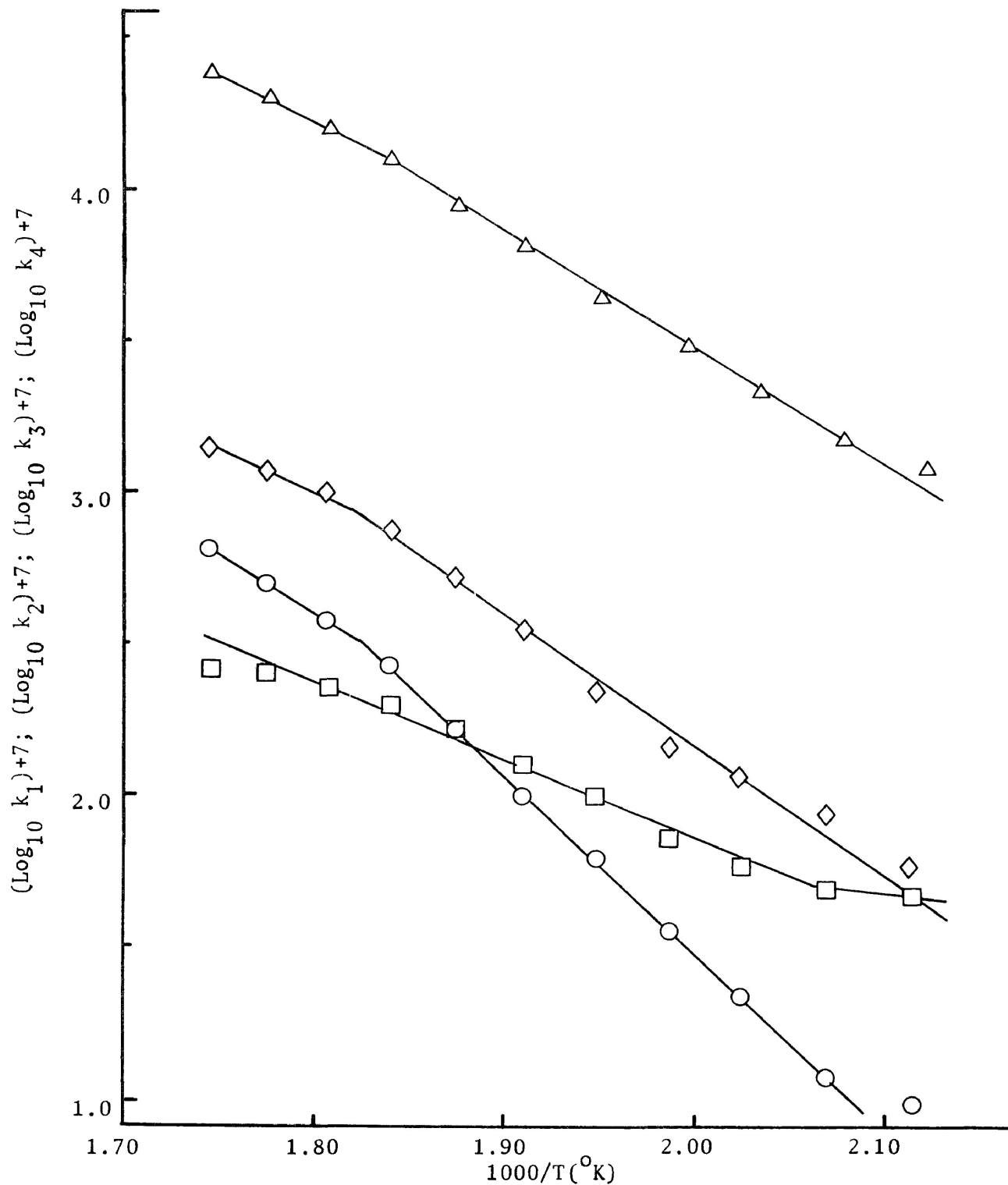


Figure 3.3.3 Arrhenius plots for the decomposition of 2-propanol over $V_2O_5:9.09\%Li_2SO_4$: \square k_1 , acetone formation; \circ k_2 , propylene formation; \triangle k_3 , propane formation and \diamond k_4 , 2-propanol consumption.

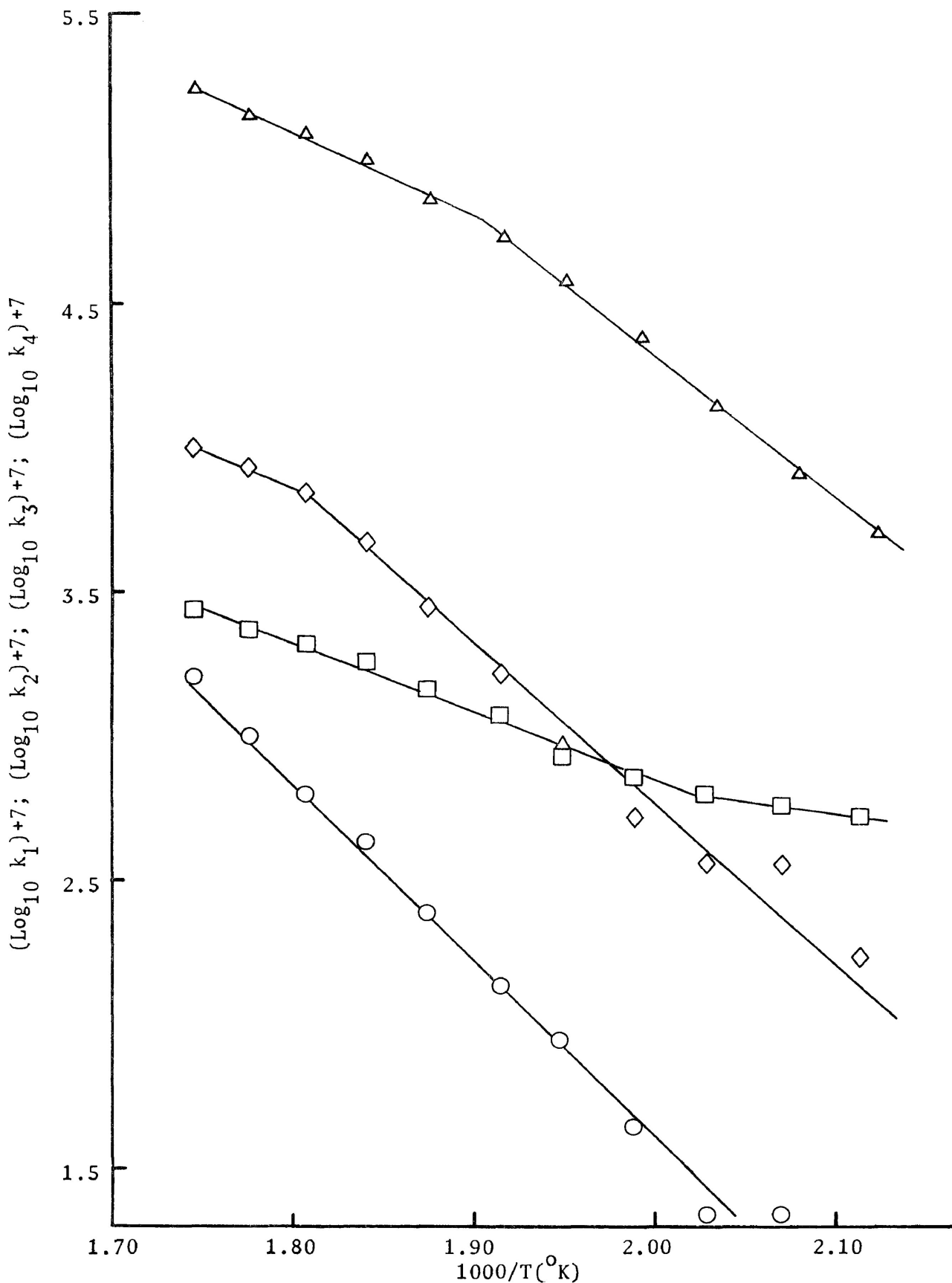


Figure 3.3.4 Arrhenius plots for the decomposition of 2-propanol over $\text{V}_2\text{O}_5:9.09\%\text{Na}_2\text{SO}_4$: \square k_1 , acetone formation; \circ k_2 , propylene formation; \triangle k_3 , propane formation and \diamond k_4 , 2-propanol consumption.

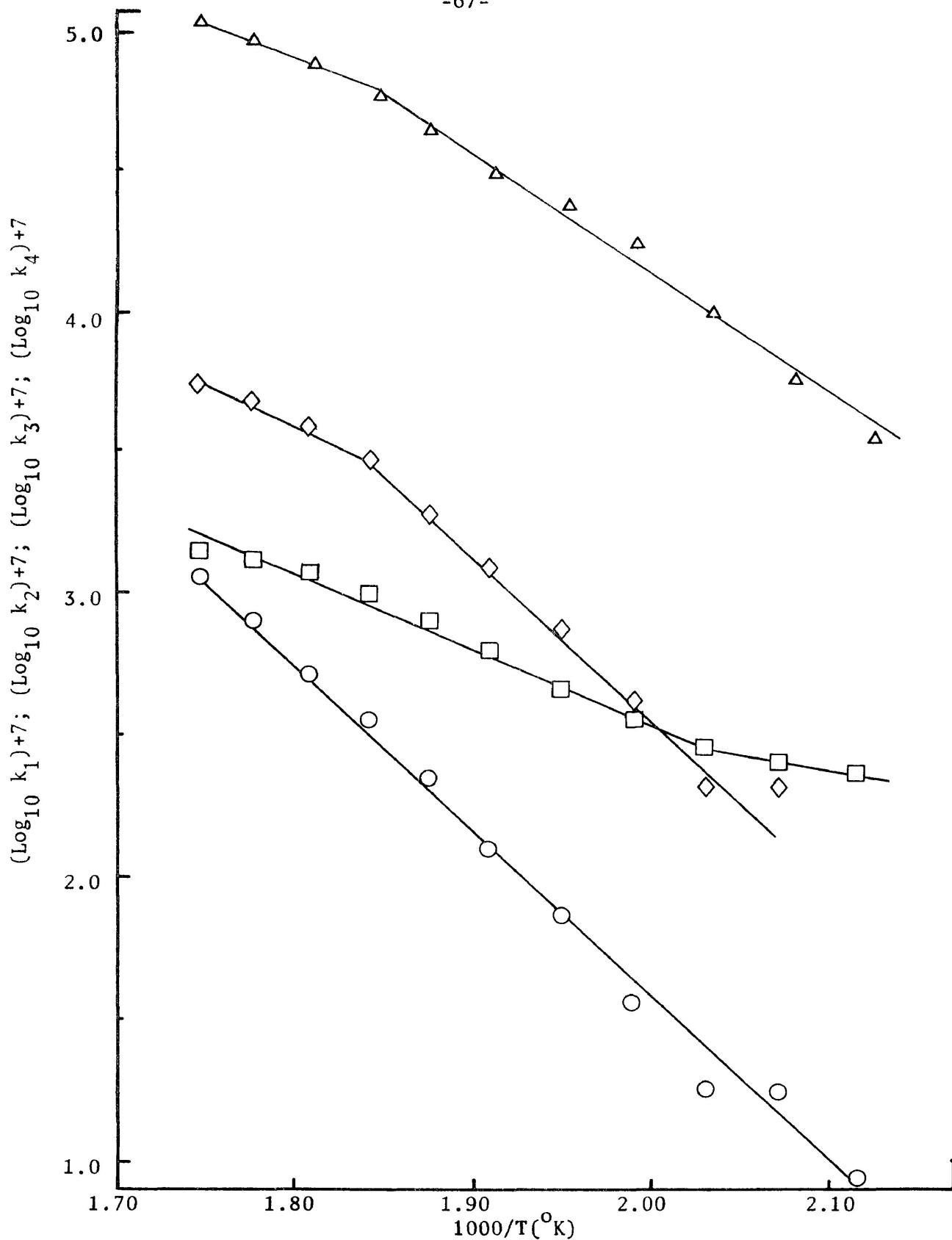


Figure 3.3.5 Arrhenius plots for the decomposition of 2-propanol over $V_2O_5:9.09\%Rb_2SO_4$: \square k_1 , acetone formation; \circ k_2 , propylene formation; \triangle k_3 , propane formation and \diamond k_4 , 2-propanol consumption.

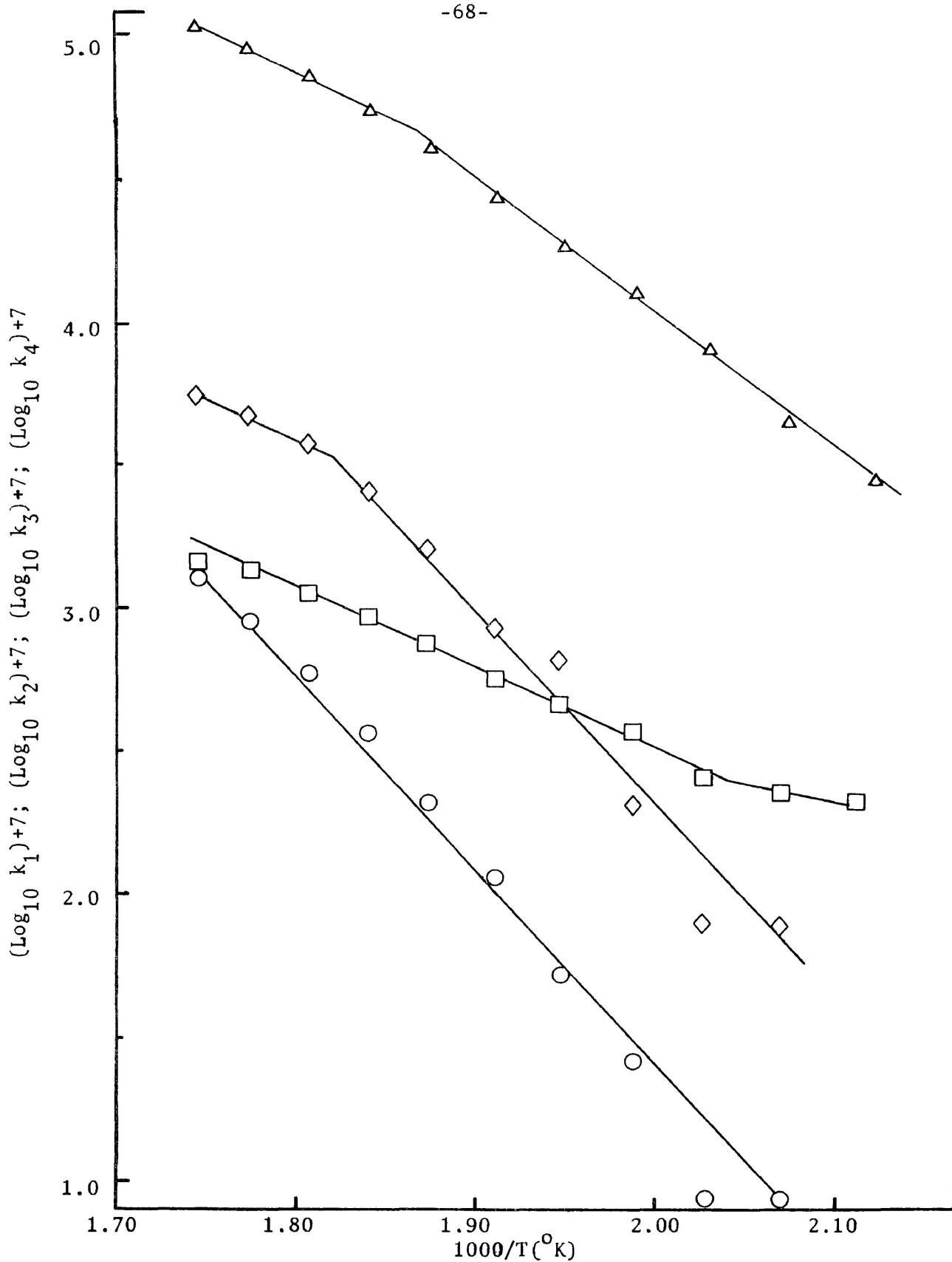


Figure 3.3.6 Arrhenius plots for the decomposition of 2-propanol over $\text{V}_2\text{O}_5:9.09\%\text{Cs}_2\text{SO}_4$: \square k_1 , acetone formation; \circ k_2 , propylene formation; \triangle k_3 , propane formation and \diamond k_4 , 2-propanol consumption.

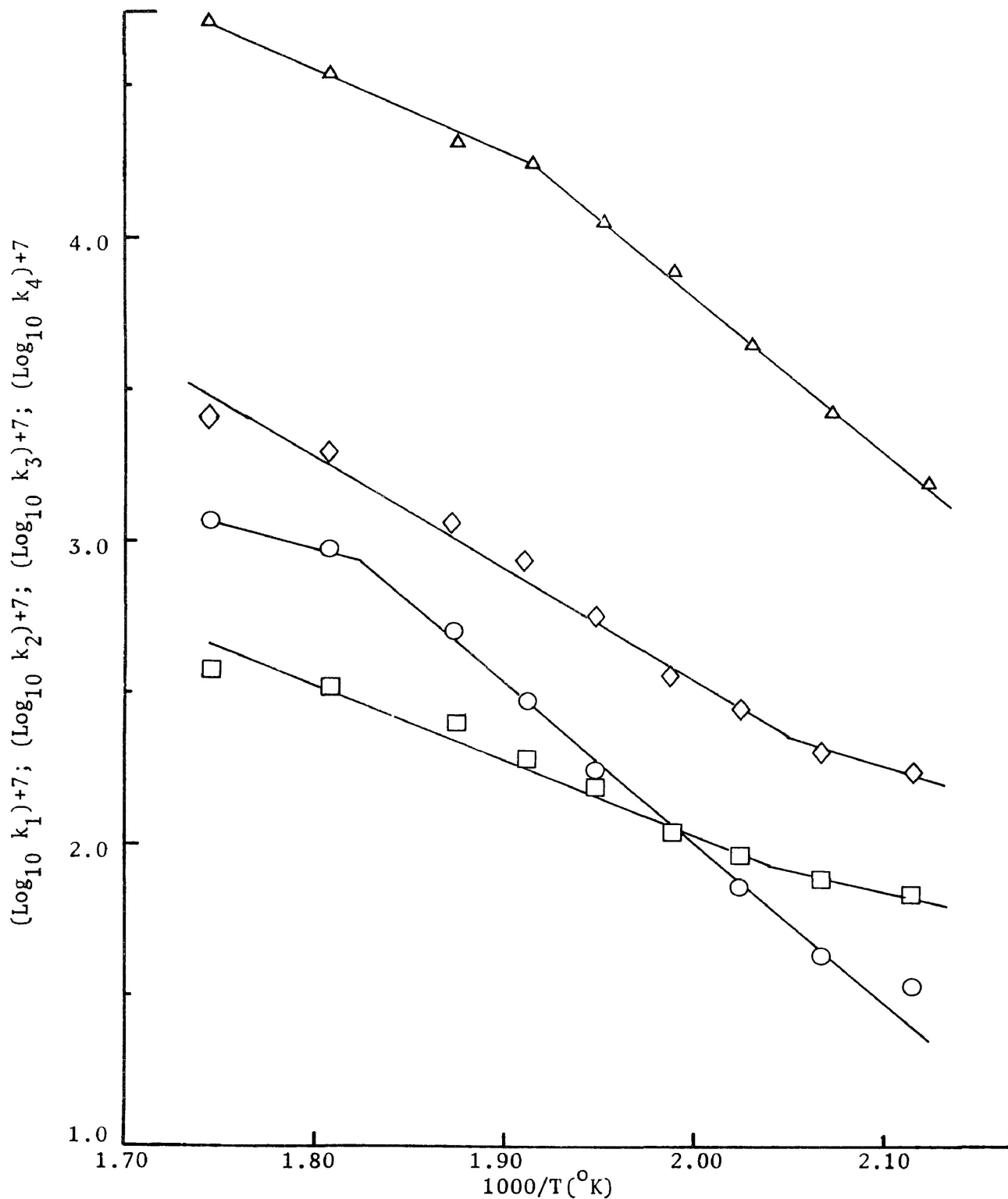


Figure 3.3.7 Arrhenius plots for the decomposition of 2-propanol over $\text{V}_2\text{O}_5:1.01\%\text{K}_2\text{SO}_4$: \square k_1 , acetone formation; \circ k_2 , propylene formation; \triangle k_3 , propane formation and \diamond k_4 , 2-propanol consumption.

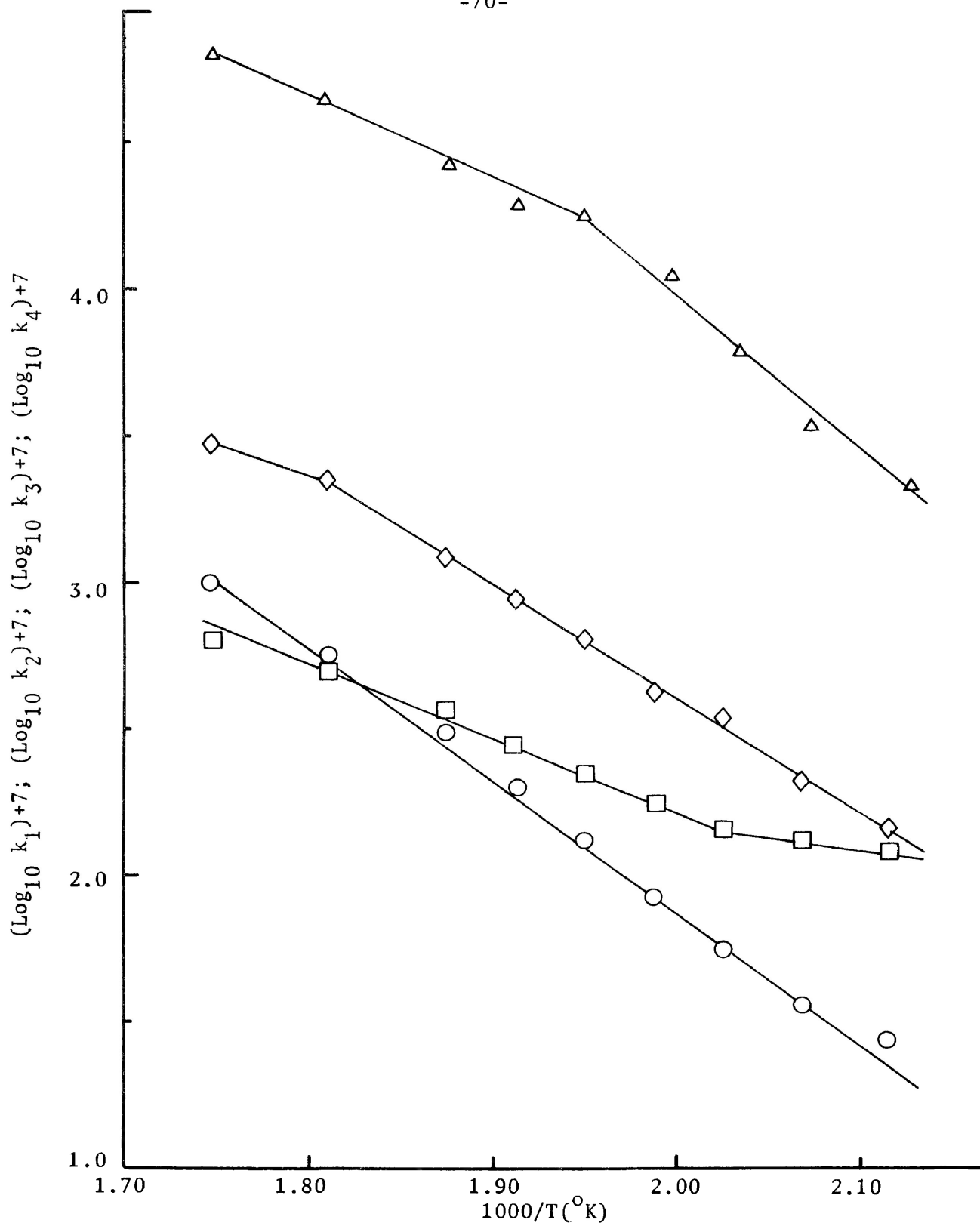


Figure 3.3.8 Arrhenius plots for the decomposition of 2-propanol over $V_2O_5:2.00\%K_2SO_4$: \square k_1 , acetone formation; \circ k_2 , propylene formation; \triangle k_3 , propane formation and \diamond k_4 , 2-propanol consumption.

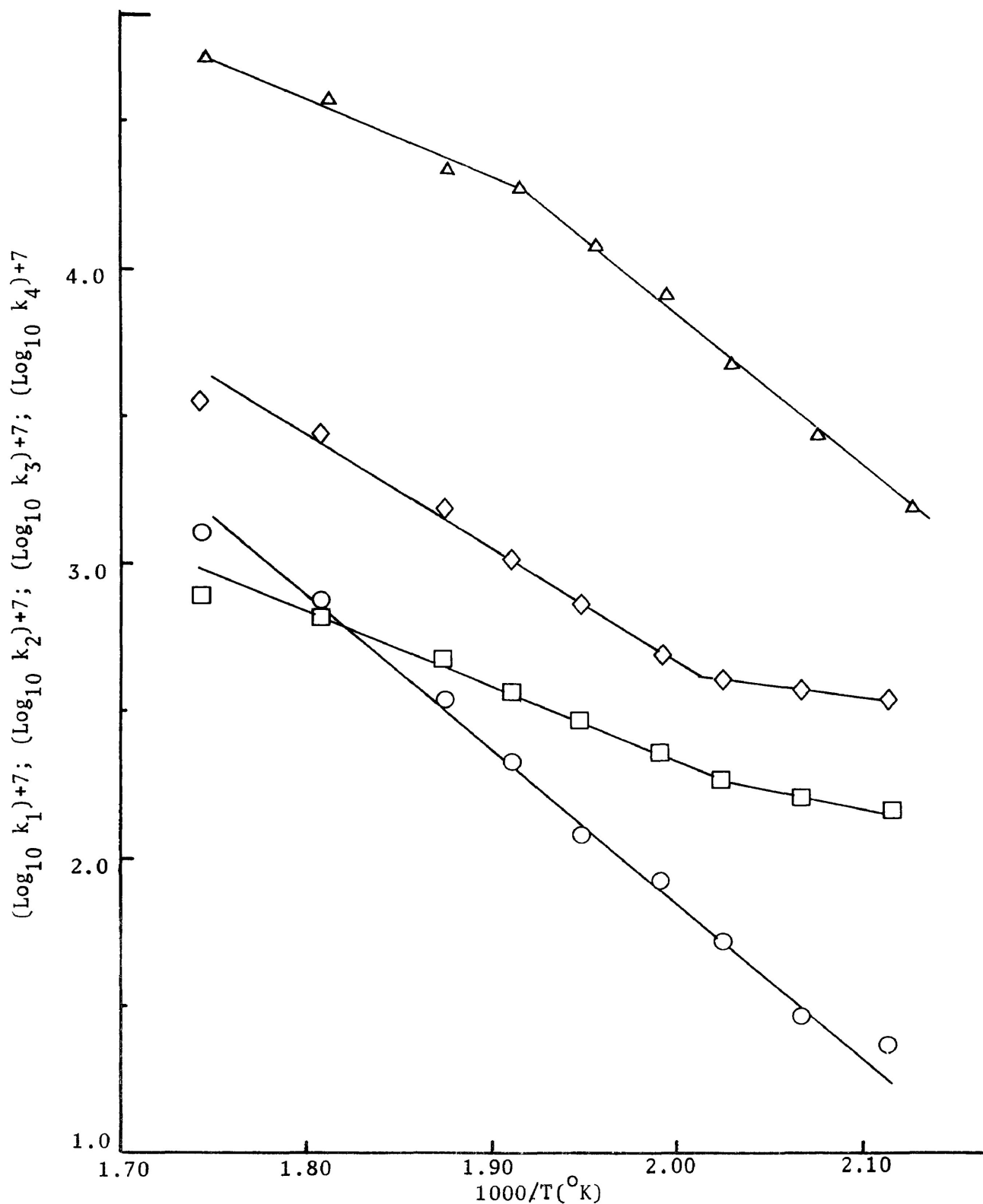


Figure 3.3.9 Arrhenius plots for the decomposition of 2-propanol over $V_2O_5:4.98\%K_2SO_4$: \square k_1 , acetone formation; \circ k_2 , propylene formation; Δ k_3 , propane formation and \diamond k_4 , 2-propanol consumption.

Table 3.3.1 Apparent activation energies for 2-propanol consumption.

Catalyst	Activation energy in temperature range 300-270°C (kcal.mole ⁻¹)	Activation energy in temperature range 260-200°C (kcal.mole ⁻¹)
V ₂ O ₅	11.4	21.1
V ₂ O ₅ :9.09%Li ₂ SO ₄	13.1	20.3
V ₂ O ₅ :9.09%Na ₂ SO ₄	11.9	24.9
V ₂ O ₅ :9.09%K ₂ SO ₄	19.6	26.1
V ₂ O ₅ :9.09%Rb ₂ SO ₄	14.5	26.1
V ₂ O ₅ :9.09%Cs ₂ SO ₄	13.1	30.5
V ₂ O ₅ :1.01%K ₂ SO ₄	17.7	17.7-6.9
V ₂ O ₅ :2.00%K ₂ SO ₄	9.2-17.2	17.2
V ₂ O ₅ :4.98%K ₂ SO ₄	18.3	18.3-4.3

Table 3.3.2 Apparent activation energies for acetone production.

Catalyst	Activation energy in temperature range 300-230°C (kcal.mole ⁻¹)	Activation energy in temperature range 220-200°C (kcal.mole ⁻¹)
V ₂ O ₅	9.8	3.1
V ₂ O ₅ :9.09%Li ₂ SO ₄	12.5	2.7
V ₂ O ₅ :9.09%Na ₂ SO ₄	11.4	4.6
V ₂ O ₅ :9.09%K ₂ SO ₄	11.0	1.8
V ₂ O ₅ :9.09%Rb ₂ SO ₄	12.4	5.1
V ₂ O ₅ :9.09%Cs ₂ SO ₄	13.1	6.0
V ₂ O ₅ :1.01%K ₂ SO ₄	12.8	6.5
V ₂ O ₅ :2.00%K ₂ SO ₄	11.9	4.6
V ₂ O ₅ :4.98%K ₂ SO ₄	12.5	6.0

Table 3.3.3 Apparent activation energies for propylene production.

Catalyst	Activation energy in temperature range 300-270°C (kcal.mole ⁻¹)	Activation energy in temperature range 260-200°C (kcal.mole ⁻¹)
V ₂ O ₅	16.1	22.9
V ₂ O ₅ :9.09%Li ₂ SO ₄	17.2	27.7
V ₂ O ₅ :9.09%Na ₂ SO ₄	27.7	27.7
V ₂ O ₅ :9.09%K ₂ SO ₄	30.5	30.5
V ₂ O ₅ :9.09%Rb ₂ SO ₄	27.7	27.7
V ₂ O ₅ :9.09%Cs ₂ SO ₄	30.5	30.5
V ₂ O ₅ :1.01%K ₂ SO ₄	8.1-23.9	23.9
V ₂ O ₅ :2.00%K ₂ SO ₄	20.3	20.3
V ₂ O ₅ :4.98%K ₂ SO ₄	23.9	23.9

Table 3.3.4 Apparent activation energies for propane formation.

Catalyst	Activation energy in temperature range 300-270°C (kcal.mole ⁻¹)	Activation energy in temperature range 260-200°C (kcal.mole ⁻¹)
V ₂ O ₅	10.0	17.4
V ₂ O ₅ :9.09%Li ₂ SO ₄	13.9	17.4
V ₂ O ₅ :9.09%Na ₂ SO ₄	13.7	23.8
V ₂ O ₅ :9.09%K ₂ SO ₄	13.7	23.8
V ₂ O ₅ :9.09%Rb ₂ SO ₄	11.0	19.2
V ₂ O ₅ :9.09%Cs ₂ SO ₄	13.7	22.9
V ₂ O ₅ :1.01%K ₂ SO ₄	11.9	24.7
V ₂ O ₅ :2.00%K ₂ SO ₄	11.9	23.8
V ₂ O ₅ :4.98%K ₂ SO ₄	12.8	24.7

Apparent activation energies for the various reactions were calculated from the Arrhenius plots and the results are shown in Tables 3.3.1 to 3.3.4.

3.4 Surface Area Determinations

The surface areas of all catalysts were found to change significantly after conditioning, with the exception of the vanadium pentoxide melt containing 9.09 mole percent potassium sulphate, Table 3.4.1. Surface areas measured after reaction and after the 24 hour conditioning period were found not to change appreciably. Figures 3.4.1 and 3.4.2 show typical 'BET' plots for $V_2O_5:9.09\%K_2SO_4$ before and after conditioning respectively.

3.5 X-ray Diffraction

X-ray powder patterns of the catalysts before reaction, with the exception of the melt containing 9.09 mole percent sodium sulphate, showed lines attributable to vanadium pentoxide, see Appendix II.

After catalysis, all catalysts exhibited a different powder pattern. The extreme cases were the cesium sulphate and 9.09 mole percent potassium sulphate melts. The latter gave a distinct but altered powder pattern while the pattern obtained with the former sample was typical of an amorphous solid, Appendix II. The other catalyst samples exhibited very faint, broad diffraction lines.

A sample of used $V_2O_5:9.09\%Li_2SO_4$ catalyst which was heated in air at $450^\circ C$ for 1 hour gave a distinct powder pattern. An additional sample was heated in air at $600^\circ C$ for 12 hours. This sample regained its orange-brown colour and the diffraction pattern was similar to that of $V_2O_5:9.09\%Li_2SO_4$ which was unused, Appendix II.

Table 3.4.1 The effect of the reaction on the surface areas of the catalysts.

Catalyst	Surface area before use* ($\text{m}^2 \cdot \text{g}^{-1}$)	Surface area after conditioning and after reaction ($\text{m}^2 \cdot \text{g}^{-1}$)	Ratio of surface area before use to area after reaction
V_2O_5	0.93	9.17	0.10
$\text{V}_2\text{O}_5:9.09\%\text{Li}_2\text{SO}_4$	2.27	12.70	0.18
$\text{V}_2\text{O}_5:9.09\%\text{Na}_2\text{SO}_4$	0.36	1.11	0.32
$\text{V}_2\text{O}_5:9.09\%\text{K}_2\text{SO}_4$	0.72	0.83	0.87
$\text{V}_2\text{O}_5:9.09\%\text{Rb}_2\text{SO}_4$	1.54	2.77	0.56
$\text{V}_2\text{O}_5:9.09\%\text{Cs}_2\text{SO}_4$	1.14	2.83	0.40
$\text{V}_2\text{O}_5:1.01\%\text{K}_2\text{SO}_4$	-----	8.58	-----
$\text{V}_2\text{O}_5:2.00\%\text{K}_2\text{SO}_4$	-----	4.88	-----
$\text{V}_2\text{O}_5:4.98\%\text{K}_2\text{SO}_4$	-----	3.85	-----

*ie. before conditioning and reaction.

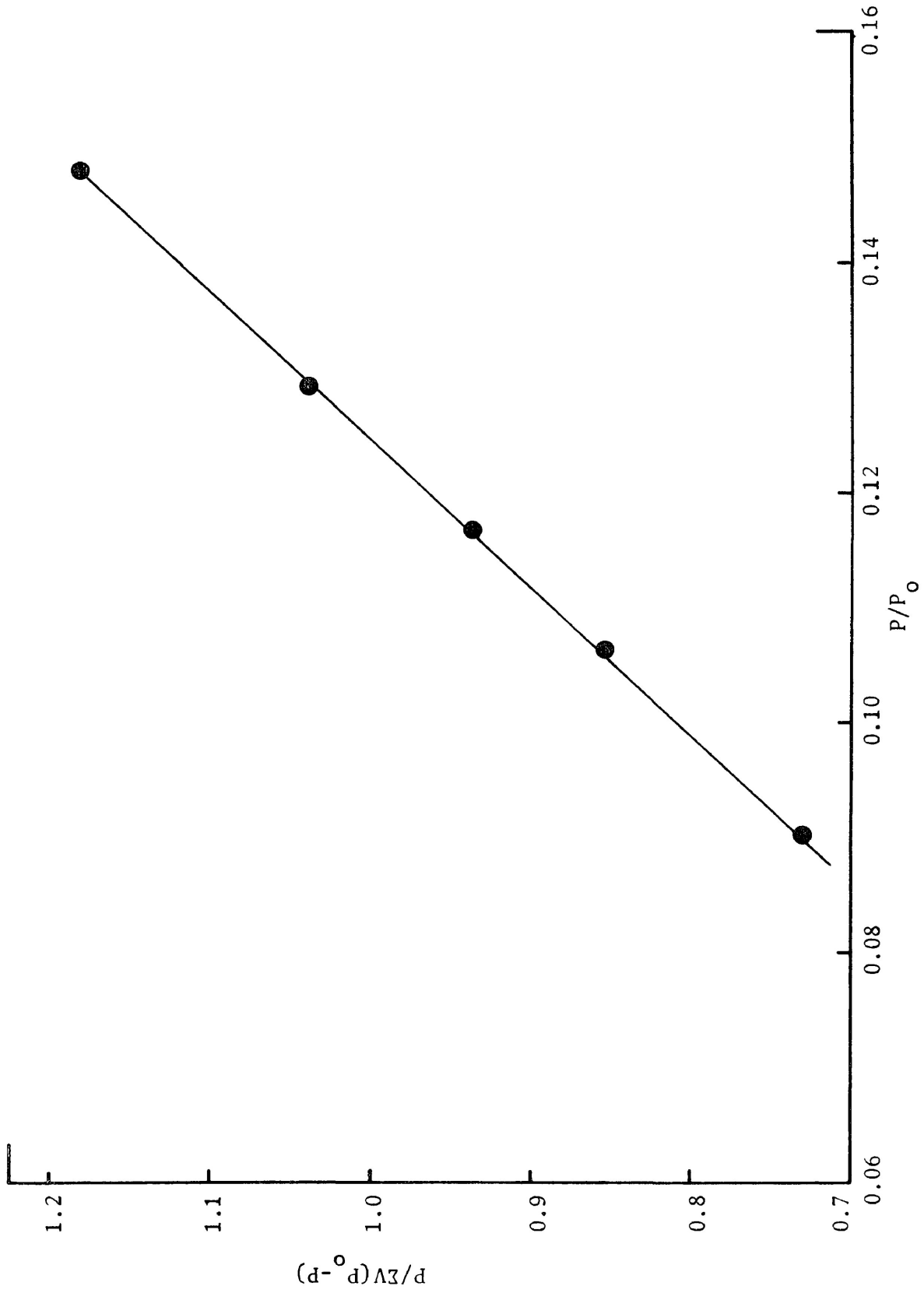


Figure 3.4.1 Typical Krypton surface area plot for 'unused' $V_2O_5:9.09\%K_2SO_4$.

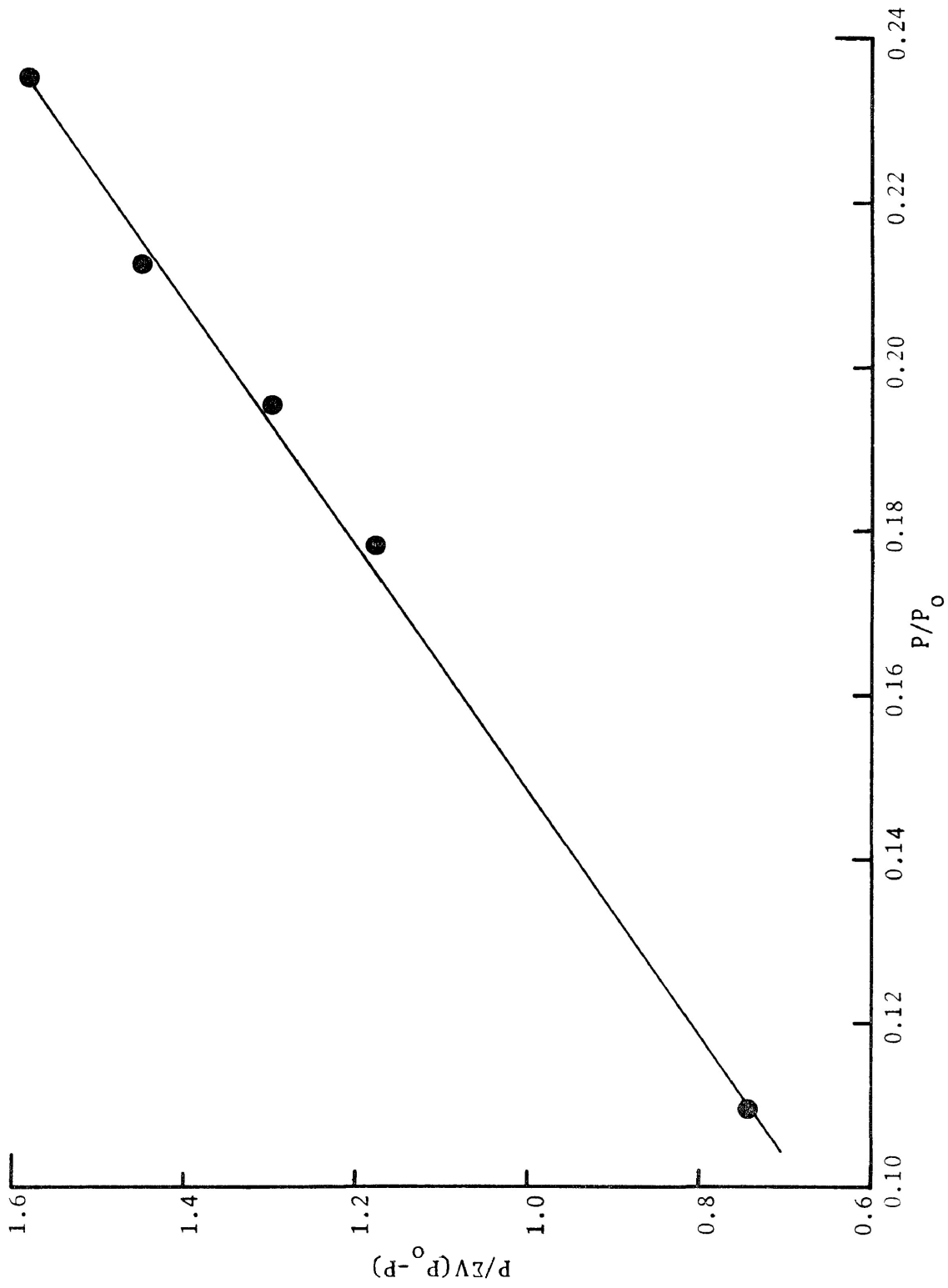


Figure 3.4.2 Typical Krypton surface area plot for 'used' $V_2O_5:9.09\%K_2SO_4$

4. DISCUSSION

4.1 Diffusion Effects

It is well established that gas transport phenomena and diffusion effects play an important role in the determination of experimental kinetic data (74). The process which determines the overall rate may be one or a combination of the following steps (71):

- (1) Transport of reactants to the catalyst surface.
- (2) Adsorption of reactants.
- (3) Surface reaction.
- (4) Desorption of products.
- (5) Transport of products away from the surface.

When steps (1) and/or (5) are rate determining the reaction is said to be diffusion controlled.

Diffusion processes on porous catalysts can be classified as; (i) mass transfer to and from the catalyst surface (external diffusion) and (ii) mass transfer in and out of catalyst pores (internal diffusion) (75). Surface diffusion is frequently detected by varying the flow rates, Section 3.1.1, while the influence of pore diffusion is often assessed from particle size experiments, Section 3.1.2, (72, 75).

Variations in the total flow rate indicated that propane production was influenced by transport phenomena at higher temperatures, Figure 3.1.2. Activation energies for propane formation, Table 3.3.4, at higher temperatures were $<14 \text{ kcal.mole}^{-1}$ which lies towards the

upper limit of the range usually associated with diffusion processes (71). At these temperatures the chemical rate of propane formation may approach that of the transport process and thus the reaction may then be influenced by transport factors. At temperatures lower than 260°C the rate of propane formation has decreased considerably, Figure 3.2.4, and the reaction then becomes independent of transport phenomena, as indicated by the results of the flow rate investigations at 230°C, Section 3.1.1, and the values of activation energies, Table 3.2.4.

The rates of reaction for propylene and acetone formation were not affected by variations in total flow at lower temperatures and showed only a slight variation at higher temperatures. Surface diffusion effects may, therefore, be negligible for these reactions, Section 3.1.1. Variations in the rate of 2-propanol consumption as the total flow was altered can be related to changes in the rate of propane formation, as discussed previously, Section 3.1.1.

Internal diffusion processes were investigated by varying the particle size of the $V_2O_5:9.09\%K_2SO_4$ catalyst, Section 3.1.2. These experiments indicated that rates of reaction were unaffected by changes in particle size at the temperatures investigated, Table 3.1.1.

It may be concluded that internal diffusion phenomena were not rate controlling in the range of conditions used in this work while external diffusion processes linked with propane formation were limited to higher temperatures. At lower temperatures, where kinetic experiments were carried out, both external and internal diffusion processes were not rate controlling.

4.2 Catalytic Decomposition of 2-propanol

4.2.1 Conditioning Effects

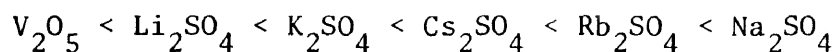
The decomposition of 2-propanol over vanadium pentoxide and modified vanadium pentoxide catalysts involved a hydrogenation-type reaction forming propane, dehydrogenation to acetone and dehydration to propylene. Contributions of other reactions, in the temperature range used, were absent. Thus condensation reactions previously observed by McCaffrey et. al. (37) on manganese oxides were not detected with the present catalysts.

The effect of catalyst ($V_2O_5:9.09\%K_2SO_4$) conditioning on product distribution has been described in Section 3.2.1. Initially 2-propanol reacted on the catalyst surface to produce propylene and acetone both of which may on desorption leave surface sites occupied by hydrogen. As more sites become occupied by hydrogen, propylene and acetone production decreased while propane production became evident, Figure 3.2.1. Propane may be produced by hydrogen extraction from the surface. A more detailed discussion of possible mechanisms is given in Section 4.2.5.

4.2.2 Selectivities for Acetone Formation

The selectivity ratios for acetone formation increased as reaction temperatures decreased from 300^o to 200^oC indicating a preference towards the dehydrogenation reaction at lower temperatures, Table 3.2.1.

Between 300^o and 260^oC the selectivity ratios, for vanadium pentoxide and the melts containing 9.09 mole percent of the alkali metal sulphates, exhibited the following trend:



Below 250°C the order changed and no apparent trends were observed.

The Cs_2SO_4 , Na_2SO_4 and K_2SO_4 melts showed the highest selectivity values.

The series of catalysts containing varying mole percentages of K_2SO_4 exhibited no apparent trends in selectivity towards acetone formation, other than a tendency to increase in value as the reaction temperatures decreased, Table 3.2.1.

4.2.3 Activation Energies

The experimental activation energy for 2-propanol consumption ranged from a minimum of $20.3 \pm 1 \text{ kcal.mole}^{-1}$ for $\text{V}_2\text{O}_5:9.09\%\text{Li}_2\text{SO}_4$ to a maximum value of $30.5 \pm 1 \text{ kcal.mole}^{-1}$ for $\text{V}_2\text{O}_5:9.09\%\text{Cs}_2\text{SO}_4$, Table 3.3.1, between 200° and 260°C. In the high temperature region the values ranged from $11.4 \pm 1 \text{ kcal.mole}^{-1}$ for V_2O_5 to $19.6 \pm 1 \text{ kcal.mole}^{-1}$ for $\text{V}_2\text{O}_5:9.09\%\text{K}_2\text{SO}_4$ which may reflect the influence of transport effects created by the intervention of the propane-forming reaction.

The catalysts containing varying amounts of K_2SO_4 gave activation energies around $18.5 \pm 1 \text{ kcal.mole}^{-1}$ between 260° and 200°C. However breaks in the Arrhenius plots, Figure 3.3.7 and Figure 3.2.9, were observed at 220°C for the catalysts containing 1.01 and 4.98 mole percent K_2SO_4 .

The activation energy values from 260° to 200°C, for the melts containing the various alkali metal sulphates, Table 3.3.1, were in good agreement with the previous values of $26 \text{ kcal.mole}^{-1}$ (37) and $25.4 \text{ kcal.mole}^{-1}$ (76) obtained for the overall decomposition of 2-propanol over manganese (II) oxide between 320°C and 365°C.

Between 300° and 270°C the apparent activation energies for

propane formation varied from 10.0 ± 1 kcal.mole⁻¹ for V₂O₅ to 13.9 ± 1 kcal.mole⁻¹ for V₂O₅:9.09%Li₂SO₄, Table 3.3.4. The low activation energies in this region are most likely a consequence of the diffusion effects observed for the propane-forming reaction, Section 4.1. In the 'low' temperature region the activation energies ranged from a low of 17.4 ± 1 kcal.mole⁻¹ for V₂O₅ to a high of 24.7 ± 1 kcal.mole⁻¹ for V₂O₅:1.01%K₂SO₄.

The activation energies for acetone formation fall into two distinct kinetic regions. At higher temperatures (300-230°C) the values lay between 9.8 ± 1 and 13.1 ± 1 kcal.mole⁻¹, while at lower temperatures (220-200°C) the values were very low, 1.8 ± 1 to 6.5 ± 1 kcal.mole⁻¹. The low activation energies are unusual since the acetone reaction was found to be free of diffusion effects over the low temperature range, Section 4.1.

Two kinetic regions for acetone formation were reported by McCaffrey et. al. (39) for a series of manganese oxide catalysts. The activation energies at higher temperatures ranged from 26 to 28 kcal.mole⁻¹ while at lower temperatures they varied from 5 to 8 kcal.mole⁻¹. The two regions were explained in terms of differences in the rate-controlling steps or by variations in the energy of activation between adsorbate molecules and adsorption sites (77).

Changes in the type of surface conduction, similar to those suggested as explaining the results of 2-propanol decompositions over chromia at 400°C (78), may also account for the observed kinetic break.

The apparent activation energies for propylene formation showed a fair tendency to remain constant over the entire temperature range studied, Table 3.3.3. At higher temperatures several catalysts exhibited somewhat lower activation energies, the most notable being the melt

containing 1.01 mole percent K_2SO_4 where the value dropped from 23.9 ± 1 to 8.1 ± 1 kcal.mole⁻¹. Similar phenomena to those discussed for the acetone activation energies may account for the kinetic break in the Arrhenius plots.

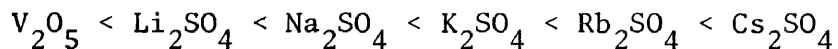
The activation energies for propylene formation are comparable with values of 20.9 kcal.mole⁻¹ obtained for the dehydration of 2-propanol over V_2O_3 (79). However, the activation energies for acetone formation are considerably lower than the value of 20.6 kcal.mole⁻¹ reported for V_2O_3 (79). McCaffrey et. al. (80) found activation energies of 22 and 42 kcal.mole⁻¹ respectively for dehydrogenation and dehydration of 2-propanol from 74° to $104^\circ C$. Again these activation energies, for both dehydration and dehydrogenation were much higher than those determined in the present study— indicative perhaps of the increase in the degree of severity in catalyst conditioning in the present study over that adopted in the previous work.

The catalysts used here were conditioned for a much longer period and at higher temperatures in what has been reported (81) to be a very efficient reducing atmosphere. This would have the effect of reducing the oxygen to vanadium ratio, as exhibited under much milder reducing conditions (82, 83), to considerably less than that in the study by previous workers (80).

Further, it has been shown (39) that a decrease in the oxygen content of a series of manganese oxide catalysts resulted in a decrease in the activation energies for the dehydration of 2-propanol. This would tend to support the hypothesis that the overall decrease in the observed activation energies over those previously reported, resulted from a decrease in the oxygen to vanadium ratio. The overall decrease

in activation energy may further suggest destabilization of the dehydration intermediate brought about by a decrease in the strength with which the dehydration centres are held by the surface (84, 85).

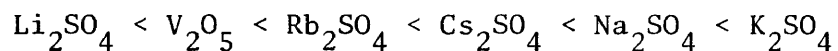
A further trend was observed in the variation of activation energy with the nature of the alkali metal cation with the melts containing 9.09 mole percent alkali metal sulphate, Table 3.3.3. These activation energies, with minor exceptions within experimental error, exhibited the following trend:



This is the same order as that observed for the increase in mobility of oxygen in this series of catalysts (49, 50). The trend may therefore be indicative of the change which occurs in the oxygen/vanadium ratio of the individual catalysts during conditioning prior to reaching the steady state.

4.2.4 Reaction Rates and Kinetics

In general the rates for propylene formation, acetone formation and 2-propanol consumption, over vanadium pentoxide and the melts containing 9.09 mole percent alkali metal sulphate showed the following trend in activity:

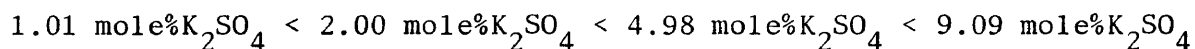


However below 280°C fluctuations in the rates for several of the catalysts caused slight changes in this order.

The rates for propane formation gave the same general pattern but between 260° and 220°C fluctuations in the rates for the Na₂SO₄ and

K_2SO_4 melts were evident.

All the reaction rates for the melts containing varying mole percentages of K_2SO_4 at any defined temperature can be expressed in the form of an activity series:



A similar pattern has been reported for the rates of oxygen exchange and the oxidation of hydrogen over vanadium pentoxide melts containing potassium sulphate (52). It should be noted, however, that as the catalyst additive concentration was varied from $V_2O_5:0.1K_2SO_4$ to $V_2O_5:1.0K_2SO_4$ a maximum in the rate of exchange was observed for the $V_2O_5:0.3K_2SO_4$ catalyst (52).

On the basis of a Langmuir-Hinshelwood model, the pseudo-zero order rate dependencies with respect to concentration of all components in the dehydration and dehydrogenation reactions may be interpreted in terms of a very rapid saturation of any surface sites present which might be amenable to the adsorption of the component. Alternatively an extremely rapid desorption of the adsorbed species into the gas phase may also account for the zero order kinetics.

The experimental reaction rate for the propane-forming reaction exhibited a rate order of 0.3 with respect to 2-propanol, Section 3.2.3, while all other components caused only temporary disturbances in steady state conditions, Section 3.2.4 to 3.2.6, indicating a zero order rate dependency on the concentrations of these components.

These temporary effects can be interpreted in terms of 'settling' changes at the catalyst surface. The reaction equilibrium or steady

state is initially disturbed or upset by the introduction of a reaction component, but, with time, it recovers and remains unaffected by further changes in the concentration of the added component.

The experimental data for partial pressure changes of 2-propanol, Section 3.2.3, were treated by means of statistical analysis, utilizing the APL computer programmes, FIT, LHDATA and LH (Appendix I), in an attempt to derive rate equations consistent with the observations for the propane reaction. The following kinetic equation:

$$r = \frac{kP_{alc}}{1 + kP_{alc}} \quad \dots 4.2.1$$

where k is the rate constant for the decomposition of the alcohol and P_{alc} is the partial pressure of 2-propanol, yielded a correlation coefficient of 0.998 for the correlation graph, Figure 4.2.1.

Equation 4.2.1 implies Langmuir-Hinshelwood type kinetics in which the rate of reaction is proportional to the amount of alcohol adsorbed on the surface which is governed by a Langmuir isotherm where the adsorbate occupies one surface site (86).

4.2.5 Reaction Mechanisms

The heterogeneous decomposition of 2-propanol has been interpreted in terms of various mechanisms (22, 87, 88). The dehydration reaction in particular, which has been used as an indication of the acid-base properties of the catalyst, can and has been explained in terms of various elimination mechanisms (89, 90).

Knözinger (89) proposed E-2 type reaction intermediates for the dehydration of primary, secondary and tertiary alcohols over alumina

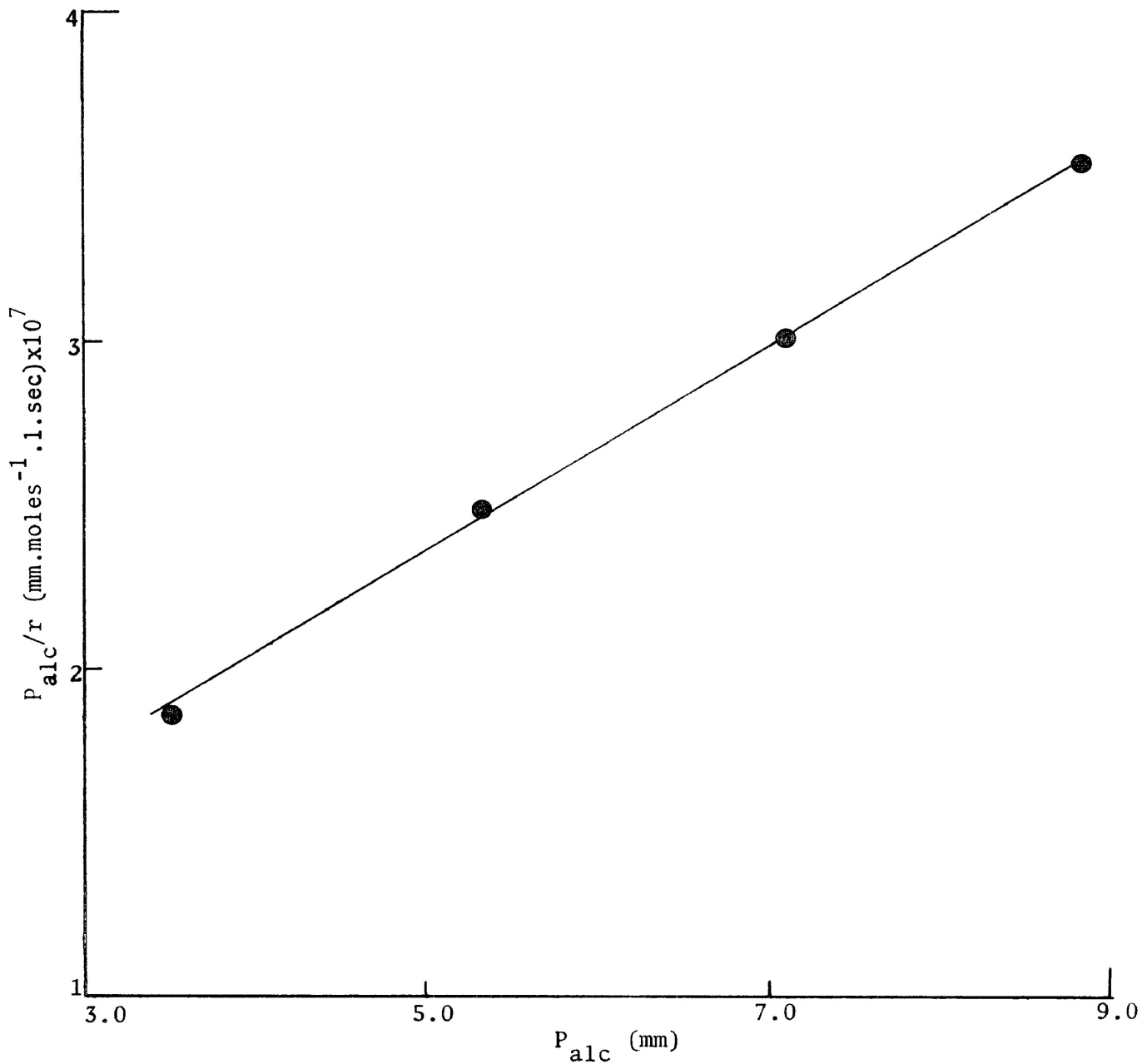
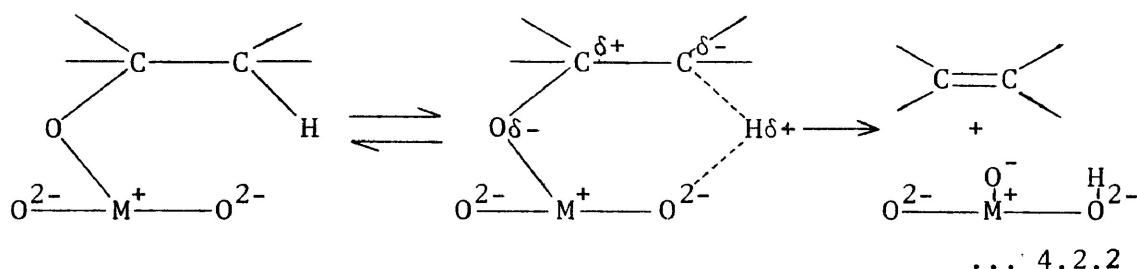


Figure 4.2.1 Comparative plot for the rate of propane formation from the rate expression $r = \frac{kP_{alc}}{1+kP_{alc}}$.

below 200°C. At higher temperatures, depending on the reactant structure, dehydration was thought to proceed via E-1 type mechanism intermediates (89).

In general, there are three possible mechanisms for elimination reactions over polar catalysts; the E-1; the cis-E-2 and the trans-E-2 (91). The E-1 mechanism has often been ruled out for many catalysts since it requires strong acidic centres, which are not usually present on the surface (92).

For thoria catalysts the cis- and trans-E-2 mechanisms were considered to be unfavourable and a modified E-1 mechanism, the E-1cB, involving basic centres on the surface (92) was proposed:



In an investigation of the acid-base properties of the SnO₂-V₂O₅ system (93) it was suggested that the activity for dehydration of 2-propanol to propylene represents the surface acidity and the ratio of dehydrogenation rate to dehydration rate was a rough index of the basicity. The incorporation of V₂O₅ into SnO₂ catalysts was found to alter the acid-base properties of the system and on basic catalysts dehydrogenation was favoured while on acidic catalysts dehydration was reported as being predominant (93). Krylov (29) has also suggested that dehydration is favoured on acidic oxides.

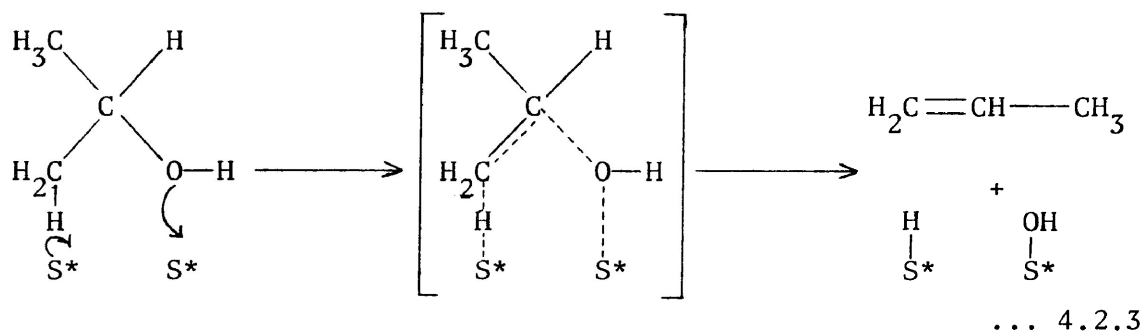
This seems to be in conflict with more recent results presented

by Canesson and Blanchard (92) who suggested that basic centres were preponderant in the dehydration of secondary alcohols over thoria. Clearly, then, there is still some controversy as to the effect of acid-base properties of the catalysts on the dehydration of alcohols.

Mechanisms for the dehydrogenation have been suggested as involving initial adsorption at an electronegative surface site with subsequent two-point adsorption (87).

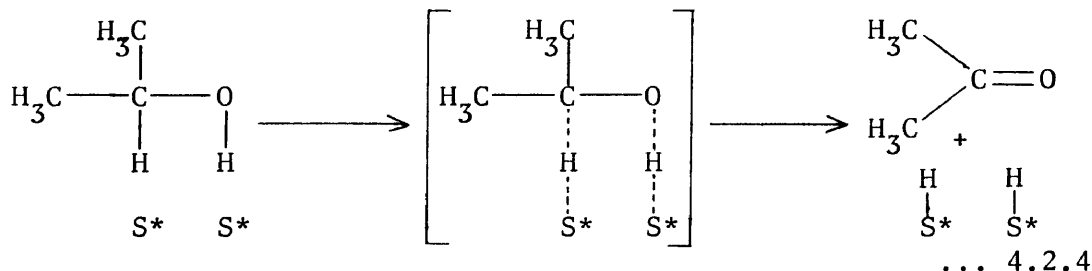
The reactions involved in this work can be explained in terms of intermediates typical of elimination type mechanisms.

Propylene may be formed via an E-2 type mechanism on adjacent vacant surface sites:



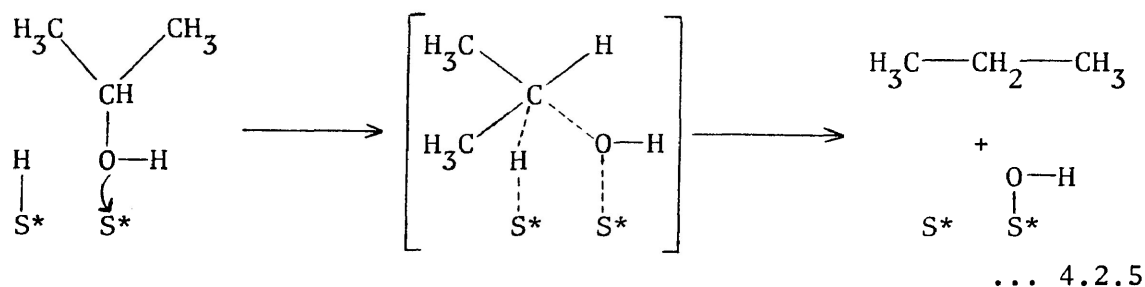
The attachment of the alcohol to the surface through the hydroxyl group and a β hydrogen has been reported as involving little strain even on plane surfaces (94)

Acetone production may involve the following intermediate:



A two point adsorption intermediate has been previously reported for acetone formation (87).

For both mechanisms, Equations 4.2.3 and 4.2.4, 2-propanol is adsorbed on a 'clean' surface and reacts with unoccupied surface sites to produce propylene and acetone. Both schemes suggest that some of the surface sites are occupied by hydrogen (atomic) and hydroxyl groups. As more sites are occupied by hydrogen 'dehydration' may become limited to a one-point adsorption centre (E-1 type) and if hydrogen is available on a neighbouring site then hydrogen abstraction from this site may give propane:



The level of propane formed should increase to some limiting value with propylene production decreasing accordingly. This trend was, in fact, observed for the V₂O₅:9.09%K₂SO₄ catalyst, Section 3.2.1. The derived rate equation for propane formation, 4.2.1, supports the one point adsorption process proposed for the propane reaction.

The mechanism implies that propane would form directly from 2-propanol and not from hydrogenation of propylene. This hypothesis has been supported in some measure by Balandin et. al. (95) who studied the formation of propane from 2-propanol on a V₂O₃ catalyst at 315°C. From isotopic labelling of added propylene they concluded that propane

was formed almost entirely by the hydrogenolysis of the alcohol and not by hydrogenation of the propylene. The absence of hydrogen in the gas stream, Section 2.3, also suggests that hydrogen was retained on the surface and perhaps involved in propane formation.

As Knözinger reported (89) E-1 mechanisms involving one-point adsorption are favourable at higher temperatures which may explain the increase in the rate of propane formation with increase in temperature, Figure 3.2.4.

4.3 Surface Areas

The addition of alkali metal sulphates to vanadium pentoxide caused some changes in surface areas, however, after conditioning the surface areas of all the catalysts had increased, some quite significantly, Table 3.4.1. The increase may be due to reduction of the catalyst during conditioning.

The ratio of the surface areas before use to the surface areas after reaction was found to follow the same trend as the surface 'Tammann' temperature for the alkali metal sulphate additives, Figure 4.3.1. This 'Tammann' temperature was taken as 0.3 times the melting temperature (T_m) of the alkali metal sulphate. Vanadium pentoxide was also considered and fell into the same pattern.

The temperature $0.3 T_m$, commonly assumed to be a lower limit, is the temperature above which ionic diffusion begins to occur thus allowing vacancies to migrate away from the contact area (96). At temperatures above $0.3 T_m$ defects in the surface of a solid become mobile so that surface migration of ions can also occur (97), although these effects have been reported for temperatures as low as $0.25 T_m$ (96, 98).

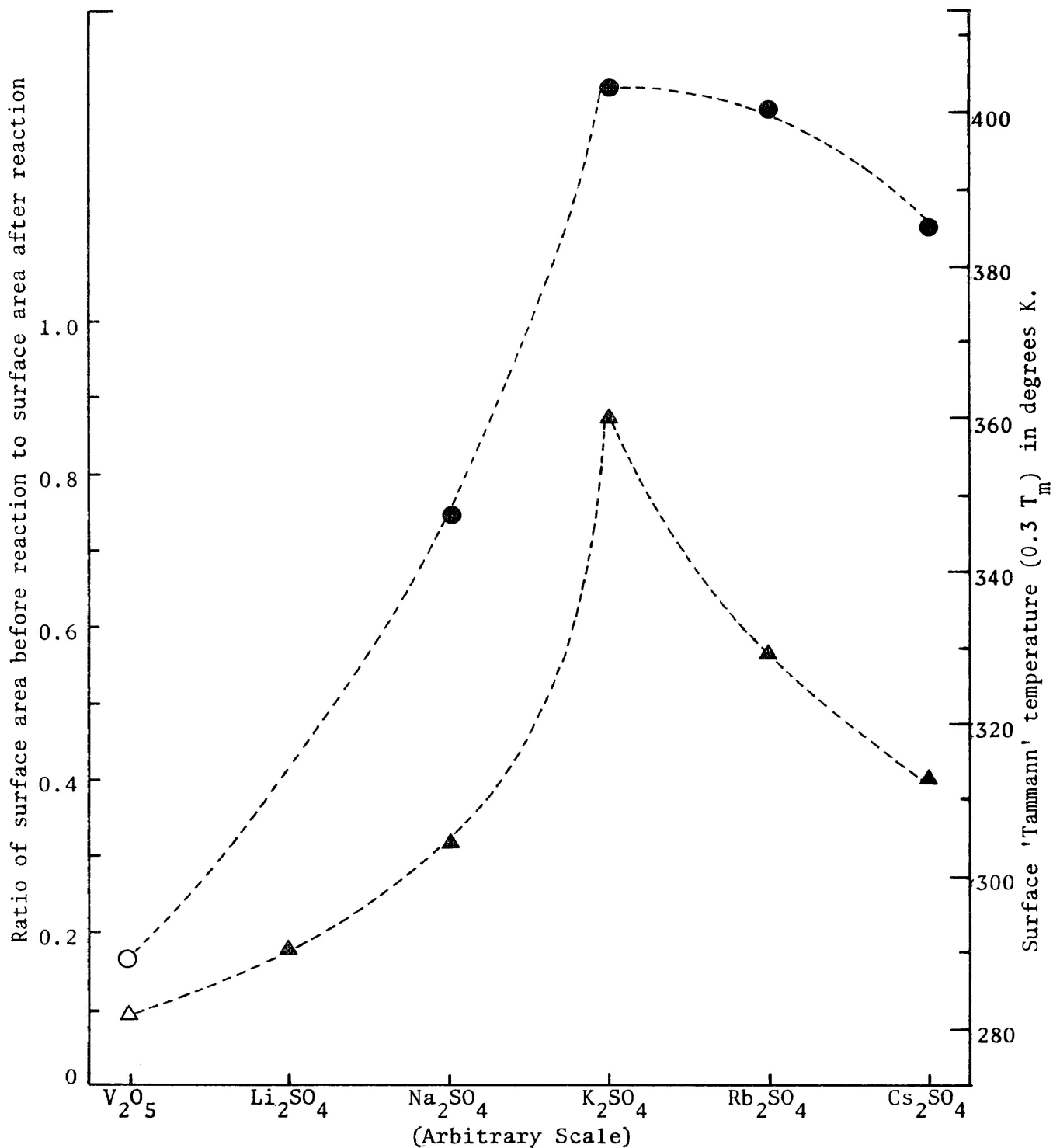


Figure 4.3.1 Correlation diagram between the ratio of surface area before and after reaction for; Δ V_2O_5 and the melts containing 9.09 mole percent of; the alkali metal sulphate, \blacktriangle , and the surface 'Tammann' temperature ($0.3 T_m$) for; \circ V_2O_5 and the added alkali metal sulphates, \bullet .

'Tammann' temperatures are frequently used when discussing sintering of solids— an effect which usually causes a decrease in surface area, thus it seems unusual for increases in surface areas to be related to 'Tammann' temperatures. It is important to note however, that with the exception of the V_2O_5 the values of $0.3 T_m$ are for the alkali metal sulphates and not the actual catalysts used. Values for $0.3 T_m$ for the actual catalysts used and Li_2SO_4 have not been calculated since their melting points could not be determined accurately.

The values for $0.3 T_m$ and $0.25 T_m$ lie below the range of temperatures used in this work, thus changes in surface areas might be related to surface migrations on the various sulphates.

The rates of reaction when normalized to the surface areas after reaction exhibited the trends previously discussed. It is interesting to note however, that the rates when related to a unit weight rather than to a unit surface do not differ greatly from catalyst to catalyst which again emphasizes the importance of catalyst surface area. The same effect has been reported for the rates of isotopic oxygen exchange over a similar series of vanadium pentoxide catalysts (49).

4.4 X-ray Analysis

The X-ray diffraction patterns of the catalysts before reaction, with the exception of the melt containing Na_2SO_4 , showed lines attributable to vanadium pentoxide, Appendix II.

Sodium sulphate melted with V_2O_5 has been reported to form bronzes containing compounds such as $NaVO_3$, $Na_4V_2O_7$ and Na_3VO_4 (99), traces of which may be present in the Na_2SO_4 melt used in this work.

Reduction of the catalysts during reaction was apparent from the complete change in all the X-ray diffraction patterns obtained from

reacted catalysts, Appendix II. Previously, McCaffrey et. al. (80) reported partial reduction of V_2O_5 , used in 2-propanol decompositions between 74-104°C, as indicated by a colour change from pale-orange to brown-green. However and perhaps not surprisingly, in view of the limitations of the technique in detecting trace components, the X-ray diffraction pattern showed only the V_2O_5 oxide structure. A similar reduction has been observed in the oxidation of methyl alcohol at 300-350°C (100).

Vanadium pentoxide, used in vapour phase oxidation reactions, has been shown to thermally dissociate evolving oxygen (101). X-ray diffraction patterns of these V_2O_5 samples, between 20° and 460°C, showed the structure to be unchanged, however, chemical reaction in the same temperature range distorted the crystal structure.

Changes in colour of all the present catalysts were observed after reaction and indicated that some reduction of the solids had occurred. The catalysts, with the exception of the 9.09 mole percent Na_2SO_4 melt which was grey-black and V_2O_5 which was pale-orange, were a brown-orange colour before reaction, while after reaction all were black.

The diffraction patterns after reaction showed some lines attributable to non-stoichiometric oxides of vanadium as well as some lines which could not be accounted for from published data. These new lines may be due to the presence of organometallic complexes, perhaps similar to vanadium isopropoxide and/or alkali metal vanadium oxides formed on the catalyst surface. The possibility is being investigated further in these laboratories.

Changes in the X-ray powder patterns may also be a result of

displacement of the lines as a result of the non-stoichiometry of the catalysts (102). Line broadening effects caused by; lattice distortion or lattice strain in which interplanar spacings vary from region to region in the crystal; imperfections in the packing of the atoms in the crystal (stacking faults); or small crystallite size (96) may also account for the changes in the X-ray powder patterns.

The X-ray diffraction patterns of used $V_2O_5:9.09\%Li_2SO_4$ samples which were subsequently heated in air, Section 3.5, showed that the original catalyst structure could be recovered by this form of exposure to oxygen at higher temperatures. Thus the powder patterns obtained for these samples were very similar to those of the catalyst before reaction with only a few additional lines present, Appendix II. This recovery process suggests that loss of oxygen from the bulk of the catalyst may cause reduction and that the additional lines in the used samples may be related to the presence of traces of organometallics and/or alkali metal vanadium oxides.

5. CONCLUSION

It has been shown that 2-propanol decomposes to give three distinct products: acetone; propylene and propane over vanadium pentoxide and modified vanadium pentoxide catalysts.

It has been proposed that Langmuir-Hinshelwood kinetics in conjunction with modified E-1 and E-2 type elimination reaction mechanisms can account for all of the products. It was further suggested that the activity and selectivity of the catalyst is a function of the vanadium/oxygen ratio and the mobility of surface oxygen.

A correlation between the ratio of surface area of the catalysts before and after reaction and the surface 'Tammann' temperature ($0.3 T_m$) of the additives, was found to exist. This feature was also considered to be a function of oxygen mobility.

6. SUGGESTIONS FOR FURTHER WORK

Studies of the catalyst surface using ESCA or related methods could be undertaken in an endeavour to identify more closely the surface sites, and perhaps the different phases, found in the used catalysts.

Isotopic labelling experiments could give more information on reaction mechanisms and possible reaction intermediates.

Further, the solids could be studied in separate experiments, using semiconductivity and X-ray techniques, as well as ESCA or Electron Microprobe methods, since these materials have intrinsic importance as fast switching devices in electronics.

REFERENCES

1. O. V. Krylov, 'Catalysis by Non-Metals', Academic Press, New York, (1970), pp. 115-134.
2. E. F. McCaffrey, Ph.D. Thesis, The Queen's University of Belfast, (1972).
3. F. H. Constable, Proc. Roy. Soc. , A107, 270, 279, (1925) and A113, 113, 254, (1927).
4. W. G. Palmer and F. H. Constable, Proc. Roy. Soc., A107, 255, (1925).
5. W. E. Garner, D. A. Dowden and J. F. Garcia de la Banda, Anales Real. Soc. Espan. Fis. Quim., 50B, 35, (1954).
6. F. F. Volkenstein, Probl. Kinetiki i Kataliza, 8, 202, (1955).
7. G. M. Schwab and E. Schwab-Agallidis, J. Am. Chem. Soc., 71, 1806, (1949).
8. A. Eucken and K. Heuer, Z. Phys. Chem., 196, 40, (1950).
9. A. Eucken, Naturwissenschaften, 36, 48, (1949).
10. M. E. Winfield, 'Catalysis' edited by P. H. Emmett, 7, Reinhold, New York, (1960).
11. V. N. Ipatieff, Ber., 37, 2986, (1904).
12. P. Sabatier and A. Mailhe, Compt. Rend., 150, 823, (1910).
13. R. N. Pease and C. C. Yung, J. Am. Chem. Soc., 46, 1163, (1924).
14. H. Adkins and P. P. Perkins, J. Am. Chem. Soc., 47, 1163, (1925).
15. H. Adkins and F. Bischoff, J. Am. Chem. Soc., 47, 807, (1925).
16. F. C. Whitmore, J. Am. Chem. Soc., 54, 3274, (1932).
17. W. S. Brey Jr. and K. A. Krieger, J. Am. Chem. Soc., 71, 3637, (1949).

18. J. G. M. Bremner, *Research (London)*, 1, 281, (1948).
19. K. V. Topchieva, K. Yun-Pin and I. V. Smirnova, 'Advances in Catalysis', 9, 799, Academic Press, New York, (1957).
20. O. V. Krylov and E. A. Fokina, *Probl. Kinetiki i Kataliza, Akad. Nauk. S. S. S. R.*, 8, 248, (1955).
21. E. Wicke, *Z. Electrochem.*, 53, 282, (1949).
22. O. V. Krylov, *Russ. J. Phys. Chem.*, 39, 1422, (1965).
23. A. J. Lundeen and R. Van Hoozer, *J. Am. Chem. Soc.*, 85, 2180, (1960).
24. F. F. Volkenstein, 'Electronic Theory of Semiconductors', Pergamon Press, New York, (1962).
25. P. Fuderer-Luetic and I. Brihta, *Croat. Chim. Acta*, 31, 75, (1959).
26. G. C. Bond, 'Catalysis by Metals', Academic Press, New York, (1962).
27. A. Dandy, *J. Chem. Soc.*, 5956, (1963).
28. A. A. Balandin, *Kinetics and Catalysis*, 4, 707, (1963).
29. O. V. Krylov and E. A. Fokina, *Dokl. Akad. Nauk. S. S. S. R.*, 120, 133, (1958).
30. R. L. Gale, J. Haber and F. S. Stone, *J. Catal.*, 1, 32, (1960).
31. R. G. Greenler, *J. Chem. Phys.*, 37, 2094, (1962).
32. N. P. Keier, *Probl. Kinetiki i Kataliza, Akad. Nauk. S. S. S. R.*, 8, 224, (1955).
33. G. M. Schwab and L. Wandinger, *Z. Electrochem.*, 60, 929, (1956).
34. Y. Dechatre and S. J. Teichner, *Bull. Soc. Chim. France*, 2804, (1967).
35. S. Kolboe, *J. Catal.*, 13, 208, (1969).
36. A. Bielanski, J. Deren, J. Haber and J. Sloczynski, *Actes du deuxieme Congr. Intern. de Catalyse Paris*, (1960), p. 1653, Technip., Paris, (1961).

37. D. G. Klissurski, E. F. McCaffrey and R. A. Ross, *Can. J. Chem.*, 49, 3778, (1971).
38. E. F. McCaffrey, T. A. Micka and R. A. Ross, *J. Phys. Chem.*, 76, 3372, (1971).
39. E. F. McCaffrey, D. G. Klissurski and R. A. Ross, *J. Catal.*, 26, 380, (1972).
40. V. M. Frovlov, O. V. Krylov and S. Z. Roginskii, *Dokl. Akad. Nauk. S. S. S. R.*, 126, 107, (1959).
41. G. M. Schwab, G. Greger, S. Krawczynski and J. Penzkofer, *Z. Phys. Chem. (Frankfurt)*, 15, 363, (1958).
42. K. I. Matveer and G. K. Boreskov, *Probl. Kinetiki i Kataliza, Akad. Nauk. S. S. S. R.*, 8, 165, (1955).
43. G. M. Zhadreva, V. I. Vladimirova and O. M. Vinogradova, *Dokl. Akad. Nauk. S. S. S. R.*, 133, 1375, (1960).
44. H. Otwinowski, E. Treszanowicz and S. Ciborowski, *Actes du deuxieme Congr. Intern. de Catalyse, Paris*, (1960, Astract 85).
45. J. E. Germain, B. Gras and J. Beaufils, *Compt. Rend.*, 26, 4735, (1965).
46. J. E. Germain, B. Gras and J. Beaufils, *Anales. Real. Soc. Espan. Fis. Quim.*, Ser B61, 233, (1965).
47. J. Deren and E. Fryt, *Bull. Acad. Polon. Sci. Ser. Sci. Chim.*, 14, 407, (1966).
48. G. K. Boreskov, 'Catalysis in Sulfuric Acid Production', *Russian State Press for Chemical Literature*, (1954).
49. V. N. Bibin and L. A. Kasatkina, *Kinetics and Catalysis*, 5, 653, (1964).
50. A. P. Dzisyak, G. K. Boreskov, L. A. Kasatkina and V. E. Kochurikhin, *Kinetics and Catalysis*, 2, 727, (1961).
51. L. A. Kasatkina, G. K. Boreskov and P. N. Sokolov, *Russ. J. Phys. Chem.*, 34, 168, (1960).
52. G. K. Boreskov, L. A. Kasatkina, V. V. Popovskii and Yu. A. Balovnev, *Kinetics and Catalysis*, 1, 207, (1960).

53. P. Jiru, D. Tomkova, V. Jara and J. Wankova, *Z. Anorg. und Allgem. Chem.*, 121, 303, (1960).
54. J. J. Carberry, *Catalysis Reviews*, 3, 61, (1969).
55. R. H. Clark, W. E. Graham and A. G. Winter, *J. Am. Chem. Soc.*, 47, 2748, (1925).
56. C. N. Hinshelwood, 'The Kinetics of Chemical Change', Oxford University Press, (1949).
57. P. B. Weisz and C. D. Prater, 'Advances in Catalysis', 6, Academic Press, New York and London, (1954).
58. A. A. Balandin, *Izv. Akad. Nauk. S. S. S. R., Ser. Chim.*, 4, 761, (1961).
59. A. A. Balandin, *Izv. Akad. Nauk. S. S. S. R., Otd. Khim. Nauk.*, 3, 416, (1961).
60. R. Kokes, H. Tobin and P. H. Emmett, *J. Am. Chem. Soc.*, 77, 5860, (1955).
61. J. E. Lovelock, *Anal. Chem.*, 33, 162, (1961).
62. C. Orr and J. M. Dallavalle, 'Fine Particle Measurement', Macmillan Co., London, (1960).
63. S. Brunauer, P. H. Emmett and E. Teller, *J. Am. Chem. Soc.*, 60, 309, (1938).
64. S. Brunauer, L. E. Copeland and D. L. Kantro, 'The Solid-Gas Interface', Vol. 1, edited by E. A. Flood, Marcel Dekker Inc., New York, (1967).
65. R. A. Beebe, J. B. Beckwith and J. M. Honig, *J. Am. Chem. Soc.*, 67, 1554, (1945).
66. S. J. Gregg and K. S. Sing, 'Adsorption, Surface Area and Porosity', Academic Press, New York and London, (1967).
67. American Society for Testing Materials Index, (1972).
68. J. M. Thomas and W. J. Thomas, 'Introduction to the Principles of Heterogeneous Catalysis', Academic Press, New York, (1967).
69. J. F. Zimmerman, *J. Phys. Chem.*, 53, 562, (1949).
70. A. C. Riddiford, *J. Phys. Chem.*, 56, 745, (1952).

71. G. C. Bond, 'Heterogeneous Catalysis: principles and application', Academic Press, Oxford, (1974).
72. D. A. Dowden and G. W. Bridger, 'Advances in Catalysis', 9, 669, (1957).
73. R. W. Blue, V. C. F. Holm, R. B. Regier, E. Fast and L. F. Heckelsberg, Ind. Eng. Chem., 44, 2710, (1950).
74. C. N. Satterfield, 'Mass Transfer in Heterogeneous Catalysis', M.I.T. Press, Cambridge Mass. and London, (1970).
75. A. Clark, 'The Theory of Adsorption and Catalysis', Academic Press, New York and London, (1970).
76. A. A. Balandin, A. A. Tolstopyatova and V. H. Matusheko, Izv. Akad. Nauk. S. S. S. R., 1333, (1960).
77. S. J. Teichner, J. Catal., 4, 724, (1965).
78. J. F. Garcia de la Banda, J. Catal., 1, 136, (1962).
79. A. A. Tolstopyatova, V. A. Naumov and A. A. Balandin, Russ. J. Chem., 38, 879, (1964).
80. E. F. McCaffrey, D. G. Klissurski and R. A. Ross, Proc. of the 5 th. Int. Cong. Cat., Miami Beach Fla., Catalysis Vol. 1 edited by J. W. Hightower, 3-151, (1973).
81. I. M. Hoodless, Personal Communication.
82. P. V. Gel'd, S. I. Alyamovskii and I. I. Matveenko, Russ. J. Inorg. Chem., 5, 815, (1960).
83. L. G. Maidanovskaya and L. M. Kurina, Nauchn. Osnovy Podbara. i Proviz. Katalizatorov, Akad. Nauk. S. S. S. R., Sibirsks, Otd., 232, (1964).
84. D. E. R. Bennett and R. A. Ross, J. Chem. Soc. A, 1524, (1968).
85. D. E. R. Bennett and R. A. Ross, J. Catal., 18, 122, (1968).
86. E. K. Rideal, 'Concepts in Catalysis', Academic Press, New York and London, (1968).
87. O. V. Krylov, Russ. J. Phys. Chem., 39, 1554, (1965).
88. J. C. Kuriacose, C. Daniel and N. Balakrishnan, Indian J. Chem., 7, 367, (1968)

89. H. Knözinger and A. Scheglila, *J. Catal.*, 17, 252, (1970).
90. H. Knözinger, 'The Chemistry of the hydroxyl group', edited by S. Patai, Interscience, London, pp. 641-718, (1971).
91. H. Noller, P. Andreu and M. Hunger, *Angew. Chem. Int. Ed.*, 10, 172, (1971).
92. P. Canesson and M. Blanchard, *J. Catal.*, 42, 205, (1976).
93. M. Ai, *J. Catal.*, 40, 318, (1975).
94. G. Forester, H. Noller and K. Thomke, *J. Catal.*, 44, 492, (1976).
95. A. A. Balandin, G. V. Isagulyants, N. P. Sokolova and I. K. Zakharycheva, *Izv. Akad. Nauk. S. S. S. R., Otd. Khim., Nauk.*, 1549, (1961).
96. S. J. Gregg, 'The Surface Chemistry of Solids', Chapman and Hall Ltd., London, (1965).
97. G. F. Huttig, *Kolloid. Z.*, 98, 263, (1942).
98. D. J. M. Bevan, J. P. Shelton and J. S. Anderson, *J. Chem. Soc.*, 1729, (1948).
99. A. A. Fotiev and B. V. Slobodin, *Russ. J. Chem.*, 10, 80, (1965).
100. G. K. Boreskov, B. I. Popov, V. N. Bibin and E. S. Kozishnikova, *Kinetics and Catalysis*, 9, 657, (1968).
101. B. V. Spitsyn and L. G. Maidanovskaya, *Zhur. Fiz. Chim.*, 33, 180, (1959).
102. G. Pannetier and P. Souchay, 'Chemical Kinetics', Elsevier, London, (1967).

APPENDIX I

The computer programmes given in this Appendix make use of the APL programming language.

Index to Appendix I

<u>Programme</u>	<u>Remarks</u>
KRBET	Used in surface area calculations.
FIT	Used in calculations of standard error of estimate and correlation coefficients.
LHDATA	Used for fitting experimental data to rate equations.
LH	Used for fitting experimental data to rate equations and plotting the results.

```

[1] * XREF:ALPHA;ZETA
[2] *ENTER THE VALUE FOR, VB (IN M.L.S.), FOR THE TUFF USTF.
[3] VB+I
[4] *ENTER THE VALUE FOR, VC (IN M.L.S.), FOR THE TUFF USTF.
[5] VC+I
[6] * ENTER THE NAME OF YOUR SAMPLE, MAKING SURE THAT IT IS ENCLOSED IN SINGLE QUOTATION MARKS.
[7] NAME+I
[8] *ENTER THE WEIGHT (IN GRAMS) OF THE SAMPLE USED.
[9] WT+I
[10] * WHAT IS THE INTERNAL DIAMETER OF THE TUFF USTF (IN IN.). IF YOU DO NOT KNOW ENTER THE NUMBER ZERO.
[11] ID+I
[12] *(ID=0)/END
[13] VI+47.37
[14] VA+13.6
[15] C1:HOW MANY POINTS HAVE YOU OBTAINED FOR THE P.F.T. PLOT.
[16] POINTS+I
[17] *ENTER YOUR TRUE PRESSURE READINGS (IN TOPP) AS A VECTOR, FOR EXAMPLE:-
[18] *PRESSURE FOR CHARGE 1,PRESSURE FOR CHARGE 2, PRESSURE FOR CHARGE 3, ETC. FOR ALL CHARGES
[19] C2+TTP+I
[20] *(POINTS=(0+0TTP)+2)/C2
[21] * YOU HAVE ENTERED THE WRONG NUMBER OF PRESSURE READINGS FOR THE NUMBER OF POINTS YOU ARE PLOTTING.
[22] *P-ENTER THE NUMBER OF POINTS YOU WISH TO PLOT AND THE CORRECT NUMBER OF PRESSURE READINGS.
[23] +C1
[24] C2:J1+J2+J3+J4+J5+J6+J7+J8+2
[25] C3:CPP[J1]+CPP[J2]-CPP[J3]*0.19+(37.2*(J1+2)*CPP[J1]*2)+(14.5*J1*CPP[J1])+1
[26] *(J1+J1+2)≤0)/C3
[27] Y+0047.37
[28] C4:V[J2]+VA+VT+VI
[29] +((J2+J2+2)≤0)/C4
[30] VTP+(273+293*760)*V*CPP
[31] VA+VC+273:77.5*760
[32] VPHTP+VVC+VI+VVS+VAD+C+PPC+YAX+Cp0
[33] C5:VTPP[J3]+CPP[J3]*FA
[34] +((J3+J3+2)≤0)/C5
[35] C6:VVC[J4]+VHTP[J4]+VPHTP[J4]
[36] +((J4+J4+2)≤0)/C6
[37] C7:VTA[J5]+0.07475*CPP[J5]

```

```

[37] +((J5+J5+2)≤0)/C7
[38] J+I+1
[39] VYSY[J]+VNTP[J]
[40] C6:J+J+2
[41] VYSY[J]+TVOL[J-1]+VNTP[J]-VIA[J-1]
[42] +(J<(0-1))/C8
[43] C9:VADS[J6]+VADS[J6-(J6≠2)*2]+VYSY[J6-1]-TVOL[J6]
[44] +((J6+J6+2)≤0)/C9
[45] VC+VADS+V7
[46] C10:PPO[J7]+CPH[J7]+1.754
[47] +((J7+J7+2)≤0)/C10
[48] C11:YAX[J8]+PPO[J8]+(VC[J8]*(1-PPO[J8]))
[49] +((J8+J8+2)≤0)/C11
[50] *ROLL UP TO A NEW SHEET AND PRESS ENTER TO GET TABLE.
[51] *****
[52] * THE DATA FOR THE P.F.T. PLOT FOR 'NAME' IS GIVEN IN THE FOLLOWING TABLE.
[53] *
[54] *
[55] * TRUE CORRECTED VOLUME VOLUME VOLUME TOTAL VOLUME VOLUME VOLUME P/PO P/PC
[56] * PRESSURE (MLS) AT NEP VOLUME AT NEP VOLUME AT NEP (MLS) (MLS) (MLS) (MLS) (MLS) (MLS) (MLS)
[57] * (TORR) (TORR)
[58] *
[59] *-----*
[60] *
[61] * I2P+ 10 6 DFT VFC+(ERR[J],COP[J],VFI),VMSPT[J],MCHL[J],VMSY[J],VMSI[J],PPO[J],YAX[J],VIA[J]
[62] * I2+1
[63] * I2P+(10*(ERR[J2]-1)+110)+H
[64] * +((I2+I2+1)≤0)/1+I2C
[65] * PIES
[66] * +((I+I+1)>0)/G
[67] *
[68] *
[69] * THE SHEET NUMBER IS FOUND FOR THE SHEET IN THE SHEET NUMBER FOR THE SHEET. THE SHEET NUMBER
[70] * CORRELATION SHEET NUMBER WILL BE SUBTRACTED FROM THE SHEET NUMBER TO GET THE SHEET NUMBER.
[71] * HAVE THE SHEET NUMBER (IN THE) OF THE SHEET. SHEET NUMBER WILL NOT BE FOUND.

```

```

V X FIT Y;N;SY;SX;MY
[1] I←((M←pX)×+/X×Y)-(SY←+/Y)×CX←+/X
[2] I←I÷(I×+/X*2)-CX*2
[3] P←(SY-I×SX)÷N+O×(Y←+/Y)÷N
[4] 2 1 ρ ' ' ; N
[5] ' INTERCEPT ' ; R
[6] ' STANDARD ERROR OF ESTIMATE ' ;
[7] ' CORRELATION COEFFICIENT ' ;
[8] 3 1 ρ ' ' ;

```

```

V R LIMITA P
[1] P←[+0×ρ[+1 FOR ALL DATA TO PF MULTIPLIFF TY P TYPE 1, IF NOT + TYFF 0
[2] X←P*P
[3] G←(I×5)ρ ' ×P '
[4] 5 1 ρ ' ' ; DATA FOR R = /P ; G ; ' / (1+AP+...) *N FOR N = 1 2 3
[5] Q(4,ρR)ρP,PR,(PR*0.5),(PR+X×P÷P)÷3
[6] 5 1 ρ ' ' ; DATA FOR R = /P*0.5 ; G ; ' / (1+AP*0.5+...) *N FOR N = 1 2 3
[7] Q(4,ρR)ρP1,(X×P1÷R),(X×P1+R)*0.5),(X×P1+P*0.5)+P)÷3
[8] 5 1 ρ ' ' ; DATA FOR R = /P*2 ; C ; ' / (1+P*2+...) *N FOR N = 1 2 3
[9] Q(4,ρR)ρ(P2),(X×P2÷R),(X×P2+R)*0.5),(X×(P2+P*2)+R)÷3
[10] 10 1 ρ ' ' ;

```

```

V P LN P;PR;P1;P2;Y;Y1;Y2;Y3;YA;M0;B0;M1;B1;M2;B2
M0←B0+M1←B1+M2←B2+10
F←F+0×ρ[F+FOR ALL EQUAT ONE TO BE MULTIPLIED BY P TYPE 1, IF NOT TYPE 0]
R = AP/(1+AP+...)'; (F×F)ρ' ×P'
P FIT PR←P×(F1←P×F)÷R
M0←M0, M+0×ρF0←F0, R
R = AP/(1+AP+...)×2'; (F×5)ρ' ×P'
P FIT PR*0.5
M0←M0, M+0×ρF0←F0, R
R = AP/(1+AP+...)×3'; (F×5)ρ' ×P'
P FIT PR*÷3
M0←M0, M+0×ρF0←F0, D
R = AP*.5/1+AP*.5+...'; G←(F×5)ρ' ×P'
P1 FIT P3←F1×(P1←P*0.5)÷R
M1←M1, M+0×ρB1←B1, R
R = AP*.5/(1+AP*.5+...)×2', G
P1 FIT P3*0.5
M1←M1, M+0×ρB1←B1, R
G 1 ρ' !; R = AP*.5/(1+AP*.5+...)×3', G
P1 FIT P3*÷3
M1←M1, M+0×ρB1←B1, R
R = AP*2/1+AP*2+...'; G
P2 FIT P4←F1×(P2←P*2)÷R
M2←M2, M+0×ρP2←P2, R
R = AP*2/(1+AP*2+...)×2', G
P2 FIT P4*0.5
M2←M2, M+0×ρP2←P2, B
R = AP*2/(1+AP*2+...)×3', G
P2 FIT P4*÷3
M2←M2, M+0×ρB2←B2, F
12 1 ρ' !; COMPARATIVE PLOTS FOR P = AP/(1+AP+...)×N FOR N=1 2 3'

```

```

[31] Y1+Y+[/Y+(PR-P0[1])+M0[1]
[32] Y2+Y+[/Y+((PR*0.5)-B0[2])+M0[2]
[33] Y3+Y+[/Y+((PR*3)-B0[3])+M0[3]
[34] ' N=1 (O) N=2 (*) N=3 (+)'
[35] 50 100 PLOT(Y1 AND Y2 AND Y3) VS P
[36] 5 1 P ' ; 'CC'PARATIVE PLOTS FOR P = AP*.5/(1+AP*.5+...) *N FOR N=1(O) N=2(*) N=3(+) '
[37] Y1+Y+[/Y+(P3-B1[1])+M1[1]
[38] Y2+Y+[/Y+((P3*0.5)-B1[2])+M1[2]
[39] Y3+Y+[/Y+((P3*3)-B1[3])+M1[3]
[40] 50 100 PLOT(Y1 AND Y2 AND Y3) VS P1
[41] 5 1 P ' ; 'CC'PARATIVE PLOTS FOR R = AP*.4/(1+AP*2+...) *N FOR N=1(O) 2(*) 3(+) '
[42] Y1+Y+[/Y+((Y+P4)-B2[1])+M2[1]
[43] Y2+Y+[/Y+((Y*0.5)-B2[2])+M2[2]
[44] Y3+Y+[/Y+((Y*3)-B2[3])+M2[3]
[45] 50 80 PLOT(Y1 AND Y2 AND Y3) VS P2

```

▽

APPENDIX II

This appendix contains the complete experimental data obtained from X-ray analysis of the different catalyst samples.

Table A.2.1Index to Appendix II

Table Number	Sample	Remarks
A.2.2	ASTM Index data for V_2O_5	(Reference 67)
A.2.3	V_2O_5 as supplied by Ventron	Pale-orange
A.2.4	V_2O_5 pelletized and calcined at $520^\circ C$ for 10 hrs.	Brown-orange
A.2.5	$V_2O_5:9.09\%Li_2SO_4^*$ pelletized and calcined at $520^\circ C$ for 10 hrs.	Brown-orange
A.2.6	$V_2O_5:9.09\%Na_2SO_4$ pelletized and calcined at $520^\circ C$ for 10 hrs.	Grey-black
A.2.7	$V_2O_5:9.09\%K_2SO_4$ pelletized and calcined at $520^\circ C$ for 10 hrs.	Brown-orange
A.2.8	$V_2O_5:9.09\%Rb_2SO_4$ pelletized and calcined at $430^\circ C$ for 10 hrs.	Brown-orange
A.2.9	$V_2O_5:9.09\%Cs_2SO_4$ pelletized and calcined at $430^\circ C$ for 10 hrs.	Brown-orange
A.2.10	$V_2O_5:1.01\%K_2SO_4$ pelletized and calcined at $520^\circ C$ for 10 hrs.	Brown-orange

* The percentages indicated refer to mole percent of alkali metal sulphate.

Table Number	Sample	Remarks
A.2.11	V_2O_5 :2.00% K_2SO_4 pelletized and calcined at 520°C for 10 hrs.	Brown-orange
A.2.12	V_2O_5 :4.98% K_2SO_4 pelletized and calcined at 520°C for 10 hrs.	Brown-orange
A.2.13	V_2O_5 after use in the reactor	Black
A.2.14	V_2O_5 :9.09% Li_2SO_4 after use in the reactor.	Black
A.2.15	V_2O_5 :9.09% Na_2SO_4 after use in the reactor	Black
A.2.16	V_2O_5 :9.09% K_2SO_4 after use in the reactor.	Black
A.2.17	V_2O_5 :9.09% Rb_2SO_4 after use in the reactor.	Black
A.2.18	V_2O_5 :9.09% Cs_2SO_4 after use in the reactor.	Black
A.2.19	V_2O_5 :9.09% Li_2SO_4 after use in the reactor then heated in air at 450°C for 1 hr.	Black
A.2.20	V_2O_5 :9.09% Li_2SO_4 after use in the reactor then heated in air at 600°C for 12 hrs.	Brown-orange
Plate A.2.1	X-ray powder photographs for: (A) sample A.2.3; (B) sample A.2.4; (C) sample A.2.5 and (D) sample A.2.6.	
Plate A.2.2	X-ray powder photographs for: (E) sample A.2.7; (F) sample A.2.8; (G) sample A.2.9 and (H) sample A.2.10.	
Plate A.2.3	X-ray powder photographs for: (I) sample A.2.11; (J) sample A.2.12; (K) sample A.2.13 and (L) sample A.2.14.	
Plate A.2.4	X-ray powder photographs for: (M) sample A.2.15; (N) sample A.2.16; (O) sample A.2.17 and (P) sample A.2.18.	
Plate A.2.5	X-ray powder photographs for: (L) sample A.2.14; (Q) sample A.2.19 and (R) sample A.2.20.	

Table A.2.2 ASTM Index X-ray data for V_2O_5 .

Line Number	d (Å)	I/I _o
1	5.76	40
2	4.38	100
3	4.09	35
4	3.48	8
5	3.40	90
6	2.88	65
7	2.76	35
8	2.687	16
9	2.610	40
10	2.492	8
11	2.405	8
12	2.185	18
13	2.147	12
14	2.042	4
15	1.992	18
16	1.919	25
17	1.900	18
18	1.864	14
19	1.840	6
20	1.778	4
21	1.757	30
22	1.740	14
23	1.648	12
24	1.632	8
25	1.5764	10

* See reference (67).

Table A.2.3 V_2O_5 as supplied by Ventron.

Line Number	R (mm)	θ	d (Å)
1	15.25	7.63	5.80
2	20.25	10.13	4.38
3	21.65	10.83	4.10
4	26.10	13.05	3.41
5	30.95	15.48	2.89
6	32.30	16.15	2.77
7	33.30	16.65	2.69
8	34.30	17.15	2.61
9	41.25	20.63	2.19
10	42.00	21.00	2.15

Table A.2.4 V_2O_5 pelletized and calcined at 520°C for 10 hrs.

Line Number	R (mm)	θ	d (Å)
1	15.55	7.78	5.69
2	20.40	10.20	4.35
3	21.90	10.95	4.06
4	26.25	13.13	3.39
5	31.10	15.55	2.88
6	32.45	16.23	2.76
7	33.65	16.83	2.66
8	34.55	17.23	2.60
9	41.45	20.73	2.18
10	42.15	21.08	2.14

Table A.2.5 $V_2O_5:9.09\%Li_2SO_4$ pelletized and calcined at 520°C for 10 hrs.

Line Number	R (mm)	θ	d (Å)
1	15.50	7.75	5.72
2	20.40	10.20	4.35
3	21.80	10.90	4.08
4	26.20	13.10	3.40
5	31.00	15.50	2.88
6	32.45	16.23	2.76
7	34.35	17.18	2.61
8	41.30	20.68	2.18
9	42.00	21.00	2.15

Table A.2.6 $V_2O_5:9.09\%Na_2SO_4$ pelletized and calcined at $520^{\circ}C$ for 10 hrs.

Line Number	R (mm)	θ	d (Å)
1	9.35	4.68	9.45
2	12.20	6.10	7.25
3	26.35	13.18	3.38
4	29.25	14.63	3.05
5	30.75	15.38	2.91
6	41.60	20.80	2.17
7	48.60	24.30	1.87
8	50.70	25.35	1.49
9	62.10	31.05	1.49
10	67.00	33.50	1.40

Table A.2.7 $V_2O_5:9.09\%K_2SO_4$ pelletized and calcined at $520^{\circ}C$ for 10 hrs.

Line Number	R (mm)	θ	d (Å)
1	15.50	7.75	5.72
2	20.40	10.20	4.35
3	21.80	10.90	4.08
4	26.20	13.10	3.40
5	31.10	15.55	2.88
6	32.50	16.25	2.75
7	34.45	17.23	2.60
8	41.45	20.73	2.18
9	42.00	21.00	2.15

Table A.2.8 $V_2O_5:9.09\%Rb_2SO_4$ pelletized and calcined at $430^{\circ}C$ for 10 hrs.

Line Number	R (mm)	θ	d (Å)
1	15.60	7.80	5.68
2	20.40	10.20	4.35
3	21.80	10.90	4.08
4	26.20	13.10	3.40
5	31.00	15.50	2.88
6	32.30	16.15	2.77
7	34.20	17.10	2.62
8	41.35	20.68	2.18
9	42.00	21.00	2.15

Table A.2.9 $V_2O_5:9.09\%Cs_2SO_4$ pelletized and calcined at $430^\circ C$ for 10 hrs.

Line Number	R (mm)	θ	d (Å)
1	15.50	7.75	5.72
2	21.80	10.90	4.08
3	24.40	12.20	3.65
4	26.20	13.10	3.40
5	27.50	13.75	3.24
6	31.00	15.50	2.88
7	41.35	20.68	2.18
8	42.10	21.05	2.15

Table A.2.10 $V_2O_5:1.01\%K_2SO_4$ pelletized and calcined at $520^\circ C$ for 10 hrs.

Line Number	R (mm)	θ	d (Å)
1	15.50	7.75	5.72
2	20.35	10.18	4.37
3	21.85	10.93	4.07
4	26.30	13.15	3.39
5	31.00	15.50	2.88
6	32.50	16.25	2.75
7	34.40	17.20	2.61
8	41.25	20.63	2.19
9	42.10	21.05	2.15

Table A.2.11 $V_2O_5:2.00\%K_2SO_4$ pelletized and calcined at $520^\circ C$ for 10 hrs.

Line Number	R (mm)	θ	d (Å)
1	15.45	7.73	5.73
2	20.40	10.20	4.35
3	21.75	10.88	4.08
4	26.20	13.10	3.40
5	30.95	15.48	2.89
6	32.40	16.20	2.76
7	34.35	17.18	2.61
8	41.25	20.63	2.19
9	42.10	21.05	2.15

Table A.2.12 $V_2O_5:4.98\%K_2SO_4$ pelletized and calcined at $520^\circ C$ for 10 hrs.

Line Number	R (mm)	θ	d (Å)
1	15.45	7.73	5.73
2	20.40	10.20	4.35
3	21.75	10.88	4.08
4	26.20	13.10	3.40
5	31.00	15.50	2.88
6	32.40	16.20	2.76
7	34.35	17.18	2.61
8	41.20	20.60	2.19
9	42.10	21.05	2.15

Table A.2.13 V_2O_5 after use in the reactor.

Line Number	R (mm)	θ	d (Å)
All lines were broad and faint, 'd' values are only approximations			
1	25.10	12.55	3.55
2	29.80	14.90	3.00
3	32.80	16.40	2.73
4	45.00	22.50	2.01

Table A.2.14 $V_2O_5:9.09\%Li_2SO_4$ after use in the reactor.

Line Number	R (mm)	θ	d (Å)
The one line was quite broad and faint, the 'd' value is only an approximation			
1	44.70	22.35	2.03

Table A.2.15 $V_2O_5:9.09\%Na_2SO_4$ after use in the reactor.

Line Number	R (mm)	θ	d (Å)
The one line was quite broad and faint, the 'd' value is only an approximation.			
1	44.70	22.35	2.03

Table A.2.16 $V_2O_5:9.09\%K_2SO_4$ after use in the reactor.

Line Number	R (mm)	θ	d (Å)
1	12.10	6.05	7.31
2	26.00	13.00	3.45
3	28.80	14.40	3.10
4	30.55	15.28	2.96
5	32.80	16.40	2.73
6	41.00	20.50	2.20
7	50.10	25.05	1.82

Table A.2.17 $V_2O_5:9.09\%Rb_2SO_4$ after use in the reactor.

This sample gave no detectable diffraction pattern under the conditions used.

Table A.2.18 $V_2O_5:9.09\%Cs_2SO_4$ after use in the reactor.

This sample gave no detectable diffraction pattern under the conditions used.

Table A.2.19 $V_2O_5:9.09\%Li_2SO_4$ after use in the reactor then heated in air at 450°C for 1 hr.

Line Number	R (mm)	θ	d (Å)
1	9.40	4.70	9.41
2	12.20	6.10	7.25
3	15.40	7.70	5.75
4	20.30	10.15	4.37
5	26.20	13.10	3.40
6	29.40	14.70	3.04
7	30.45	15.23	2.93
8	31.10	15.55	2.88
9	32.40	16.20	2.76
10	33.00	16.50	2.71
11	34.35	17.18	2.61
12	50.80	25.40	1.80

Table A.2.20 $V_2O_5:9.09\%Li_2SO_4$ after use in the reactor then heated in air at $600^\circ C$ for 12 hrs.

Line Number	R (mm)	θ	d (\AA)
1	14.00	7.00	6.33
2	20.50	10.25	4.33
3	21.10	10.55	4.21
4	21.95	10.98	4.05
5	26.20	13.10	3.40
6	28.60	14.30	3.12
7	31.00	15.50	2.88
8	32.55	16.28	2.75
9	34.50	17.25	2.60
10	41.50	20.75	2.18
11	42.40	21.20	2.13
12	45.70	22.85	1.96



Plate A.2.1



Plate A.2.2



Plate A.2.3

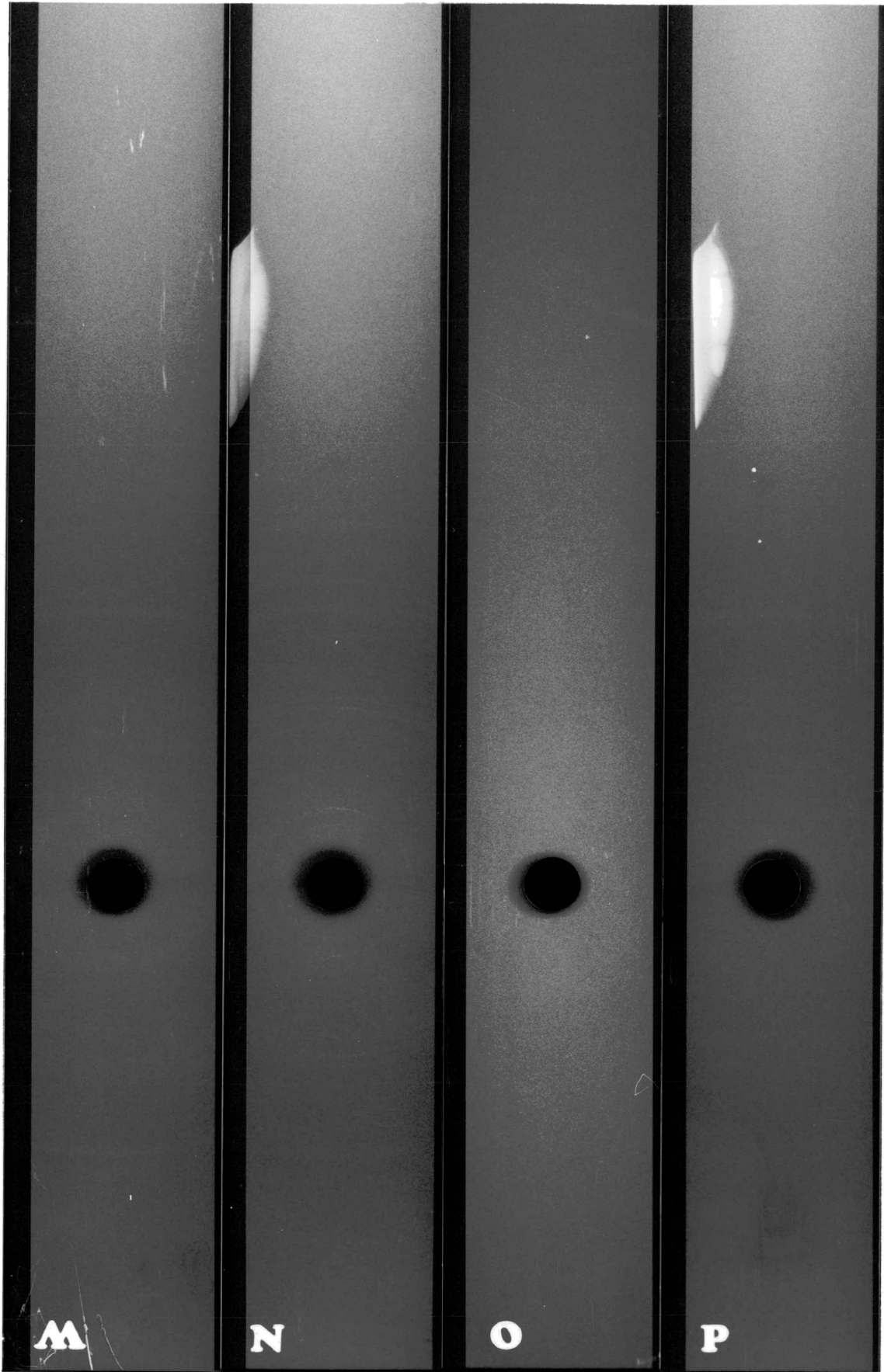


Plate A.2.4

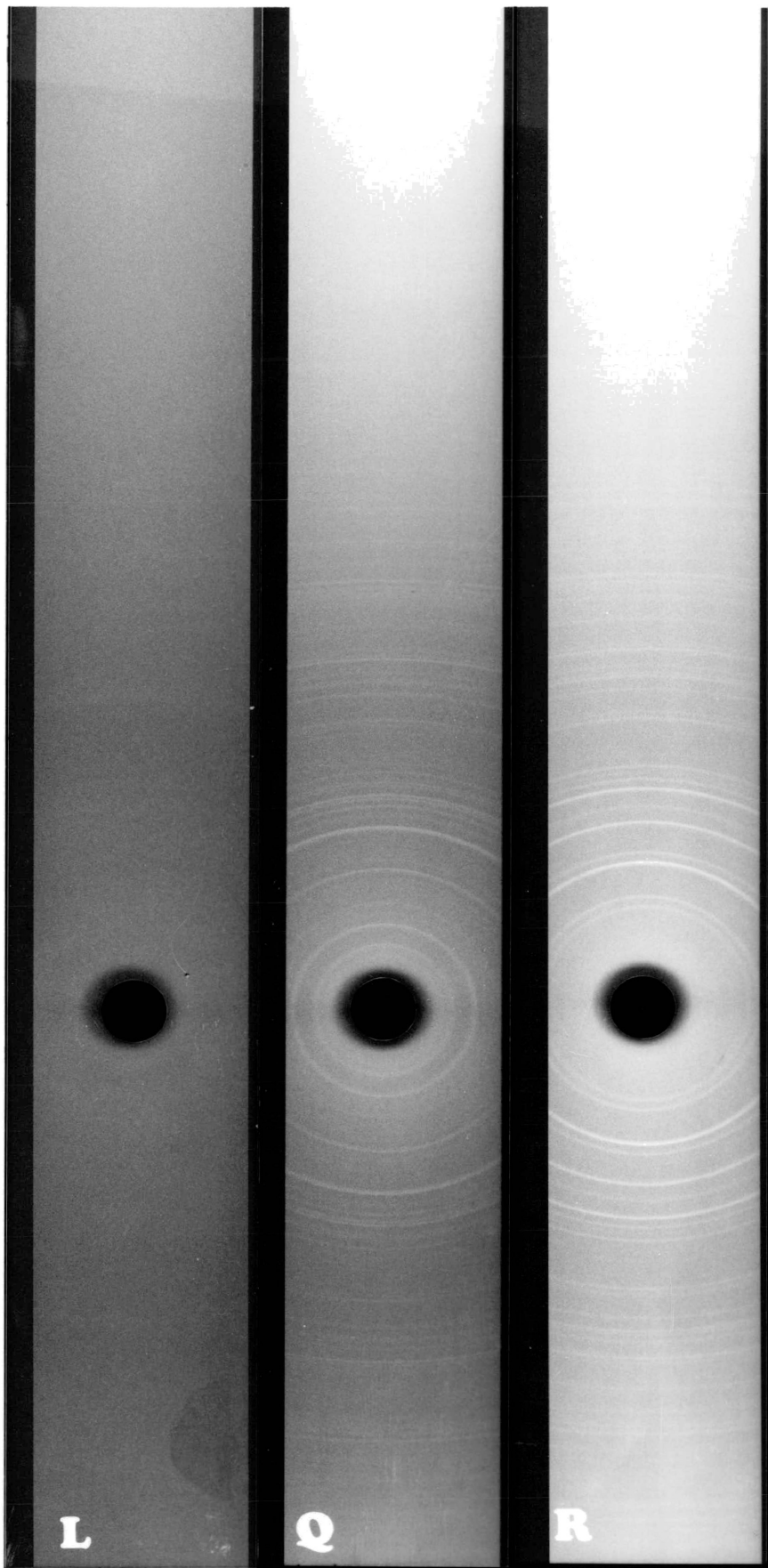


Plate A.2.5